# Effects of Defects and Strain on Ion Channeling in Solids

A Dissertation submitted for the award of the Degree of
**Doctor of Philosophy**

**By**
**AZHER MAJID SIDDIQUI**


**SCHOOL OF PHYSICS**
**UNIVERSITY OF HYDERABAD**
**HYDERABAD**
**INDIA**

MAY - 2000

# Dedicated
# to
# My Father

# (Late) Mr. Rasheeduddin Siddiqui

with the following poem which appeared in the *Student Magazine of the Aligrah Muslim University* (from where I did my P.G)....

My Tower of Strength

When you were with us
I never felt the need
to hug you, to remain with you
You were our part and parcel
which would newer part
I never thought you'd leave and go
But alas! no one thought it would be so.
So sudden that still it is shocking
Tears seem to trifle at the great loss
Regrets, depression and profound sorrow
Is all that's life
I want to tear you apart from
wherever, with whomever you are
I know that you won't come back
But still I want you back
The more I think of you,
the intensity of wanting you
Loving you and making you happy
grows stronger,
Why oh! why didn't I stay more with you
If I hadn't done that but.....
These 'Why and If make me weak.
That I long for my "Tower of Strength"
Which had been and still are You.
for i am still holding onto something
of you and "Living".

# ACKNOWLEDGEMENTS

It is perhaps not an overstatement to say that this is the most difficult part of the thesis to write. I don't know if am not aware of such a word or maybe the English language itself does not have the word (although known to be the richest of all languages) which would express my feelings when I want to acknowledge somebody. A simple word like *Thanks* or its synonym may not suffice for this, but if I am able to convey my feelings through such words, the purpose would be fulfilled.

From the day I joined the University of Hyderabad, I have been in touch with one person, the then Dean, School of Physics, Prof. Anand P Pathak, whom I found dedicated to the field of science; which inspired me to join under him for M. Phil and after successful completion of that, for Ph. D. I am immensely grateful to him for his patience, helpful guidance and constant encouragement.

I would like to thank the successive Deans, School of Physics, for providing all the facilities during my work.

As a part of my work, I had to visit several Institutes of excellence like, the Tata Institute of Fundamental Research, Mumbai; Institute of Physics, Bhubaneswar; Indira Gandhi Centre for Atomic Research, Kalpakkam; Indian Institute of Technology, Kanpur; and the Nuclear Science Centre, New Delhi. I take this opportunity to acknowledge the facilities and support (academic and otherwise) extended by these Institutions to carry out my work. It is during these visits that I got in contact with Prof. Bhupen Dev of IoP and Prof. B M Arora of TIFR, from whom I really learnt to carry out experimental research. Courtesy Prof. Dev and Prof. Arora, I am now in a position to execute a full fledged experimental project. I am again at a loss to express my gratitude to both of them.

My sincere thanks to the most helpful and sincere-most person, my senior Dr. V Harikumar who always stood by me at tough times and tried his level best to help me out. Special thanks

My brothers, sisters and all other family members also gave their full moral support and I am deeply indebted to all them.

At the fag end of my research, Bushra entered into my life and made it colourful. She came into my life as a sensation and I was very soon gifted by the most wonderful, most beautiful and the cutest of all things, my daughter, Maseera (the Wind of Paradise). Thanks to Bushra and all her family members for everything.

A bunch of thanks to my friends, Mr. Farooq, Mr. Mushtaq, Mr. Ishtiaq, Mr. Arif, Mr. Athaullah, Mr. Younus, Mr. Ateeq, Mr. Ashfaq, my cousins Mr. Syed Viqaruddin, Mr. Farrukh Siddiqui, Mr. Yasar and lot many for their whole-hearted support during my Ph. D.

I am also thankful to the Non-teaching staff, Mr. Abraham, Mr. Anand, Mr. Nagarajan and to all others who helped me directly or indirectly during the course of the time. Mr. K. Srinivas also helped me a lot in learning LaTeXand I thank him for all the help.

Last, but not the least, I am grateful to IUC-DAEF, Indore for providing financial assistance in the form of a project and also to the Council of Scientific and Industrial Research, New Delhi, India for three years of Senior Research Fellowship.

# List of Publications

## A. Refereed Publications

1. [⋆] **A.M. Siddiqui,** V. Harikumar and **A.P.** Pathak, Phy. Stat. Sol (b) **185,** 77, (1994).

2. [⋆] **Azher M. Siddiqui,** V. Harikumar, L.N.S. Prakash Goteti and A.P. Pathak, Modern Physics Letters **(B), 10,** 745, (1996).

3. **Azher M. Siddiqui,** A. Kiran and A.P. Pathak, Modem Physics Letters **(B), 11,** 1231, (1997).

4. **Azher M. Siddiqui,** Anand P. Pathak, B. Sundaravel, Amal K. Das, K.Sekar, B.N. Dev and B.M. Arora, Nucl. Instr. and Meth. (B), **142,** 389, 1998.

5. Anand P. Pathak, S.V.S. Nageswara Rao and **Azher M. Siddiqui,** Nucl. Instr. and Meth. **(B), 161-163,** 488, 2000.

## B. In Proceedings

1. **Ion** beam **mixing in Au/Si system by Nitrogen ions,** D. **K.** Sarkar, S. Choudhary, Azher M. Siddiqui, S. K. Sinha, P. Magudapathy, K. Sekar, K. G. M. Nair, S. Panchapakesan, N. S. Thampi and K. Krishan, *Emerging trends of thin films Technology and device fabrication*, 27-29 Nov. 1995, Cochin University, India.

2. **Development of RBS facility with 2MV Tandem Van de Graff accelerator at IGCAR, Kalpakkam**, S. **K.** Sinha, D. C. Kothari, P. Magudapathy, S. Panchapakesan, Azher M. Siddiqui and K. G. M. Nair, *The 4th National Seminar of Physics and Technology of Particle Accelerator and their Applications* (PATPAA) 26-29 Nov. 1996, IUC-DAEF, Calcutta, India.

3. **Quantum Models For Dechanneling By Point Defects And Extended Defects,** Anand P. Pathak, L.N.S. Prakash Goteti and Azher M. Siddiqui, Proc. *The Fifteenth International Conference on Applications of Accelerators in Research and Industry* (CAARI'98), 4-7 November 1998, Denton, Texas, USA Editors: J. L. Duggan and I. L. Morgan, American Institute of Physics (AIP) Conference Proceedings No. **475,** 765, (1999).

## C. **Others**

- **Channeling and channeling Radiation in Semiconductor Superlattices** Anand P Pathak, Azher M. Siddiqui, L. N. S. Prakash Goteti and V. Harikumar in **Semiconductor Materials and Devices** edited by O. P. Agnihotri and V. K. Jain *Narosa Publishing House, New Delhi* pp. 241 - 258 (1998).

## Conference/Workshop/School Attended:

1. Participated in Workshop *Ion Beam Applications With Low Energy Accelerator Facility at MSD, IGCAR*, Particle Irradiation Facility, MSD, Indira Gandhi Centre for Atomic Research, Kalpakkam, 26 February-3 March 1994.

2. Participated in International Conference on *Defects in Condensed Media (DCM'95)*, Materials Science Division, Indira Gandhi Centre for Atomic Research, Kalpakkam, 20-22 September 1995.

3. Participated in SERC School on *Computational Condensed Matter Physics*, Department of Physics, Himachal Pradesh University, Shimla 30 October-18 November 1995.

4. Poster Presented at the International Conference on *Frontiers in Materials Modelling and Design (MATMOD '96)*, Materials Science Division, Indira Gandhi Centre for Atomic Research, Kalpakkam, 20-23 August 1996.

5. Participated in National Conference on *Ion Beams in Materials Research* Department of Physics, University of Poona, Pune, 17-19 February 1997.

6. Participated in SERC School on *Materials for Advanced Research and Technology (SMART'97)* Crystal Growth Centre, Anna University, Chennai, 3-17 October 1997.

7. Posters Presented *In Proxy* at the *15th International Conference on Applications of Accelerators in Research and Industries (CAARI'98)* Department of Physics, University of North Texas, Denton, TEXAS, USA, 4-7 November 1998.

8. Poster Presented at the Seminar on *Semiconductor Physics and Devices*, School of Physics, University of Hyderabad, Hyderabad, 5-7 March 1999.

[*] **Not Included** in Thesis.

## Table of Contents

Chapter 1

# INTRODUCTION

Enormous theoretical and experimental research has been carried out in the area of ion-solid interaction; most of the work is concerned with the source of probes, the beam of particles-photons, electrons or ions, the interaction cross-section and the emergent e.m. radiation etc. Rutherford Backscattering is one among these fundamental processes in which an energetic positively charged particle (a proton, an $\alpha$-particle or a heavy ion) is bombarded on a target and the emerging backscattered particle/radiation flux is studied to get the information on the composition, thickness and structure etc of the target. When an ion beam impinges on a crystalline solid in a direction parallel to one of the major crystallographic directions, the ioas tend to be steered by the rows or planes into the regions between the atoms. This steering effect causes the projectiles to follow trajectories in the open channels between rows and planes. This phenomenon is known as *channeling*. The range of channeled particles is anomalously large and close impact phenomena like Rutherford Backscattering Spectrometry ($RBS$) or Inner Shell excitation yield are reduced drastically, indicating the alignment of the beam with axes or planes. Three essential requirements must be met for a particle to get channeled. First, it must find transparency in the form of an open channel between rows or planes of atoms. Secondly, there must be a force acting which steers the particle towards the middle of the channel. Thirdly, for the channeled trajectory to be stable, the particle must not approach the rows or planes of atoms too closely otherwise the gentle steering effect of many glancing collisions will be replaced by a wide angle deflection in one or more violent collisions with individual atoms. Thus one requires *transparency, steering* and *stability* (Fig. 1.1).

The first extensive and comprehensive treatment of channeling is that due to Lindhard [1] with the following four basic assumptions. First, the angles of scattering of the incident particle

are small even if the particle is a fast heavy ion. Scattering at large angles would imply that the original direction as well as correlations associated with it are completely lost. The scattering of the projectile is due to nuclear collisions where it interacts with the charge distribution of an atom as a whole, the collision being nearly elastic. Secondly, since a collision demands that the particle comes close to the atom, strong correlations between collisions occur if the particle moves at a small angle with a *row* of atoms; if it passes close to one atom in the row, it must also pass close to the neighbouring atoms in the same row. Thus the atom effectively *sees* one string of atoms at a time which is characterized by the lattice parameter $d$ only. Strings belonging to low index directions have a small value of $d$, and are most pronounced ones. Correlations weaker than those of strings are expected for crystal planes. The third assumption is that, classical orbital pictures may be used to a large extent. The classical description of many successive collisions with atoms in a string (or a plane) is "valid" at high velocities. Fourth, the idealized case of a perfect lattice, a perfect string and ideal plane are adopted. The thermal and zero point vibrations are negligible compared to the successive collisions with many atoms in a string or plane.

Assumption 2 tells us that a channeled particle will not be able to feel the interaction due to individual atoms sitting at various lattice sites but rather experiences a collective effect of all atoms sitting along that particular axial or planar direction. This is valid so long as the angle of incidence is less than a critical angle $\psi_{cri}$; the incident beam then undergoes reflection from a string or plane. For angles of incidence less than the critical angle; an aligned beam of particles is generated. In other words, it experiences only continuum strings or planes. The phenomena is also studied by defining a limiting distance of approach to the atomic rows/planes of atoms which in turn again depends on the critical angle (Fig. 1.2).

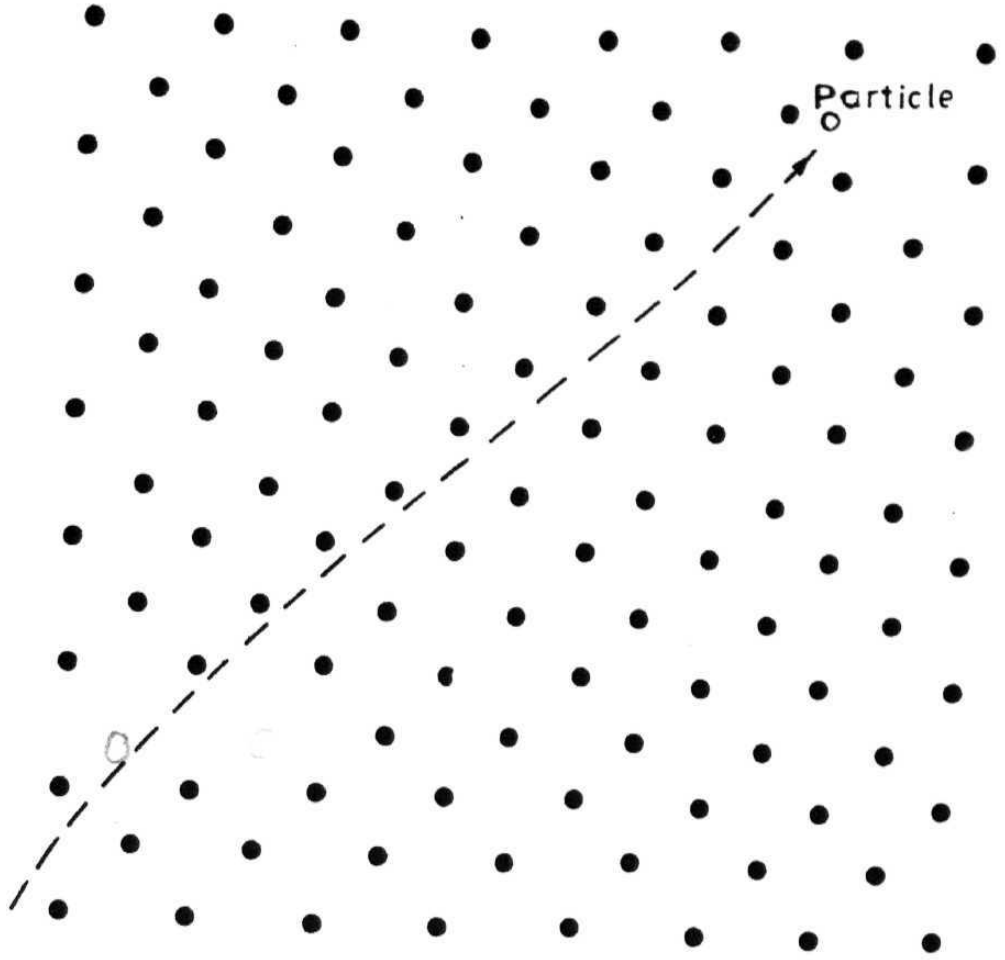


**Fig 1.1**: The Channeling phenomenon, showing how the particle is steered by glancing collisions along an open passage in the crystal [4].

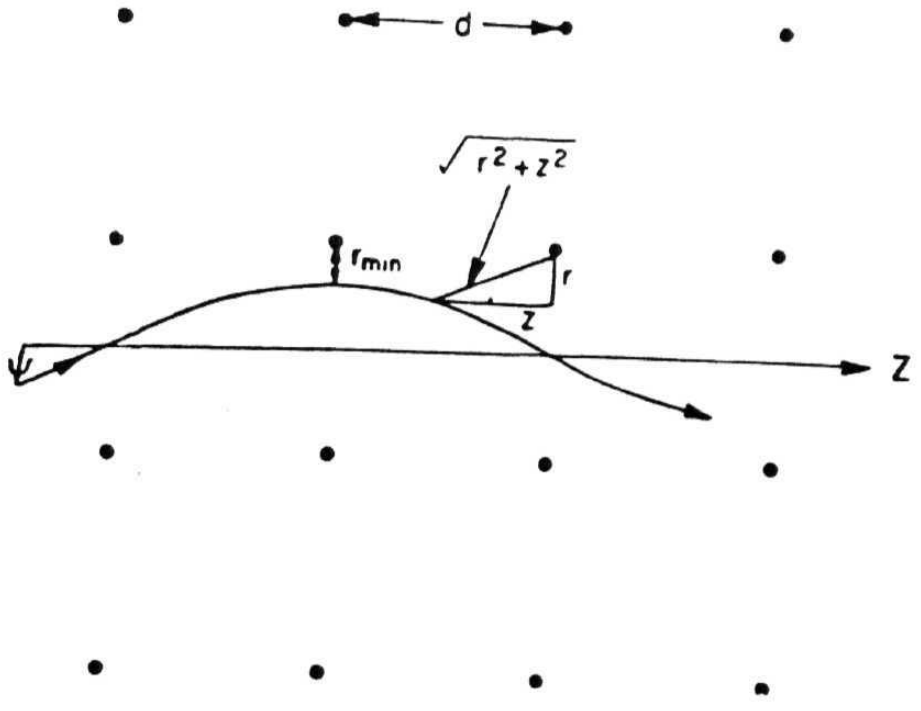


**Fig 1.2**: A channeled trajectory showing various quantities such as the incident angle, minimum distance of approach and the interatomic distance.

## 1.1 Lindhard's Continuum Model

With the basic assumptions discussed above, the channeling phenomena is explained by Lindhard in a step by step way. The particle velocity component parallel to the axial or planar direction is such that the time of flight to cross one lattice spacing is less than the collision time with any individual target atom. As a consequence, before it can feel itself to be in the potential field of one atom, it is already in the field of next atom along the string or plane and it will feel only continuum potentials. Therefore the critical angle and corresponding closest distance of approach are very essential parameters, in channeling situations. If $\psi$ is the angle the incident particle makes with the channel axis, $v$ is its velocity, $r_{min}$ the minimum distance of approach and $d$ is the interatomic spacing along the axis, then the above condition for continuum approximation written as

$$\frac{r_{min}}{v \sin \psi} > \frac{d}{v \cos \psi} \tag{1.1}$$

If $\psi$ is fc&o small, then we get

$$\frac{r_{min}}{v\psi} > \frac{d}{v}$$

**or**

$$r_{min} > \psi d \tag{1.2}$$

Under continuum approximation, $r_{min}$ is obtained by equating the repulsive interaction due to continuum string, with the transverse kinetic energy, the effect of other strings being negligible when the probe is approaching one of them.

$$U(r_{min}) = E \sin^2 \psi \approx E\psi^2 \tag{1.3}$$

The motion of a channeled particle is in effect governed by a transverse potential corresponding to the average of the crystal potential along an axis or plane, over the coordinates parallel to direction of propagation. For positive particles, the transeverse motion perpendicular to the axis or plane is confined to the region around a potential minimum between the strings or planes of

atoms. The continuum axial potential is derived by averaging the interatomic potential along the string and is given by [1-4]

$$U(r) = \int_o^\infty \frac{1}{d} V(\sqrt{z^2 + r^2}) \quad dz \tag{1.4}$$

where r is the distance from the string and V(r) is the interatomic potential. Extensive work has been done regarding the choice of interatomic potential. These potentials are derived by various methods and each of them has its own advantages and draw backs. These statistical potentials can be broadly classified in two groups namely, the power law potentials and the exponential potentials. In the first category of power law potentials come the Lindhard's potential [1] and its modifications by Pathak and Mory [2] and Pathak [3]. In the category of exponential potentials come Moliere potential [3] and the Biersack's Universal potential [4]. Lindhard's standard potential has been most frequently used [5] for calculating various parameters like critical angle etc. This potential is given by

$$V_{Li}(R) = Z_1 Z_2 e^2 \left[ \frac{1}{R} - \frac{1}{\sqrt{R^2 + C^2 a_{T.F}^2}} \right] \tag{1.5}$$

where $C$ is Lindhard constant $(= \sqrt{3})$ and $a_{T.F}$ is Thomas-Fermi screening radius given by

$$a_{T.F} = \frac{0.8853 a_0}{(Z_1^{2/3} + Z_2^{2/3})^{1/2}} \tag{1.6}$$

where $a_o$ is Bohr radius. The corresponding continuum potential for the planar case is derived Py averaging over the particular plane and is given by

$$Y(y) = N d_p \int_{-\infty}^{\infty} V(\sqrt{r^2 + y^2}) \quad 2\pi r dr \tag{1.7}$$

Here, N is the bulk density of atoms in the crystal, $d_p$ the interplanar spacing and $y$ the distance measured from the plane.

One can see the difference between the axial continuum potential and the planar potential. For the axial case, the continuum potential rapidly decreases for values of $r$ comparable to or less than the Thomas-Fermi screening distance. At small nuclear seperations, it is appropriate to use

screened potential with a screening function given by the Thomas-Fermi TF model. The general form of TF potential can be written as

$$V(R) = \frac{Z_1 Z_2 e^2}{R} \phi\left(\frac{R}{a_{TF}}\right) \tag{1.8}$$

where $Z_1$ *and* $Z_2$ are the atomic numbers of projectile and t arget atoms respectively. $\phi(x)$ is the Thomas-Fermi screening function. It is an established fact that this choice of TF screening function and hence the interatomic potentials is not unique. The TF model possesses the distinct advantage of simplicity combined with increasing validity for heavier atoms. In addition, it provides ai initial hypothesis for some more reliable theoretical potentials at close separations.

The study of point defects in the crystals, their lattice location, etc.have been among the first applications of RBS/Channeling technique, over three decades back. The interaction potential between the probe projectile and the heavy impurities is appreciably modified due to the presence of host crystal electrons (conduction and valence) on the one hand and the atomic electrons of the, impurity, on the other. The response of the electrons and, indirectly, the neighbouring metal atoms to the introduction of point charges like hydrogen or positive pions and unions is a basic problem for the theory and a starting point for the description of point defects in general (4]. Pions that are incident upon a crystalline solid occupy a lattice site and then decay into muons of energy 4.12 *MeV* which undergo channeling effects. The scattering cross-section of pions by an interstitial impurity is a topic of special interest. For a systematic study of various phenomena in the field of lattice steering of muons by the decay of pions, a reliable and yet analytically simple potential is needed.

## 1.2 Interatomic Potentials

The interaction between a positive particle and a target maybe analytically described by the TF statistical model, neglecting the velocity dependence of the ion-atom field. The potential is given by equation (1.8). For the Lindhard's model, the TF function is mathematically simple and lends

itself readily to computational purposes, and is given by [6]

$$\phi\left(\frac{R}{a}\right) = 1 - \left[1 + \left(\frac{Ca}{R}\right)^2\right]^{\frac{-1}{2}} \tag{1.9}$$

Equation (1.9) has a drawback in that for the planar case that it does not yield analytically handy expressions for various quantities as dechanneling parameters. The most widely used potential along with Lindhard's is the Moliere potential [3]

$$V_{Mo}(R) = \frac{2Z_1Z_2e^2}{d}(0.35e^{(-0.3R/a)} + 0.55e^{(-1.2R/a)} + 0.1e^{(-6R/a)}) \tag{1.10}$$

The corresponding axial and planar potentials are given by

$$U_{Ax}(r) = \frac{2Z_1Z_2e^2}{d}\left[0.35K_o\left(\frac{0.3r}{a}\right) + 0.55K_o\left(\frac{1.2r}{a}\right) + 0.1K_o\left(\frac{6r}{a}\right)\right] \tag{1.11}$$

and

$$U_{Pl}(y) = 2\pi Z_1Z_2e^2N_p\left(1.16ae^{-0.3y/a} + 0.46ae^{-1.2y/a} + 0.016ae^{-6y/a}\right) \tag{1.12}$$

Moliere potential simplifies only if one leading term is taken [10] even for the perfect crystal case. Another potential which is of most value in providing a simple functional form for ion-atom and atom-atom collisions at large distances is the Born-Mayer potential [11] which can be written as

$$V_{BM}(R) = A_{BM}\exp\left(\frac{-R}{a_{BM}}\right) \tag{1.13}$$

where $A_{BM}$ and $a_{BM}$ are determined phenomenologically by fitting elastic moduli. But this results in a purely exponential interaction potential which is not suitable for describing close ion-atom collisions. Its application is therefore restricted to interactions where the particles are heavy ions with energies in the keV range. In order to obtain some analytical results in complicated problems involving effects of defects in channeling and to study the detailed behaviour of transmitted patterns involving the solution of Boltzmann transport equation, alternative mathematical approximation of both the axial and planar potentials have been made [12, 13, 14], justified by

showing that this corresponds to the physically understandable interatomic potential [3], given by

$$V_{PM}(R) = \frac{Z_1 Z_2 e^2}{R} \frac{Ca^2}{(R+a)^2} \tag{1.14}$$

There is one small difficulty with the above equation, namely the screening function goes to $C(=\sqrt{3})$ rather than to unity for R going to zero. Also the basic requirement of charge neutrality is not met [15] by this potential. Pathak et al. handled this difficulty [16] by replacing Lindhard's constant C by a function $\frac{2(R+a)}{(R+2a)}$ without disturbing the basic simplified form to be used for analytical calculations. This potential now takes the form

$$V_{Pa}(R) = \frac{Z_1 Z_2 e^2}{R} \frac{2a^2}{(R+a)(R+2a)} \tag{1.15}$$

All these potentials, as mentioned earlier, are statistical in nature and give a rough estimate of the ion-solid interactions. In what follows in the succeeding subsections, we discuss about the simplest of all the TF functions, namely the Screened Coulomb potential for a point charge and for an ionized impurity in a host lattice.

### 1.2.1 Potential Around A Point Charge

The potential around a point charge is a screened Coulomb potential and beyond a few multiples of the screening parameter, the charge cannot be *seen* by the incoming particle. In metals, this radius is of the order of an interatomic spacing; in semiconductors it is much larger.

$$V(r) = \frac{Z_1 Z_2 e^2}{r} e^{-\lambda r} \tag{1.16}$$

This potential can be described by a dielectric function $\epsilon(q)$ invoking the concept of static screening [12]

$$\epsilon(q) = 1 + \frac{\lambda^2}{q^2} \tag{1.17}$$

A is the screening radius which decreases rapidly as $q$ increases. It is very difficult to make the electron distribution screen out potentials of short wavelength. The influence of a medium characterized by $\epsilon(q)$ on a potential V(r) is related to the Fourier transform U(q) as

$$V(r) \rightarrow U(q) = \frac{V(q)}{\epsilon(q)} \tag{1.18}$$

Thus *U(q)* can now be written as

$$U(q) = Z_1 Z_2 \frac{4\pi e^2}{\lambda^2 + q^2} \tag{1.19}$$

This is the potential for the interaction of a probe with a point charge. This indicates that the effective potential acting on the electrons is divided by a dielectric constant $\epsilon(q, \omega)$ which is a function of the wavelength and frequency of the applied perturl ation. Assuming this perturbation to be $static (\omega \rightarrow 0)$, $\epsilon(q)$ is now a function of q only. Equation (1.17) is an approximation for screening at short wavelengths. When $q \rightarrow 0$, A is related to the density of states at the Fermi level $N(E_F)$

$$\lambda^2 = 4\pi e^2 N(E_F) \tag{1.20}$$

Here $N(E_F) = \frac{3n}{2E_F}$, $E_F = \frac{\hbar^2 k_F^2}{2m}$ and $k_F = (3\pi^2 n)^{1/3}$, n being the electronic concentration of the host lattice given by the product of the number of outermost electrons and the atomic concentration. This gives

$$N(E_F) = \frac{3^{1/3} m n^{1/3}}{\hbar^2 \pi^{4/3}} = 0.358 \quad \text{states}/eV \text{ atom}.$$

Potential (1.16) decays very rapidly with increasing r, becoming invalid at separation greater than a few tenths of an angstrom. Beyond a few multiples of —, the external field is completely screened out almost entirely by the flow of electrons.

In a nutshell, we can say that a phonon of wave-vector $q$ sets up a potential due to the motion of the ions. The electrons move to screen this field. The ions therefore now interact with each other via this screened field which is inversely proportional to $\epsilon(q)$. Hence, the forces between the ions will be modified and the lattice frequency of this mode of vibration will depend on $\epsilon(q)$. The same effect is likely to be seen in other system of wave propagation in the solid, if they interact with the conduction electrons. The above calculation thus offers a general method for the investigation of the Fermi surface-although the detection of the effect may not be practically feasible.

### 1.2.2 Potential Around An Ionized Impurity In Solids

An impurity in an otherwise perfect single crystal causes dechanneling of energetic particles propagating along the major crystallographic directions [2]. Chylinski et al [8] have carried out a comparative study of $\alpha$-particle dechanneling by hydrogen and carbon interstitials in thin palladium foil; the results were based on the assumption that the interstitials act mainly by obstructing the channels and do not deform the neighbouring atomic planes by any significant amount. The extent and magnitude of the effects depend upon the strength of the potential presented by these impurities to the incoming channeled particles. This potential is complicated by two effects; first du to the atomic electrons of the impurity, which is determined by the charge state of the impurity, and second due to the electronic structure of the host material.

Considering now the interaction of a positively charged particle with a *crystal lattice*, the same equations hold good and the screening is provided by the conduction electrons of the host. And if this host lattice has interstitial impurities, then the screening becomes twofold; the atomic electrons of the impurity also contribute to the screening and the corresponding screening parameter $\lambda_a$ is given by

$$\lambda_a = \frac{0.8853 a_o}{(Z_I - Z_I^*)^{1/3}} \tag{1.21}$$

where $a_o$ = 0.0529 $nm$ (Bohr radius), $Z_I$ is the atomic number of the impurity and $Z_I^*$ the degree of ionization of the impurity atom. As stated earlier, the choice of Thomas-Fermi screening radius is not unique; for this interaction, $\lambda_a$ is the TF radius [12, 13]. Taking into account interaction between a positive probe (either $\alpha$ or $\pi^+$, $\mu^+$ or hydrogen atom) and a host lattice with partially ionized impurities! the electron gas of the host screens the interaction further. U(q) of equation (1.20) comes out to be

$$U(q) = Z_1 Z_I \frac{4\pi e^2}{\lambda_a{}^2 + q^2} \frac{q^2}{\lambda^2 + q^2} \tag{1.22}$$

which, in direct space is given by

$$V(r) = \left(\frac{1}{2\pi}\right)^3 \int\int\int \frac{4 Z_1 Z_I \pi e^2 q^2}{(\lambda_a{}^2 + q^2)(\lambda^2 + q^2)} e^{iqr} d^3q \tag{1.23}$$

Angular integration gives

$$V(r) = Z_1 Z_I \frac{2e^2}{\pi r} \int_{q=0}^{\infty} \frac{q^3 \sin qr}{(\lambda_a{}^2 + q^2)(\lambda^2 + q^2)} dq \tag{1.24}$$

Using [21]

$$I(m) = \int_0^{\infty} \frac{x \sin mx dx}{(a^2 + x^2)(b^2 + x^2)} = \frac{\pi}{2} \left[ \frac{e^{-mb} - e^{-ma}}{a^2 - b^2} \right].$$

and

$$\frac{d^2 I}{dm^2} \begin{pmatrix} a > 0, & b > 0 \\ m > 0 & a \neq b \end{pmatrix},$$

we obtain

$$V(r) = Z_1 Z_I \frac{e^2}{r} \left[ \frac{\lambda_a{}^2 e^{-\lambda_a r} - \lambda^2 e^{-\lambda r}}{\lambda_a{}^2 - \lambda^2} \right] \quad if \quad \lambda_a \neq \lambda \tag{1.25a}$$

and

$$V(r) = Z_1 Z_I \frac{e^2}{r} \left[ e^{-\lambda r} - \frac{\lambda r}{2} e^{-\lambda r} \right] \quad if \quad \lambda_a = \lambda \tag{1.256}$$

This double screened potential is due to Chylinski et al [8] and we have used this as a prelude to some of the calculations for ionized oxygen in tantalum crystal [18, 11]. In chapter 2 of the thesis, we have derived another screened potential in the long wavelength limit; this potential is then used to derive the dechanneling cross-section of a positive probe in a host with ionized point defects. Dechanneling cross-sections are modified for various charge states of impurity in different planar directions since the potential thus derived considers both the effect of both atomic electrons of the impurity and conduction electrons of the host lattice. It carries the signature of weakly decaying nature and the formulation highlights the role played by the atomic electrons of the impurity and the conduction electrons of the host lattice [23]. This model is expected to be applicable in various situations where long range electron-ion interactions affect the potentials due to heavy impurities seen by external probe particles in otherwise perfect crystals.

## 1.3 Applications of Channeling

Ion channeling is widely used to study the lattice location of impurities in crystalline materials, defect densities and also allows determination of the strain in epitaxial layered structures. Utilization of the ion channeling for characterizing synthetically modulated structures like semiconductor superlattices is another area of special interest. Strained Layer Superlattices **SLS** are layered structures of alternating composition of materials having a small mismatch ($\sim 0.1$ *to* 2.0%). This small lattice mismatch is accommodated by biaxial (compressive and tensile) strains in the plane of the layers and each layer acquires a perpendicular lattice constant due to strain accommodation [8]-[38]. The ability to tailor the energy bandgap in SLS's is one of the properties which is utilized in the manufacture of various devices like photodetectors and quantum well lasers. SLS's thus have wide ranging applications in many frontier areas of science and technology. Strain accommodation in SLS is limited by the thickness of the epilayer and beyond a critical thickness of layer, characteristic of the material grown, the system starts relaxing giving rise to misfit dislocations in the sample. Typical layer thicknesses are limited to a few hundred angstroms for lattice mismatches $\sim$ 1%. The presence of defects deteriorates the performance of these devices and thus it is important to characterize strain and strain-relief mechanisms in the structures and also the limits of strained-layer growth. Rutherford Backscattering Spectrometry (RBS/channeling) is one such technique by which one can determine the thickness, composition, defect densities and strain. For a fully commensurate structure, the magnitude of strain depends directly on the composition of the layer and the substrate. *RBS* analysis allows determination of layer composition, uniformity and thickness and can be applied readily to the superlattices. Ion channeling is a special case of RBS and is one of the sensitive characterization techniques which provides a measure of crystalline quality. $\chi_{min}$ which is the ratio of the backscattered particles when aligned (A) to a crystallographic axis to that in the random (R) condition (i.e., $\chi_{min} = Y_A/Y_R$) is a measure of the crystalline quality of the sample. A typical $\chi_{min}$ value of a very good crystalline sample will be around 2-3%. It also allows one to determine the strain in epitaxial layered structures. This is accomplished by carrying out angular scans along the off-normal axis using which, the strain in

the epilayers is evaluated. The difference between the dips on angular axis of these angular scans between epitaxial layers is a direct measure of the strain between the layers. Raman Spectroscopy also permits one to determine the strain quantitatively from the shift in the wavenumbers between commensurate and incommensurate layers. The longitudinal optic phonons in the $In_{0.1}Ga_{0.9}As$ layers exhibit two-mode behaviour, which helps in fitting the curve accordingly. In chapter 3 of the thesis we describe the growth and characterization of SLS by Ion Channeling, which is compared with XRD and Raman Spectroscopy.

## 1.4 Catastrophic Dechanneling Resonance

Another method of determination of strain in **SLS** by ion channeling is based on a resonance condition in which if the period of SLS structure matches with the average channeled-particle wavelength, there will be a rapid increase in dechanneling after a certain depth. This phenomenon is called *Catastrophic Dechanneling Resonance* **CDR** and occurs when the half wavelength $(\frac{\lambda}{2})$ of the oscillatory motion of the channeled ion matches with the path length per layer *(s)* of the $SLS$. This technique is attractive for strain analysis at, very low strains: it is the most sensitive of all the ion-channeling techniques for strain measurements. In contrast, axial channeling angular scan is the most versatile; each layer strain can be determined over a wide range of strain magnitudes and layer thickness for both single-strained layers and superlattices. $CDR$ dependence on various parameters like energy of the incident ion, incident angle, tilt angle etc. have been studied using Moliere potential on $In_{0.2}Ga_{0.8}As$ / $GaAs$ and $In_{0.1}Ga_{0.9}As/GaAs$ superlattices with $He^4$ as the probe along the (110) direction. In chapter 4 of the thesis, the CDR studies are be described in detail.

The present dissertation is thus organized as follows. In chapter 2, we derive the dechanneling cross-section of a positive probe in a host lattice with ionized point defects. Chapter 3 is application oriented and we discuss there the use of ion channeling for the strain measurement of Strained Layer Superlattices. The samples of SLS are grown at TIFR, Mumbai; the description of these samples has also been given in detail. The experiments of ion channeling have been carried

out at IoP, Bhubaneswar, IIT, Kanpur and Alabama A & M Univeristy, Alabama. Raman Spectroscopy and XRD have also been done and the results are compared with those obtained from channeling studies. In chapter 4, we discuss one more less commonly known technique namely the Catastrophic Dechanneling Resonance for strain analysis. Finally in chapter 5, we conclude the work and also discuss the future direction of work.

# References


[1] J. Lindhard, Kgl. Danske, Vindenskab, Selskab, Mat. Fys. Medd., 34, No. 14 (1965).

[2] A. P. Pathak, Rad. Eff., 61, 1, (1982).

[3] A. P. Pathak, J. Phys., C8, L439, (1975).

[4] "Channeling, Theory Observation and Applications", Ed. D. V. Morgan, (Wiley, London), 1973.

[5] D. S. Gemmel, Rev. Mod. Phys. 46, 129 (1974).

[6] G. Moliere, Z. Naturforschung, A2, 133 (1974).

[7] D.J. O'Connor and J.P. Biersack, Nucl. Inst. Meth, **B15,** 14 (1986).

[8] V. Harikumar and A.P. Pathak, Phys. Stat. Sol. (b), **177,** 269 (1993).

[9] A. Seeger, Proc. Yamada Conf. **VII,** Muon Spin Rotation and Associated Problems, Shimoda, Eds. T. Yamazaki, K. Nagamine, Hyperfine Interact. **17-19** (1985) p. 75-102.

[10] M. T. Robinson, Phys. Rev **179,** 327 (1969).

[11] M. Born and L. Mayer, Z. Physik, **75,** 1 (1975).

[12] J. Mory and Y. Quere, Rad. Eff., **13,** 57, (1972).

[13] Y. Quere, Phys. Rev. B H, 1818 (1975).

[14] J. Rosner et al, Phys. Rev **B18,** 1066 (1978).

[15] A. P. Pathak, Rad. Eff., **301,** 193, (1976).

[16] A. P. Pathak and L. T. Chaddertcn, Phys. Stat. Sol., (1981).

[17] Z. Chylinski, A. Dunlop, J. Mory and A.P. Pathak, Nucl. Ins. Methods. B **71,** 55 (1992).

[18] A. M. Siddiqui, V. Harikumar and A. P. Pathak, Phys. Stat. Sol. (b) **185,77** (1994).

[19] J.M. Ziman, Principles of Theory of Solids, Chap. 5, Cambridge University Press, (1972).

[20] I. M. Torreas, Interatomic Potentials, Academic Press, New York 22 (1972).

[21] I.S. Gradshteyn and I.M. Ryzhik, Tables of Integrals, Series and Products Academic Press, New York 1980, Formulae 3.728.2, 3.729.2.

22] Azher M. Siddiqui, V. Harikumar, L. N. S. Prakash Goteti and A. P. Pathak, Modern Physics-Letters (B), Vol 10, No. 16, 745, 1996.

[23] Azher M. Siddiqui, A. Kiran and A. P. Pathak, Modern Physics Letters (B), **11,** 1231, (1997).

[24] G. C. Osbourn, J. Appl. Phys., 53, 1586, 1982.

[25] S. T. Picraux, B. L. Doyle and J. Y. Tsao in Strained-layer Superlattices: Materials Science and Technology, Vol 33 "Semiconductors and Semimetals", ed: Thomas P Pearsall, Academic Press, New York (1991).

[26] S. T. Picraux, L. R. Dawson, G. C. Osbourn and W. K. Chu, Appl. Phys. Lett, 43, 930, 1983.

[27] S. T. Picraux, L. R. Dawson, G. C. Osbourn, R. M. Biefeld and W. K. Chu, Appl. Phys. Lett, 42, 1020, 1983.

[28] S. T. Picraux, W. K. Chu, W. R. Allen and J. A. Ellison, Nucl. Ins. and Meth, **B15,** 306, 1986.

[29] S. T. Picraux, J. Y. Tsao and D. K. Brice, Nucl. Ins. and Meth, **B19/20,** 21, 1987.

## Chapter 2

# DECHANNELING BY POINT DEFECTS

Practically all the crystals will have one defect or the other. Even in the so called perfect crystals some amount of defects are always present, however small. The most common defects are vacancies, self-interstitials, foreign atoms, stacking faults, grain boundaries, dislocations, voids, gas bubbles etc. A particle propagating through a solid can see the presence of the defects through the effects these defects will produce in the solids; either the particle path is directly obstructed or a distortion is produced in the crystal (or both). When the projectile hits the defect directly or is scattered in the potential field of the defects thereby modifying the trajectory (e.g. stacking faults, interstitial atoms, grain or twin boundaries), the effects are said to be *obstruction dechanneling*. If the defects give rise to distortion in a certain region of the crystal disturbing the regularity of the material in that region, the effects are known to be *distortion dechanneling*. The important example here is that of dislocations. Some defects such as Guinier-Preston zones, voids, gas bubbles and antiphase boundaries give rise to obstruction as well as distortion effects and a composite dechanneling is to be considered for these defects. The point defects introduced into a crystal produce obstruction dechanneling due to direct scattering of probe particles. Heavy impurity in a host lattice may result in negligibly small amount of distortion dechanneling. This fact is used to find the lattice locations of the implanted species in the crystals with the help of channeling technique. If the impurity is situated on a regular lattice site (substitutional), it will have no effect on the channeling spectrum. When it is located at an interstitial position, it may obstruct the path of the channeled particles along certain directions and may be shadowed by the atomic strings along certain other directions (Fig, 2,1). The trajectory of a particle getting channeled in a crystal lattice will be determined by the strength of the potential presented by the target atoms to the incident channeled particle. It would be interesting thus to consider the probability that

the projectile gets scattered in a crystal with impurities (interstitial or substitutional). Jousset et al [l]-[3] have studied the dechanneling of $\alpha$-particles by hydrogen and carbon interstitial in palladium crystals for the planar case, assuming that the dechanneling is caused by Rutherford scattering of $\alpha$-particles from the impurities.

The possibility of pions and muons being used as probe particles for defects studies in materials research has been looked into for the past thirty years. In the sequence of the hydrogen isotopes extending from positron ($e^+$) to triton, the positive pion ($\pi^+$) stands closest to muon. As light isotopes of hydrogen, $\pi^+$ and $\mu^+$ can tell us the details about the crystallographic sites preferred by particles of unit electrical charge. They can also be used as probe atoms that may get trapped at crystal defects in much the same way as positrons. The application of $\pi^+$ in defect studies is closely related to the diffusion studies of the $\pi^+$. With the mass lying between those of the muon and the proton, the $\pi^+$ will help us to understand quantum mechanical processes in the diffusion of light positive particles [4, 5]. It was as early as 1957 that the use of the positive muon as a probe of the condensed matter was suggested. The work of Garwin et al [6] along with other pioneering works [7] were the turning points of the invention of $\mu$SR technique. We will not discuss here the essentials of $\mu$SR techniques; but the application of muon (and analogously pion) channeling cannot be overlooked. Muons have intrinsic angular momentum (spin $\frac{1}{2}$) whereas pions are spinless particles and hence the probability of muon emission is *isotropic* in the pion rest system.

$$\pi^+ \longrightarrow \mu^+ + \nu_\mu$$

Since this is a two-particle decay, the muons resulting from it are *monoenergetic* and their kinetic energy in the pion rest system is given by

$$E_{kin} = \frac{(m_\pi - m_\mu)^2 c^2}{2m_\pi} = 4.12 MeV,$$

their momentum by

$$p = \frac{m_\pi^2 - m_\mu^2}{2m_\pi} c = 29.73 MeV/c,$$

and their velocity by

$$v = \frac{m_\pi^2 - m_\mu^2}{m_\pi^2 + m_\mu^2} c = 0.27c$$

*The* mass ratio of pion and muon is

$$m_\pi/m_\mu = 1.32$$

Wo have discussed till now, the similarities between pions and muons and therefore their uses as solid state probes. On the other hand, these particles show marked differences in some aspects and thus provide us access to different regimes of solid state parameters. The most significant difference is the lifetime of these particles. Pion has a lifetime of $2.6\times10^{-8}$ sec whereas union's lifetime is $2.2\times10^{-6}$ sec. Consequently, the observable range of rates of kinetic processes e.g. of thermalisation, diffusion, trapping, and detrapping at defects, atom formation or reactions with foreign atoms, are shifted with respect to each other by about a factor of $10^2$.

Being treated as light hydrogen isotopes, the mass difference between pions and muons is crucial. It enables us to supplement the isotope effects of lattice locations, diffusivities, reaction rates. In addition to these, pion experiments do not require special properties of the material e.g nuclear magnetic moments or high scattering cross-sections for neutrons: only crystals of good quality (high perfection) would suffice. We can thus state that it is possible to perform experiments on short-lived elementary particles of the same charge as hydrogen. Using positive pions we can partly bridge the gap between the positron, muon and the proton mass. It is much lighter than the hydrogen nuclides and thus the quantum effects are more profound. At the same time it is heavier compared to $e^+$ so that the theoretical treatment of its behaviour is similar to that of protons, deuterons, tritons and positive muons.

In times shorter than their lifetime, implanted pions are slowed down; the electrostatic repulsion of the nuclei tends to localize the $\pi^+$ in interstitial sites. Trapping at defects leads to different $\pi^+$ sites in the crystal [5]. To get information on these sites, we may use muons as signals obtained from pion decay as shown above. Pion sites in a channel lead to an increase of the muon intensity profile (channeling) whereas the pions located in the chain of host atoms lead to a decrease in it (blocking) (figure 2.2).

## Two - dimensional model

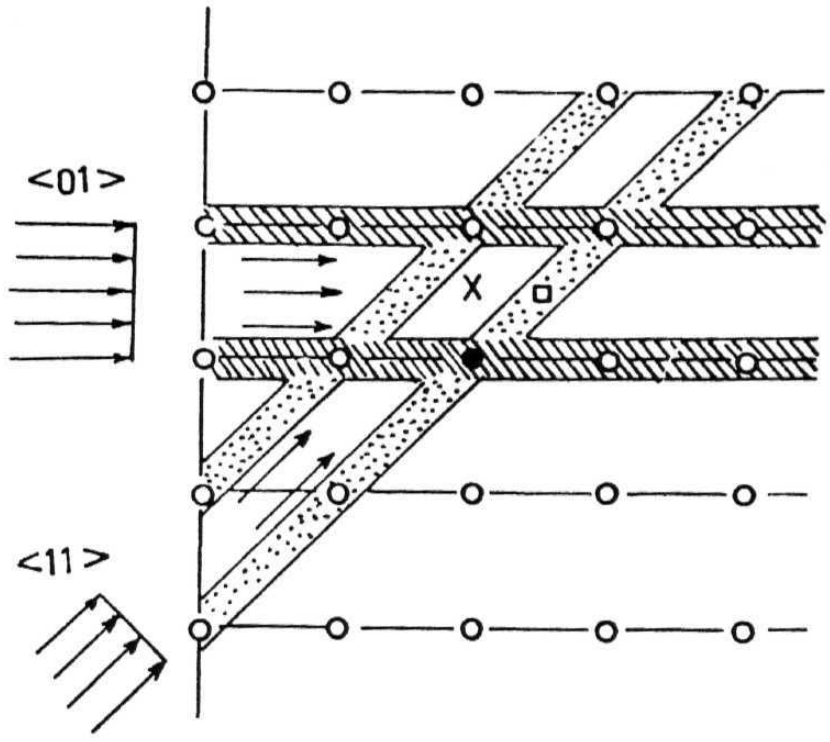


| | Directional effect? | | |
|---|---|---|---|
| | ● | x | □ |
| <01> | Yes | 50 % | No |
| <11> | Yes | No | Yes |

Fig 2.1: A two dimensional model illustrating how the channeling effect may be used to locate foreign atoms in a crystal [2].

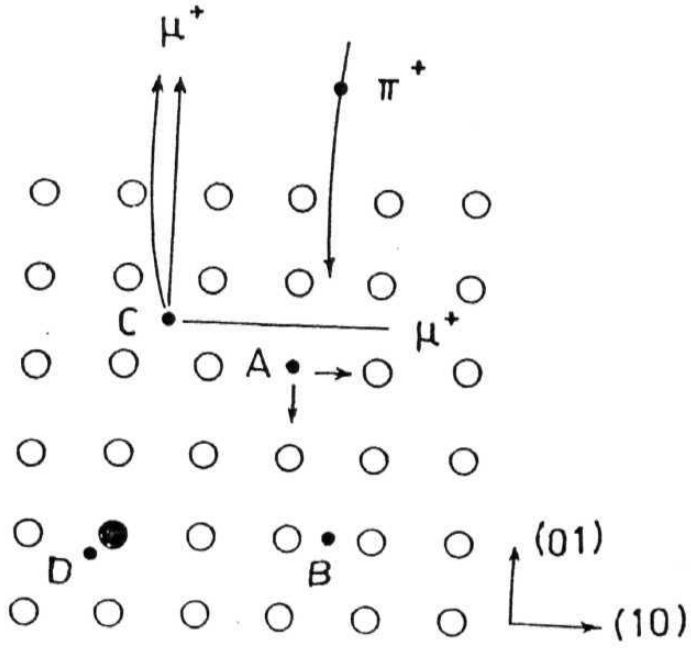


**Fig 2.2**: Different $\mu^+$ sites in a two-dimensional lattice. The decay muons may leave the crystal with increased probability from positions *B*, *C*, *D* (channeling). The muons are blocked from position A and B in <1 1> direction (blocking). Position 1) is a trapped site (not in the channel centre) [4,5].

The interaction between an incident charged particle and a host lattice is described by a screened Coulomb potential which falls off exponentially. Chylinski et al [8] have calculated the dechanneling cross-section using a double-screened potential for α-particles in palladium with hydrogen impurity. The same model was again used [9] to evaluate the dechanneling cross-section and corresponding scattering cross-sections of muons and pions propagating in tantalum crystal with oxygen impurity. Since muons and pions are considered as the light isotopes of hydrogen, the study of pion decay and muon channeling can yield more intuition to the hydrogen studies. The effects of screening are of fundamental importance for their consequences on, and in determining the behaviour of any charge carrying disturbance in a metal.

## 2.1 Scattering Cross-section of $\pi^+$/ $\mu^+$ by Defects (O in Ta)

In order to estimate the probability that a channeled particle (muon) will get scattered inside the crystal (Ta) with impurities (O), we proceed as follows. A steady beam of $\pi^+$ is bombarded on the target (Ta) for a long time such that the incident flux 'f' (the number of pions crossing unit area taken normal to the beam direction per unit time) is independent of time. The impurities present in the target crystal modify the interaction potential between the incident pions and the target atoms. There are 73 protons in the tantalum nucleus and a positive pion getting channeled inside it possesses a repulsive potential. Because of the presence of oxygen which is a lighter nuclide, the potential as experienced by the $\pi^+$ near these defects is effectively less repulsive; in other words, in the background of highly repulsive interaction with pure Ta, $\pi^+$ at the impurity sites experiences a relatively attractive potential. The probability that these pions will get trapped at these impurity sites or will be diffused can be estimated applying the scattering theory, in particular the Born approximation. The same approach is also used in the case of possible muons scattering after the decay of pions.

The differential scattering cross-section, in Born Approximation, is given by

$$\frac{d\sigma}{d\Omega} = |f(\theta, \phi)|^2$$

where $f(\theta, \phi)$ is given as

$$f(\theta,\phi) = -\frac{1}{K} Im \int_o^\infty \vec{r} e^{-i\vec{K}.\vec{r}} U(\vec{r}) d\vec{r} \tag{2.27}$$

where $K = |\vec{K}| = 2k \sin\frac{\theta}{2}$, $k^2 = 2mE/\hbar^2$ and $U(\vec{r}) = (2m/\hbar^2)V(r)$ and $V(r)$ is the double-screened potential [8, 9]

$$\begin{aligned} f(\theta) &= -\frac{2mZ_I e^2}{K\hbar^2(\lambda_a^2 - \lambda^2)} Im \int_o^\infty e^{i\vec{K}.\vec{r}} (\lambda_a^2 e^{-\lambda_a r} - \lambda^2 e^{-\lambda r}) dr \\ &= -\frac{2mZ_I e^2 K^2}{\hbar^2(\lambda_a^2 + K^2)(\lambda^2 + K^2)} \end{aligned} \tag{2.28}$$

Therefore the total scattering cross-section is

$$\begin{aligned} \sigma(\theta) &= 2\pi \int_o^\pi |f(\theta)|^2 \sin\theta d\theta \\ &= \frac{256\pi Z_I^2 m^2 e^4 k^4}{\hbar^4} \int_o^\pi \frac{\sin^5\frac{\theta}{2}\cos\frac{\theta}{2} d\theta}{(\lambda_a^2 + 4k^2\sin\frac{\theta}{2})^2(\lambda^2 + 4k^2\sin^2\frac{\theta}{2})^2} \end{aligned} \tag{2.29}$$

Let $\sin\frac{\theta}{2} = x$; $\frac{1}{2}\cos\frac{\theta}{2} d\theta = dx$;

$\theta = 0, \quad x = 0 \qquad\qquad \theta = \pi, \quad x = 1.$

Therefore

$$\sigma_t = \frac{512\pi Z_I^2 m^2 e^4 k^4}{\hbar^4} \int_o^1 \frac{x^5 dx}{(\lambda_a^2 + 4k^2x^2)^2(\lambda^2 + 4k^2x^2)^2} \tag{2.30}$$

which on integration comes out to be [10, 11]

$$\sigma_t = \frac{32\pi Z_I^2 m^2 e^4}{\hbar^4(\lambda^2 - \lambda_a^2)^2} \left[ \left( \frac{\lambda^2}{2(\lambda^2 + 4k^2)} + \frac{\lambda_a^2}{2(\lambda_a^2 + 4k^2)} \right) + \frac{\lambda^2\lambda_a^2}{4k^2(\lambda^2 - \lambda_a^2)} ln \left( \frac{\lambda_a^2(\lambda^2 + 4k^2)}{\lambda^2(\lambda_a^2 + 4k^2)} \right) \right] \tag{2.31}$$

One can infer from this formulation that as the velocity of pions increases, the scattering cross-section decreases, which implies that the probability of pions getting trapped in crvstal increases. Same trend in muons shows the greater dechanneling probabilty of muons at lower energies.

## 2.2 The Dielectric Function

The double-screened potential, as described in chapter (1), around a partially ionized impurity can be written as [8, 9]

$$V(r) = Z_I \frac{e^2}{r}\left[\frac{\lambda_a^2 e^{-\lambda_a r} - \lambda^2 e^{-\lambda r}}{\lambda_a^2 - \lambda^2}\right] \tag{2.32}$$

$Z_I$ here is the atomic number of the probe particle and since $Z_\mu - Z_\pi = 1$, it is omitted in the above equation; $\lambda_a$ is the Thomas-Fermi screening radius given by [12, 13]

$$\frac{1}{\lambda_a} = \frac{0.8853 a_o}{(Z_I - Z_I^*)^{1/3}} \tag{2.33}$$

where $a_o$ is the Bohr radius, $Z_I$ is the atomic number of the impurity, $Z_I^*$ is the degree of ionization of the impurity atom. A in eq. (1) is the screening parameter which is associated with the screening of the electron gas of host lattice and can be related to the density of states at Fermi level $N(E_F)$ by the equation

$$\lambda^2 = 4\pi e^2 N(E_F) \tag{2.34}$$

with $N(E_F) = 3n/2E_F$, $E_F = \hbar^2 k_F^2/2m$ and $k_F = (3\pi^2 n)^{1/3}$

where $n$ is the concentration of conduction electrons in the host lattice (Ta), given by the product of the number of outermost conduction electroas in each atom and the atomic concentration. The interaction between a positive probe and a host lattice with ionized point defects is described by the static screening concept connected to a dielectric function $\epsilon(q)$ [12, 14]. The detailed $q$ dependence of the static dielectric function is given by [12]

$$\epsilon(q) = 1 + \frac{6\pi e^2 n}{q^2 E_F}\left[\frac{1}{2} + \frac{4k_F^2 - q^2}{8k_F q} ln\left|\frac{2k_F + q}{2k_F - q}\right|\right] \tag{2.35}$$

The effective screening length $1/\lambda$ tends to increase as $q$ increases. Equation (5) has a singularity at $q = 2k_F$ and is not analytic at that point. As a result of this singularity, the potential, instead of being a smooth exponential function, contains well known Friedel oscillations of wave-number $2k_F$. Assume $X = \frac{q}{2k_F}$. Expanding the log terms in the parenthesis, we get

$$\epsilon(q,0) = 1 + \frac{6\pi e^2 n}{q^2 E_F}\left[\frac{1}{2} + \frac{1-X^2}{2}\left(1 + \frac{X^2}{3} + \frac{X^4}{5} + .....\right)\right], \tag{2.36}$$

which gives

$$\epsilon(q) = \frac{q^2(1-\gamma^2) + \lambda^2 - \beta^2 q^4}{q^2}, \tag{2.37}$$

$$where \quad \beta^2 = 2me^2/115\hbar^2\pi k_F^3, \qquad \gamma^2 = me^2/3\hbar^2\pi k_F \tag{2.38}$$

The Thomas-Fermi model [12, 14] defines the dielectric constant $\epsilon(q)$ which is wave vector dependent as

$$\epsilon(q) = 1 + \frac{\lambda^2}{q^2} \tag{2.39}$$

We can see that $\epsilon(q)$ of this equation is small $q$ limit of equation(2.4).

## 2.3 Screened Potential of a Positive Probe in a Host Lattice with Ionized Point Defects

Following the formulation of Chylinski et al [8, 9], we write down the potential between an impurity ( *atomic number* $Z_I$ ) and the probe particle as

$$V = \frac{Z_1 Z_I e^2}{r} e^{-\lambda_a r} \tag{2.40}$$

where

$$\frac{1}{\lambda_a} = \frac{0.8853 a_0}{(Z_I - Z_I^*)^{\frac{1}{3}}}; \quad a_0 = 0.0529\ nm \quad (Bohr\ \ radius). \tag{2.41}$$

The Coulomb potential between a target particle $Z_2$ and a probe $Z_1$ in the direct and Fourier space can be written as [9]

$$V(r) = \frac{Z_1 Z_2 e^2}{r} \leftrightarrow V(q) = Z_1 Z_2 4\pi \frac{e^2}{q^2} \tag{2.42}$$

It is here that we invoke the dielectric function due to electron gas derived in the previous section. The double screened potential for such a system of interacting particles can now be written as

$$U(q) = Z_1 Z_2 \frac{4\pi e^2}{\lambda_a^2 + q^2} \frac{q^2}{\lambda^2 + q^2} \tag{2.43}$$

When $q$ becomes comparable to $2k_F$, there is considerably more structure to $\epsilon(q)$ which is not analytic at $q = 2k_F$. The potential then, as predicted by Lindhard [14], at large distances goes as

$$\phi(r) \sim \frac{1}{r^3}\cos(2k_F r) \tag{2.44}$$

Substituting the value of $\epsilon(q)$ from equation(2.6) and noting that

$$U(q) = \frac{V(q)}{\epsilon(q)}$$

$$U(q) = \frac{4\pi Z_1 Z_2 e^2}{(q^2(1-\gamma^2) + \lambda^2 - \beta^2 q^4)(\lambda_a^2 + q^2)}, \tag{2.45}$$

which after integration comes out to be

$$U(r) = \frac{Z_1 Z_2 e^2}{r}\left[\frac{1}{\beta^2}\left(\frac{x^2\cos xr}{z(x^2+\lambda_a^2)} - \frac{y^2 e^{-yr}}{2z(\lambda_a^2 - y^2)} + \frac{\lambda_a^2 e^{-\lambda_a r}}{(\lambda_a^2 + x^2)(\lambda_a^2 - y^2)}\right)\right], \tag{2.46}$$

where

$$a = \frac{(1-\gamma^2)}{2\beta^2}, \qquad b = \frac{\lambda^2}{\beta^2}, \qquad z = (a^2+b)^{\frac{1}{2}}, \tag{2.47}$$

$$x = (z+a)^{\frac{1}{2}}, \qquad y = (z-a)^{\frac{1}{2}} \tag{2.48}$$

The weakly decaying nature of this double screened potential shows its signature in the potential given by the above equation(2.15) which is otherwise not observed elsewhere [14]. It is also evident from the above equation that the electrons screen out the field of external charge and the characteristic distance beyond which the field is effectively screened out is —• In other words, the electron gas distributes itself in the presence of external charge distribution so as to shield or screen the fields produced by that distribution. The figures (2.3 to 2.6) show the variation of the potential thus derived for carbon and hydrogen impurities in various states of ionization [7]. We expect this model to be applicable in various situations where long range electron-ion interactions affect the potentials due to heavy impurities seen by external probe particles in otherwise perfect crystals.

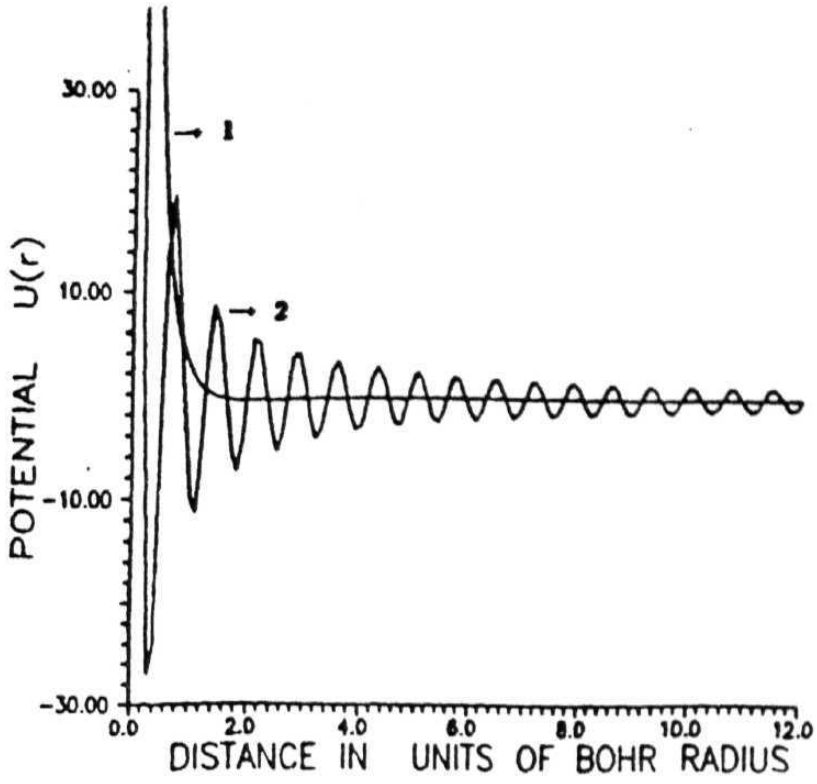


Fig 2.3: Variation of Double Screened Potential for (1) small and (2) large values of $q$ as a function of distance for singly ionized carbon.

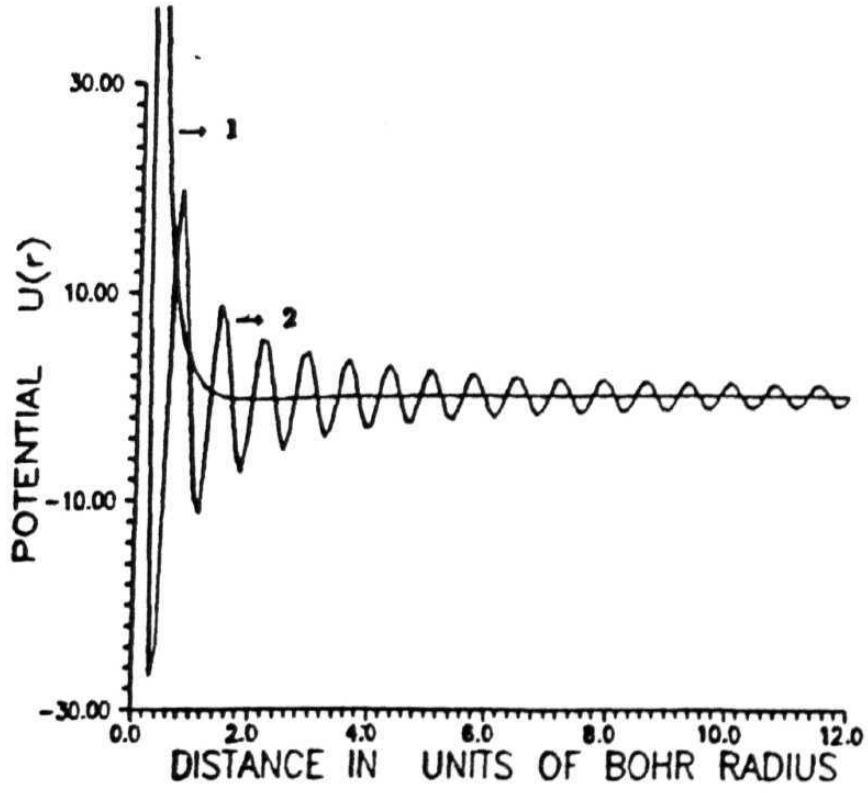


Fig 2.4: Variation of Double Screened Potential for (1) small and (2) large values of $q$ as a function of distance for doubly ionized carbon.

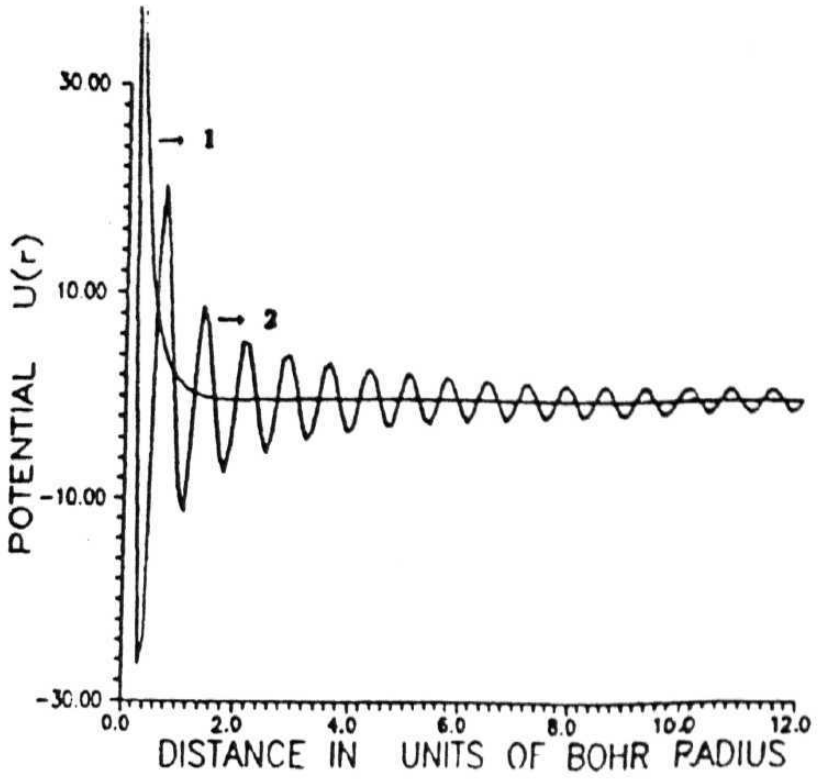


Fig 2.5: Variation of Double Screened Potential for (1) small and (2) large values of $q$ as a function of distance for triply ionized carbon.

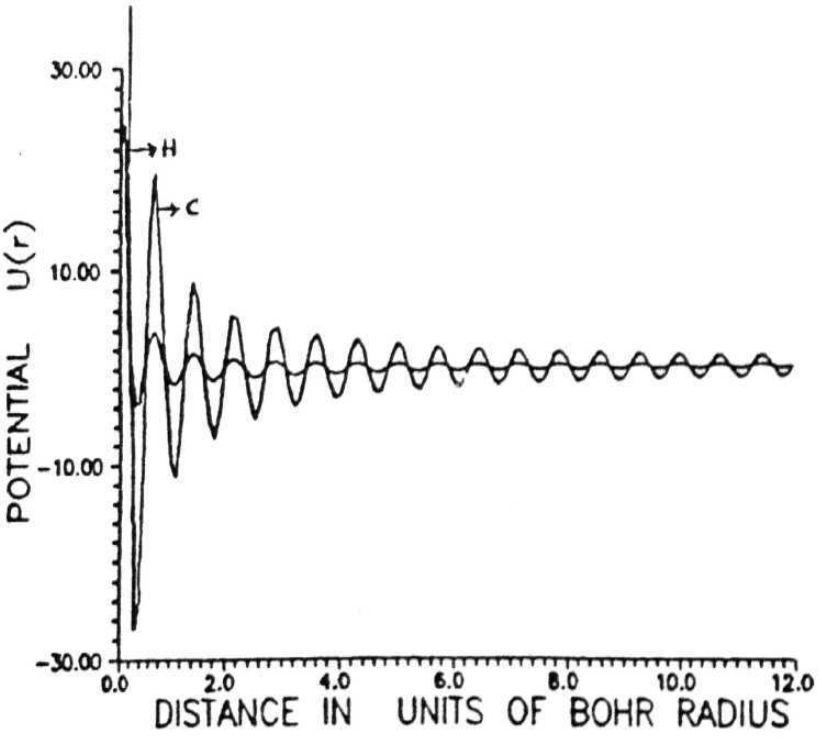


Fig 2.6: Variation of Double Screened Potential as a function of distance for singly ionized Carbon and Hydrogen.

## 2.4 Dechanneling Cross-section of Energetic Particles by Ionized Point Defects

When a charged particle is incident on a crystal, electrons are readjusted and there will he changes in the charge state of the incoming probe particle. The[1] interaction between atomic electrons of the target and the probe is in general not taken into account. One talks about the interaction of the target and the probe with conduction electrons of target providing the screening. When we consider the effects of atomic electrons of impurity along with conduction electrons of host lattice, there is an increase in screening beyond the distance $1/\lambda_a$. The impurities present in the target crystal modify the interaction potential between the probe particles and the target atoms 11]. The electrons around the impurity are not simply heaped up but haloes of electrons will be distributed around the impurity and correspondingly the potential function will also have similar variations as shown in the figures. The planar potential between a channeled particle (in our case a $\pi^+$ or a $\mu^+$) and the two planes between which it moves was given by Lindhard [1]; in the hyperbolic approximation it can be written as

$$V(x) = \frac{AY}{Y^2 - x^2} \tag{2.49}$$

where

$$A = 6\pi Z_{Ta} e^2 N_p a_T^2 \quad , Y = d + a_T/2$$

and

$$a_{TF} = \frac{0.8853 a_o}{(Z_\mu^{2/3} + (Z_2^{2/3})^{1/3}}$$

$N_p$ is the atomic density of the channeling planes ($= Nd_p$, $d_p$ is the interplanar distance). The critical angle for channeling is defined by

$$E\psi_c^2 + V(x = 0) = V(x_c) \tag{2.50}$$

Substituting the value of V(x) from equation (2.18), the critical angle can now be written as

$$\psi_c^2 = \frac{Ax_c^2}{Y(Y^2 - x_c^2)} \frac{1}{E} \tag{2.51}$$

Following the formulation of Chylinski et al [8], the dechanneling cross-section for the potential {equation (2.15)} [8, 9] can be written as

$$\sigma(E) = KE^{-1/2}\left[\frac{1}{\beta^2}\left(\frac{\lambda_a}{(\lambda_a^2 + x^2)(\lambda_a^2 - y^2)} - \frac{y}{2z(\lambda_a^2 - y^2)}\right)\right]. \tag{2.52}$$

where

$$K = \frac{Z_\mu Z_1 \pi e^2}{x_c}\sqrt{\frac{Y(Y^2 - x_c^2)}{A}},$$

and

$$x_c = \left(\frac{d_p}{2}\right) - a_T$$

Using the parameters listed in tables (1) and (2), we calculated the dechanneling cross-section of $\alpha-$particles by carbon and hydrogen impurity atoms in palladium crystal which are shown in table (3). We have also evaluated the dechanneling cross-section of a 4.12 MeV $\mu^+$ by oxygen impurity atoms in Ta using equation (2.18), which is shown in table (4). The results arc[1] compared with the work of Chylinski et al [8]. Our results match with their experimental values in the case of carbon impurity.

**Table 1:**

The values of the parameters used for calculating dechanneling cross-section of a 4.8 MeV $\alpha$ by carbon and hydrogen impurities in Pd

| Planar direction | Atomic conc. (**N**) $10^{21} cm^{-3}$ | Interplanar distance ($d_p$) ($10^{-1}$nm) | $x_c$ ($10^{-1}$nm) | $Y$ ($10^{-1}$nm) | $A$ (eV nm) | $K$ ($\mathrm{eV}^{1/2}$ nm) |
|---|---|---|---|---|---|---|
| {100} | 68.0 | 3.892 | 1.822654 | 2.007673 | 10.05474 | 3.54296 |
| {111} | 68.0 | 2.246 | 0.999654 | 1.184673 | 5.80240 | 4.93282 |

| $\lambda$ ($10^{-1}\mathrm{nm}^{-1}$) | $\beta$ ($10^{-1}$nm) | $z$ ($10^{2}\mathrm{nm}^{-2}$) | $x$ ($10^{-1}$ nm) | $y$ ($10^{-1}$ nm) |
|---|---|---|---|---|
| 2.44949 | 0.036160 | 350.6714 | 26.3579 | 2.5700 |

**Table 2:**

The values of the parameters used for calculating dechanneling cross-section of a 4.12 MeV $\mu$ by oxygen impurity in Ta.

| Planar direction | Atomic conc. (**N**) $10^{21} cm^{-3}$ | Interplanar distance ($d_p$) ($10^{-1}$nm) | $x_c$ ($10^{-1}$nm) | $Y$ ($10^{-1}$nm) | $A$ (eV nm) | $K$ ($\mathrm{eV}^{1/2}$ nm) |
|---|---|---|---|---|---|---|
| {100} | 55.0 | 1.65 | 0.71593 | 0.879509 | 2.13704 | 5.23774 |
| {111} | 55.0 | 0.952628 | 0.367297 | 0.530822 | 1.23382 | 7.83221 |

| $\lambda$ ($10^{-1}\ \mathrm{nm}^{-1}$) | $\beta$ ($10^{-1}$nm) | $z$ ($10^{-2}\mathrm{nm}^{-2}$) | $x$ ($10^{-1}$ nm) | $y$ ($10^{-1}$ nm) |
|---|---|---|---|---|
| 1.732051 | 1.02276 | 41.8013 | 8.9453 | 1.8932 |

**Table 3:**

The dechanneling cross-section ($\sigma$) of a 4.8 MeV $\alpha$ by carbon and hydrogen impurities in palladium crystal.

For Carbon Impurity

| Planar direction | Experimental $\sigma$ $(10^{-5}nm^2)$ Ref.[8] $Z_1^* \leq 2$ | $\sigma$ $(10^{-5}nm^2)$ Finite q | | | $\sigma$ $(10^{-5}nm^2)$ Small q [1] | |
|---|---|---|---|---|---|---|
| | | Singly ionized | Doubly ionized | Triply ionized | Singly ionized | Doubly ionized |
| {100} | - | 2.743 | 2.874 | 3.043 | - | - |
| {111} | 3.6 to 5.6 | 3.819 | 4.001 | 4.237 | 6.766 | 6.978 |

| Planar direction | $\lambda_a$ $(10nm^{-1})$ | | |
|---|---|---|---|
| | Singly ionized | Doubly ionized | Triply ionized |
| {100} | 3.650028 | 3.388389 | 3.078558 |
| {111} | 3.650028 | 3.388389 | 3.078558 |

For Hydrogen Impurity

| Planar direction | $\lambda_a$ $(10nm^{-1})$ | | $\sigma$ $(10^{-5}nm^2)$Finite q | | $\sigma$ $(10^{-5}nm^2)$Small q [1] | |
|---|---|---|---|---|---|---|
| | No ionization | Single ionization | No ionization | Single ionization | No ionization | Single ionization |
| {100} | 2.134561 | 0.00 | 6.15 | 1.143 | - | - |
| {111} | 2.134561 | 0.00 | 0.8571 | 1.591 | 1.019 | 1.304 |

**Table 4:**

The dechanneling cross-section ($\sigma$) of a 4.12 MeV $\mu^+$ by oxygen impurity atoms in Ta

| Planar direction | $\lambda_a$ $(10nm^{-1})$ | | | $\sigma$ $(10^{-5}nm^2)$ | | |
|---|---|---|---|---|---|---|
| | Singly ionized | Doubly ionized | Triply ionized | Singly ionized | Doubly ionized | Triply ionized |
| {100} | 4.083242 | 3.878732 | 3.650028 | 3.692 | 3.909 | 4.170 |
| {111} | 4.083242 | 3.878732 | 3.650028 | 5.521 | 5.846 | 6.236 |

# References


[1] J. C. Jousset, J. Mory and J. J. Quillico, J. Phys. (Letters), 35, L229 (1974).

[2] J. J. Quillico and J. C. Jousset, Phys. Rev. **B11**, 1791 (1975).

[3] A. Dunlop, L. Lorenalli and J. C. Jousset Phys. Stat. Sol. (a) 49, 643 (1978).

[4] A. Seeger, Proc. Yamada Conf. VII, Muon Spin Rotation and Associated Problems, Shimoda, Eds. T. Yamazaki, K. Nagamine, Hyperfine Interact. **17-19** (1985) p. 75-102.

[5] K. Maier, Proc. Yamada Conf. VII, Muon Spin Rotation and Associated Problems, Shimoda, Eds. T. Yamazaki, K. Nagamine, Hyperfine Interact. **17-19** (1985) pg. 3-15; Discussions same Volume pg. 14-15.

[6] R.L. Garwin, L.M. Lederman and M. Weinrich, Phys. Rev. **105,** 1415 (1957).

[7] G.W. Forin and C.J. Mullin, Phys. Rev. **108,** 477 (1957).

[8] Z. Chylinski, A. Dunlop, J. Mory and A.P. Pathak, Nucl. Ins. Methods. B **71,** 55 (1992).

[9] A. M. Siddiqui, V. Harikumar and A. P. Pathak, Phys. Stat. Sol. (b) 185,77 (1994).

10] I.S. Gradshteyn and I.M. Ryzhik, Tables of Integrals, Series and Products Academic Press, New York 1980, Formulae 3.728.2, 3.729.2, 2.112.2 and 2.113.3.

[11] Azher M. Siddiqui, V. Harikumar, L. N. S. Prakash Goteti and A. P. Pathak, Modern Physics Letters (B), Vol 10, No. 16, 745, 1996.

[12] J. M. Ziman, Principles of Theory of Solids, Chap. 5, Cambridge University Press, (1972).

[13] I. M. Torrens, Interatomic Potentials, Academic Press, New York 22 (1972).

[14] Neil W. Ashcroft and N. David Mermin, Solid State Physics, Chap. 17, (1976).

[15] Azher M. Siddiqui, A. Kiran and Anand P. Pathak, Modern Physics Letters (B), 11, 1231, 1996.

[16] J. Lindhard, Kgl. Danske, Vindenskab, Selskab, Mat. Fys. Medd., 34, No. 14 (1965).

Chapter 3

# CHARACTERIZATION OF STRAINED-LAYER SUPERLATTICES

The tailoring of bandstructures of semiconductor devices to enhance their electronic and optical properties has become, over the past two decades, one of the major driving forces in semiconductor physics. The three major phenomena used for band tailoring are; (i)alloying of two or more semiconductors, (ii)use of heterostructures to cause quantum confinement of formation of *superlattice* and (iii)use of built-in strain via lattice mismatch epitaxy. Alloying of two materials is one of the oldest techniques to modify and improve the properties of materials. In semiconductors, this is motivated by the sole objective to alter the bandgap of the material to a pre-chosen value; and also to create a material with proper lattice constant to match or mismatch with an available substrate. There are other potential advantages also like improved carrier transport, fabrication of heterostructures etc.

When two semiconductors A and B are mixed via an appropriate growth technique, then the information on the crystalline structure of the lattice and the ordering of the atoms (arrangement of A and B atoms in the alloy) are to be considered very carefully. While in most semiconductors the two or more components of the alloy have the same crystal structure, mixing a diamond lattice material (e.g Ge) with a zinc-blende material (e.g. GaAs) can lead to some very interesting structures [1]. Figure 3.1 shows the changes in the bandgaps of various material combinations; the solid lines represent direct bandgap regions and the dotted lines the indirect gap regions. The ordering of the atoms in the alloy is also extremely important since the band-structure depends strongly on ordering. The arrangements of the atoms A and B in the alloy may have the following cases:

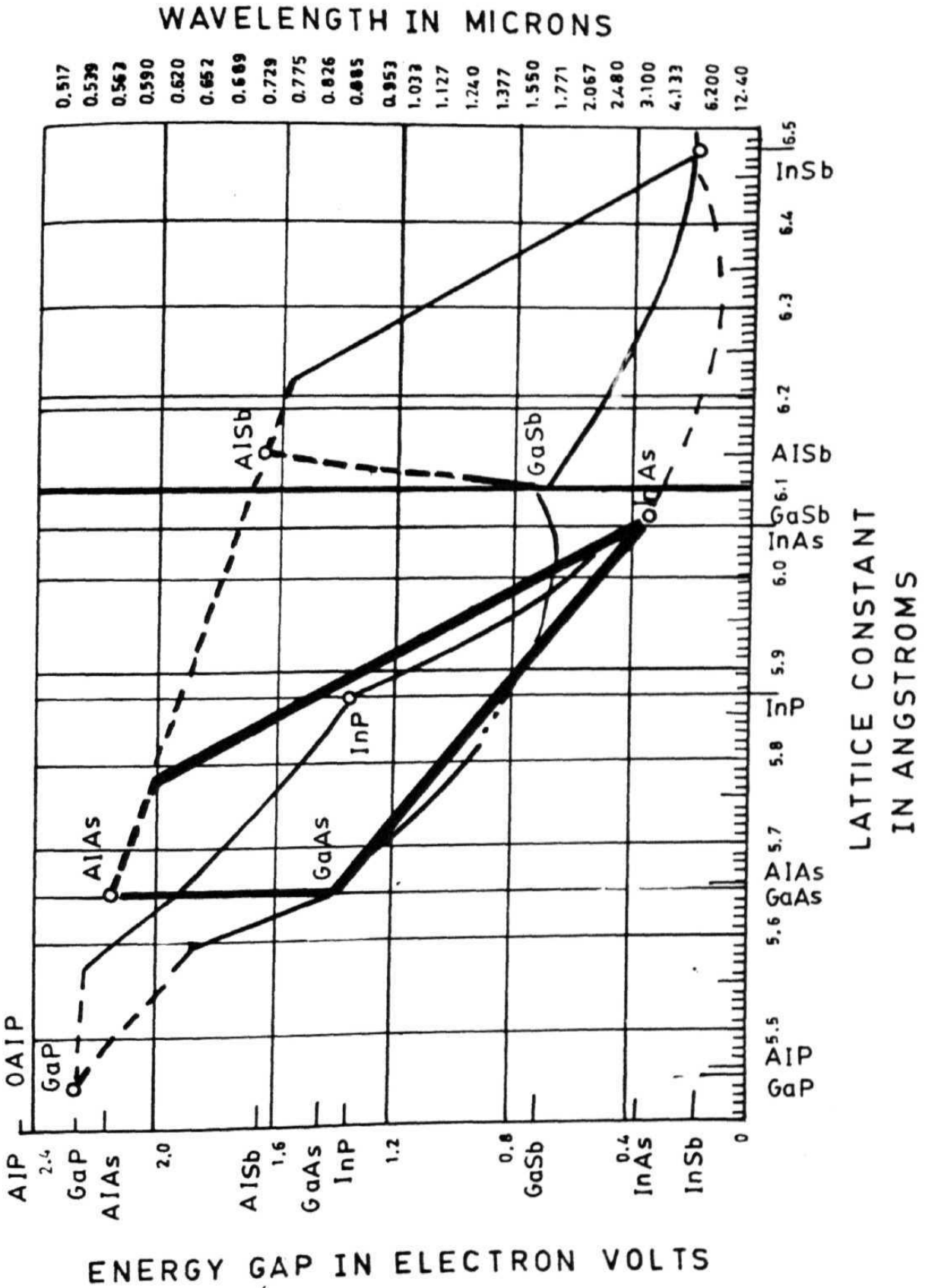


**Fig 3.1**: The bandgap range achievable by alloy formation in some III-V compund semiconductors [1].

- All of the A atoms are localized in one region while the B atoms are localized in another region. Such alloys are called phase separated.
- The probability that an atom next to an A-type atom is A is X and the probability that it is B is (1-X). Such alloys are called random alloys.
- The A and B atoms form a well-ordered periodic structure leading to a superlattice.

A few specific cases of these alloys are, (i) GaAs-AlAs alloy which gives AlGaAs system; the most important component of high speed electronic and optoelectronic devices. Nearly all kinds of quantum well structures can be formed utilizing its perfect lattice match with GaAs. It also interestingly exliibits switching of the bandgap from direct to indirect. (ii) lnAs-GaAs alloy giving rise to the InGaAs system. These are active components of very high speed electronic and optoelectronic devices. InAs and GaAs have a lattice mismatch of 7%. InGaAs also shows excellent low and high field transport properties and is *the ones studied in this work*. (iii) HgTe-CdTe giving HgCdTe. HgTe and CdTe are very well lattice matched, do not show miscibility gap and span a bandgap of 0 to 1.5 eV. HgCdTe has a direct bandgap throughout the composition range and is used for very small bandgap device applications. Also, it can be grown on CdTe, ZnTe and even Si and GaAs substrates. (iv) Si-Ge alloy; this alloy allows the heterostructure concepts to be used in Si technology since it can be a component of Si-SiGe structure. Apart from this, these structures don't find potential applications in the optoelectronic devices. Silicon and germanium have a lattice mismatch of 4% and hence a suitable substrate to grow this alloy on cannot be found easily.

The basis of all the advantages of bandgap tailoring is the *charge confinement* that is achieved through this process. This is done by growing a thin layer ($\sim$ 100 $\AA$ ) of one semiconductor sandwiched inside a different semiconductor with different bandgap. The electrons (or holes) are then confined in the smaller gap material by the potential barriers arising from the bandgap discontinuity at the interface. As a result, the quantization energy shifts the band edge to a higher energy; the electrons and holes are brought closer and the density of states becomes independent of energy. If the confinement is realized in one dimension, the resulting device is quantum well,

two dimensional confinement gives a quantum wire and three dimensional confinement gives a quantum dot. The present discussion is focussed on quantum well devices; the fabrication of these devices by the latest epitaxial growth technologies is relatively simple as compared to the processing of quantum wires or dots. The original idea of fabrication of a quantum well structure was proposed by Esaki and Tsu [2].

## 3.1 Epitaxial Growth

The fabrication of these types of devices became possible only after the major advancements in the technology of epitaxial crystal growth techniques like Molecular Beam Epitaxy *MBE*, Metal Organic Chemical Vapour Deposition *MOCVD*, Organo Metallic Vapour Phase Epitaxy *OMVPE*, Atomic Layer Epitaxy *ALE* and Hot Well Epitaxy *HWE*. Epitaxy literally means outer, upon or attached to *(Greek epi)* + arrangement or order *(taxis)*. The thickness of the layers grown ran be controlled to one atom layer at the rate of one micron per minute with the help of these techniques. Much improved crystalline quality, accurate control over substitutional doping and control of interface roughness to less than a couple of monolayers could also be achieved. Thus, by growing materials with different bandgaps, bandgap "tailoring" or "engineering" can be achieved. Therefore epitaxial growth, used to grow layers of elemental and compound semiconductors, as-compared to all other crystal growth techniques, which provides better control of purity and perfection as well as doping level, is a well controlled phase transition leading to a single crystalline solid, and is the exclusive growth technique for semiconductor alloys such as $Al_xGa_{1-x}As/GaAs$ and $In_xGa_{1-x}As/GaAs$. The thermodynamics of the phase transition is the first basic tool to be considered carefully. Since this is a dynamic and not an equilibrium process, the kinetics of both the mass transport and of surface processes must also be considered carefully. Defect generation is another problem to be dealt with, since the epitaxial growth is normally at low temperatures and has a high growth rate. In OMVPE, the growth is carried out in a cold wall reactor; the growth is generated by the following reaction

$$Ga(CH_3)(g) + AsH_3(g) \rightarrow GaAs(s) + 3CH_4(g)$$

for trimethyle-Ga and

$$Ga(C_2H_5)_3(g) + AsH_3(g) \rightarrow GaAs(s) + 3C_2H_6(g)$$

for triethyle-Ga. The absence of *Cl* precludes the etching reaction and simplifies the kinetics by eliminating the possibility of adsorption of chloride species on the surface. The ratio of As to Ga in the input gas stream is greater than one for the most favourable growth conditions. The flow rate is linearly proportional to the gallium flow rate.

Crystalline defects such as grain boundaries, stacking faults, twins and dislocations are known to get generated during the growth process, deteriorating the device properties. These defects have been shown to act as non-radiative recombination centres in many materials [4, 5], and reduce the minority carrier lifetime and growth efficiency in LED [6, 7] apart from degrading the performance of transistors, solar cells, detectors and other devices. Considerable effort has been devoted to the study and elimination of these crystalline defects in semiconductor materials.

All these growth techniques, till recently, concentrated on the use of lattice-matched epitaxy, limiting the associated development of electronic and optoelectronic semiconductor device structures considerably. Wavelengths of laser emission, frequency response and output power of a traasistor, all suffered limitations in lattice-matched systems. Strained-Layer Superlattices (SLS) have unique electronic and optoelectronic properties [8]; in these structures the lattice parameter of the deposit is different from that of the substrate which is accommodated by strain in the layers. In lattice-matched epitaxy (fig. 3.2a), the deposit and the substrate have the same lattice parameter; the epilayer atoms getting deposited onto the substrate locate the potential minima corresponding to the substrate lattice sites easily. In St rained-Layer structures, deposit atoms are constrained to the substrate interatomic spacings in the plane of the interface [9], although the lattice parameters of the substrate and the epilayer are different, resulting in a strain in the epilayer and at the interface (fig. 3.2b). The magnitude of this strain directly depends on the composition of the layer and the substrate. This elastic strain energy for a given lattice mismatch increases with the epilayer thickness and beyond a critical thickness, all the strain in the epilayer is relaxed. This process occurs via the introduction of slipped regions into the crystal, bounded by

line defects called the "misfit dislocations". Structures that are strained are termed commensurate or coherent and the strain relaxed materials (fig. 3.2c) are called discommensurate structures. Misfit dislocations are the unwanted defects in the solid which deteriorate the performance of the devices and hence it is important to characterize strain, strain-relieving mechanisms and the limits of strained layer growth. A number of theories exist for the critical layer thickness [5-15] for given structures; the most relevant being the one due to Matthews and BlacJceslee [10, 11, 12].

The critical layer thickness for $In_{0.1}Ga_{0.9}As$ material lies between 100 A- 300 A. With a view to determine the exact thickness at which tin's system ($In_{0.1}Ga_{0.9}As/GaAS$SLS) relaxes, we have grown a series of such structures and characterized them by ion channeling. Other complimentary characterization techniques like High Resolution XRD and Raman Spectroscopy have also been carried out on these structures and the results are compared. The description of these SLS and also some samples that were obtained earlier is given in the forthcoming section.

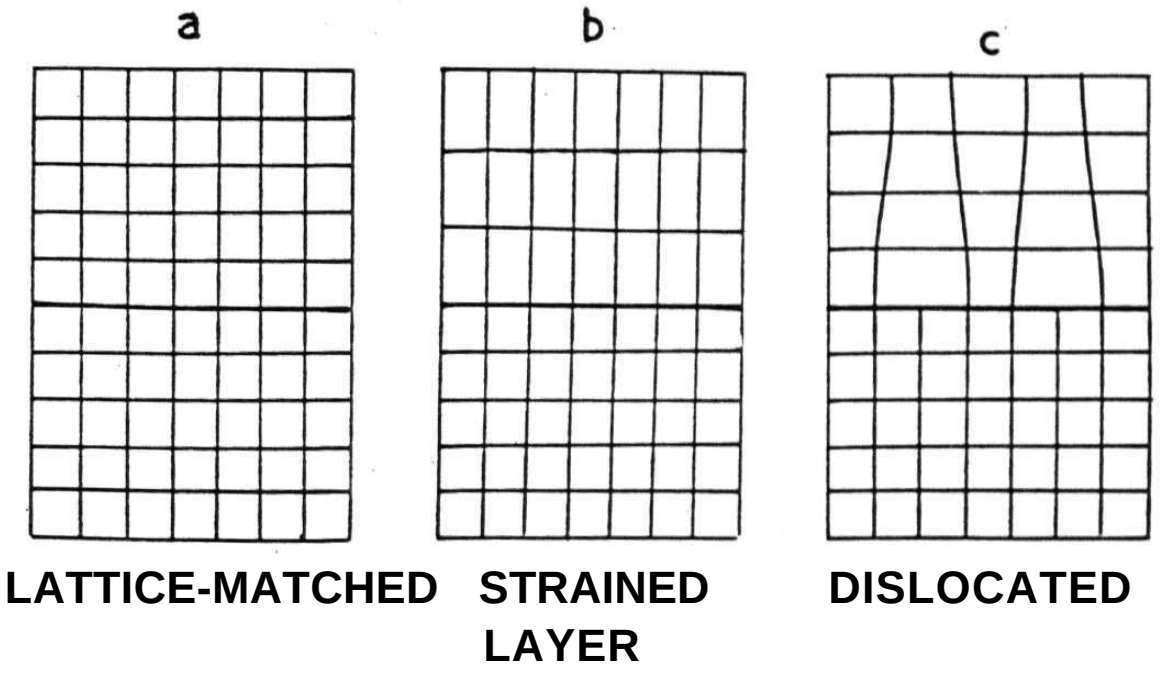


Fig 3.2: Schematic illustration of (a) lattice-matched heteroepitaxy, (b) coherently lattice-mismatched heteroepitaxy and (c) relaxed lattice-mismatched heteroepitaxy [9].

## 3.2 Sample Description

Some of the SLS samples were obtained from the Tata Institute **of Fundamental** Research, Mumbai, India. These are listed below.
(100) growth direction on GaAs substrate

- 30 alternating layers of $In_{0.6}Ga_{0.4}As$ with thickness 55 A and GaAs with thickness 225 A a top cap-layer of GaAs $0.3\mu$ thick and a buffer of $0.6\mu$.
- 30 alternating layers of $In_{0.5}0.5As$ with thickness 45 A and GaAs with thickness 225 A a top cap-layer of GaAs $0.12\mu$ thick and a buffer of $0.6\mu$.
- 30 alternating layers of $In_{0.6}Ga_{0.4}As$ with thickness 55 A **and** GaAs with thickness 900 A a top cap-layer of GaAs 0.12/J thick and a buffer of $0.6\mu$.
- 5 alternating layers of GaAs of 200 A and $In_{0.2}Ga_{0.8}As$ of 70 A.

Some samples have been grown on the *Organo Metallic Vapour Phase Epitaxy(OMVPE)* facility at the Solid State Electronics laboratory of Tata Institute of Fundamental Research, Mumbai. All the experiments have been carried out *on these samples.* The sample specifications are shown below.

Table 3.1: Samples grown at TIFR. Indium content in all the cases is 0.1. /All samples grown on GaAs substrate and 5000 A thick GaAs buffer.

| Sample No. | Specification | Thickness (In the same order) |
|---|---|---|
| 9702 | GaAs/InGaAs/GaAs(Buffer) | 250 Å/ 350 Å/5000 Å |
| 9706 | InGaAs/GaAs(Buffer) | 300 Å/5000 Å |
| 9850 | InGaAs/GaAs(Buffer) | 100 Å/5000 Å |
| 9851 | InGaAs/GaAs(Buffer) | 200 Å/5000 Å |
| 9853 | GaAs/InGaAs/GaAs(Buffer) | 300 Å/500 Å/5000 Å |
| 9854 | GaAs/InGaAs/GaAs(Buffer) | 300 Å/200 Å/5000 Å |

## 3.3 Rutherford Backscattering Spectroscopy/Channeling

Rutherford backscattering Spectrometry (RBS/channeling) is one **technique** which can determine the thickness, composition, defect densities, uniformity and strain, and can be applied readily to the superlattices [8, 9, 11].

RBS is based on four basic physical concepts corresponding to specific physical phenomena; each one has a particular capability or limitation of backscattering Spectrometry. These are listed below with brief descriptions.

### 3.3.1 Basic Physical Concepts

- *Energy transfer from a projectile to a target nucleus in an elastic two body collision.* This process leads to the concept of kinematic factor and to the capability of mass perception. When a projectile of mass $M_1$ moving with an energy $E_o$ collides elastically with a stationary particle (target) of mass $M_2$, energy will be transferred from the moving to the stationary particle. This interaction is assumed to be elastic with the condition that the projectile energy $E_o$ must be much large than the binding energy of the atom and nuclear reactions and resonances are absent. If $E_1$ is the energy with which the projectile is scattered back, $\theta$ is the scattering angle and $\phi$ the recoil angle, then the kinematic factor it is defined as the ratio of the projectile energy after the collision to that before the collision;

$$k = \frac{E_1}{E_o} \tag{3.53}$$

The energy and momentum conservation principles give

$$k_{M_2} = \left\{ \frac{[1 - \left(\frac{M_1}{M_2}\right)^2 \sin^2\theta]^{\frac{1}{2}} + \left(\frac{M_1}{M_2}\right)\cos\theta}{1 + \left(\frac{M_1}{M_2}\right)} \right\}^2 . \tag{3.54}$$

Thus, with a knowledge of $E_1, E_o$ and hence $k$, the mass of the target can be found out.

*The probability that an elastic two-body collision occurs.* This loads to the concept of scattering cross-section which in turn leads to quantitative analysis of atomic composition. Suppose a narrow beam of particles impinges on a wide target; a detector is placed at an angle *0* from the direction of incidence which counts each particle scattered in the differential solid angle direction $d\Omega$. If Q is the total number of particles that have impinged on the target and dQ is the number of particles recorded by the detector, then the differential scattering cross-section $\frac{da}{d\Omega}$ is defined as

$$\frac{d\sigma}{d\Omega} = \frac{1}{Nt}[(\frac{dQ}{d\Omega})/Q] \tag{3.55}$$

where $N$ is the volume density of atoms in the target and $t$ is its thickness. *Ni,* therefore is the areal density of the target. The. average number of scattering events falling within a "finite" solid angle $\Omega$ is then given by

$$\sigma = \frac{1}{\Omega}\int_{\Omega}(\frac{d\sigma}{d\Omega})d\Omega \tag{3.50}$$

The total number of particles detected or the backscattering yield is written as

$$Y = \sigma\Omega QNt \tag{3.57}$$

**i.e.**

$$\begin{pmatrix} \text{number. of} \\ \text{detected particles} \end{pmatrix} = \sigma\Omega \begin{pmatrix} \text{total number of} \\ \text{incident particles} \end{pmatrix} \cdot \begin{pmatrix} \text{number of target} \\ \text{atoms per unit area} \end{pmatrix}$$

Thus, when $\sigma$, $\Omega$ are known and the number of incident and detected particles are counted, the number of atoms per unit area, $Nt$, can be determined quite accurately.

- *Average energy loss of an atom moving through a dense medium.* This leads to the concept of stopping cross-section and to the capability of depth perception. The likelihood of a Rutherford scattering collision is very less and most often, the projectile penetrates into the target. As it pushes itself through the target, it slows down and its kinetic energy

decreases. The amount of energy lost per unit distance A:r, which is measured by recording the energy difference before and after the transmission through the target, defines the specific energy loss

$$\lim_{\Delta x \to 0} \frac{\Delta E}{\Delta x} = \frac{dE}{dx}(E) \tag{3.58}$$

The energy at a given depth *x* below the surface is then given by

$$E(x) = E_o - \int_o^x (\frac{dE}{dx})dx \tag{3.59}$$

$\frac{dE}{dx}$ is a function of energy and not x and so $\int_o^x (\frac{dE}{dx})dx$ cannot be evaluated without the knowledge of the energy as a function of $x$, $E(x)$. But $E(x)$ is unknown in the equation; the difficulty is resolved by regarding $x$ as a function of $E$, rather than $E$ as a function of $x$. Then,

$$dx = \frac{dx}{dE}(E)dE \tag{3.60}$$

Therefore,

$$x = \int_E^{E_o} (\frac{dx}{dE})dE = \int_E^{E_o} (\frac{dE}{dx})^{-1}dE \tag{3.61}$$

Or

$$x = (E - E_o)(\frac{dE}{dx})^{-1} \mid_{E_o} \tag{3.62}$$

If S is the target area illuminated by the beam, N the atom density in the target and $\Delta x$ the thickness of the target, then $\frac{dE}{dx} = \frac{SN\Delta x}{S} = N\Delta x. Therefore \Delta E$ is set proportional to $N\Delta x$ and the proportionality factor is known as the "Stopping Cross-Section $\xi$".

$$\xi = (\frac{1}{N})(\frac{dE}{dx}) \tag{3.63}$$

- *Statistical fluctuations in the energy loss of an atom moving through a dense medium.* This process leads to the concept of *energy straggling* and to a limitation in the ultimate mass and depth resolution of the backscattering spectrometry. An energetic particle that moves through a medium loses its energy via many individual encounters. As a result, identical energetic particles, which all have the same initial velocity, do not have the same energy after passing through a thickness $\Delta x$ of a homogeneous medium; they are no more monoenergetic. This results in fluctuations in the energy loss which places a finite limit for the precision on both the mass and depth perception. For these reasons, it is very important to have quantitative information on the magnitude of energy straggling for any given combination of energy, target material, target thickness and projectile.

When the incident ion beam is directed along a high-symmetry crystal direction, ion channeling occurs [20, 21]. $\chi_{min}$ which is the ratio of the backscattered particles when aligned (A) to a crystallographic axis to that in the random (R) condition (i.e., $\chi_{min} = Y_A/Y_R$) is a measure of the crystalline quality of the sample. A $\chi_{min}$ value of a very good crystalline sample will be around 2-3%. With ion channeling one can determine the tetragonal distortion in the epilayer and consequently the in-plane strain (whether compressive or tensile) can be determined. Therefore, the use of ion channeling in conjunction with *RBS* provides a measure of the crystalline quality as a function of depth and also allows determination of the strain in epitaxial layered structures. Strain measurements by ion-channeling technique in multi-layered structures is based on the tetragonal distortions induced in the layers.

To align the sample that is cut so that the [001] axis is normal to the incident beam, the axis of rotation of the goniometer is given a tilt of $3^o$ from the incident direction. A "$\phi$" rotation is then given in steps of 1.5° and the backscattered yield is recorded each time. The same procedure is adopted for a tilt of $6^o$. The position of the most pronounced minima are recorded on polar coordinates. The lines connecting the minima then correspond to {100}, {110} and {111} planes. The intersection of these lines correspond to the [001] axial direction. The coordinates of the point of intersection give the goniometer position that will line up the [001] axis with the be [21].

The two components of strain are defined as

$$\epsilon_{\perp} = \frac{d_L^{\perp} - d^{\perp})}{d^{\perp}} \tag{3.64}$$

$$\epsilon_{\parallel} = \frac{(d_L^{\parallel} - d^{\parallel})}{d^{\parallel}} \tag{3.65}$$

where $d_L^{\perp}$ and $d_L^{\parallel}$ are the interplanar spacings of the strained layer in the direction perpendicular and parallel to the interface respectively. $d^{\perp}$ and $d^{\parallel}$ are the corresponding values for the free lattice of the epilayer material. The tetragonal distortion in the epilayer $\epsilon_t$ is related to $\epsilon_{\parallel}$ and $\epsilon_{\perp}$ as

$$\epsilon_t = \epsilon_{\parallel} - \epsilon_{\perp} = \frac{\Delta\theta}{\sin\theta\cos\theta} \tag{3.66}$$

where *0* is the angle between the positions of [100] and [110] directions where wo get minimum yield in the substrate and *AG* is the difference in the position of the minimum yield dip of substrate and epilayer.

## 4.4 High Resolution XRD

High Resolution X-Ray Diffraction (HRXRD) has become an essential and versatile tool to characterize heteroepitaxial structures, and, often complementary to other characterization techniques. XRD is very sensitive to the lattice strain. Point defects are too small to be observed by conventional imaging techniques but they do have appreciable effects on the X-ray intensity profile. With the advent of increasingly perfect single crystals and crystalline layers, a need for refined characterization emerged and *HRXRD* stands one among the most powerful and non-destructive techniques. Under the optimum conditions, HRXRD is capable of detecting strains with a sensitivity of about $10^{-5}$ [22]. It provides information on the interface structure with monolayer precision.

HRXRD gives a Fourier transform of a crystal volume of typically 1 $mm$ x 1 $mm$ x $(5 - 50)\mu m$. The data are X-ray intensity distributed in the vicinity of a reciprocal lattice point (or a Bragg peak), which is integrated over the direction normal to the diffraction plane by a detector wide-open in that direction. A high angular resolution, and thus a high strain sensitivity is achieved by

monochromating and/or collimating the incident X-ray beam, the procedure for which is given in ref. [22].

The relation between the chemical composition and the lattice parameter form the basis for HRXRD. The lattice parameters of the alloys gradually change with the chemical composition and can be approximated by a linear interpolation of the lattice parameters of the binary end members. This relation is known as Vegard's Law [23, 24]. With HRXRD, the lattice parameter and the lattice mismatch can be determined exactly and from this the chemical composition can be deduced. Consider the system of AlGaAs on GaAs. Because of the similar lattice parameters $\{a_o(GaAs) = 5.563\mathring{A},\ a_o(AlAs) = 5.6611\ \mathring{A}\}$, the lattice mismatch determination at, the $Cu - K\alpha_1 - GaAs$ {(004) reflection } must, be accurate to 2.7 x $10^{-5}$ corresponding to an angular width of the layer peak ($\Delta\Omega \sim 0.001$), if the chemical composition is to be determined with an accuracy of 1 %.

Another analytical aim of HRXRD is the determination of layer thickness. In measurements of extremely thin single layers, the small reflectivity presents the difficulties, rather than the angular width of the layer peak. Therefore for carrying out HRXRD, one needs to have an angular resolution of at least 0.001° and a dynamical range of intensity.

As stated earlier, HRXRD measures the intensity of scattered X-rays; these are distributed in the neighbourhood of a reciprocal lattice point. $k_o$ is defined as the incident wave vector, $k$ as the diffracted wave vector inside the crystal and $K_o$ and $K$ are defined as the incident and diffracted wavevectors outside the crystal, conventionally. So the reciprocal lattice point serves as a reference position in the reciprocal lattice space in describing the distribution of scattered intensity as a function of deviation *(q)* of the scattered wave-vector *K* from the reciprocal lattice point. The $\bar{q}$-vector lies within the diffraction plane because the scattered intensity distributed in the direction normal to the diffraction plane is integrated by a wide-open detector.

If we define $\theta_B$ as the angle at which the Bragg reflection takes place, ($\theta_{BS}$,the Bragg angle for the substrate and $\theta_{BL}$, that for the epilayer), then the Bragg condition is written as

$$2d \sin\theta_B = \lambda \tag{3.67}$$

Differentiating the above equation, we get

$$\frac{\Delta d}{d} = \epsilon_{\perp} = -cot\theta_B \Delta\theta \tag{3.68}$$

For GaAs samples and materials grown on them, (004) (224) ($\bar{2}\bar{2}4$) (115) and ($\bar{1}\bar{1}5$) are the directions in which the Bragg equation is satisfied. If $\omega_s$ is the incident angle of the X-ray beam to the substrate and $\omega_L$, that to the epilayer, $\tau_S$ the inclination of the Bragg plane to the substrate and $\tau_L$ that to the epilayer, then $\omega_S = \theta_{BS} + \tau_S$ is called the High Incident angle and $\omega_S = \theta_{BS} - \tau_S$, the Low Incident angle for the substrate. Similarly $\omega_L = \theta_{BL} + \tau_L$ is the High Incident angle and $\omega_L = \theta_{BL} - \tau_L$, the Low Incident angle for the epilayer. We then have [25, 26],

$$\epsilon_{\perp} = \frac{\cos\tau_S \sin\theta_{BS}}{\cos\tau_L \sin\theta_{BL}} - 1 \tag{3.69}$$

$$\epsilon_{\parallel} = \frac{\sin\tau_S \sin\theta_{BS}}{\sin\tau_L \sin\theta_{BL}} - 1 \tag{3.70}$$

The tetragonal distortion $\epsilon_f$ is then given by

$$\epsilon_f = \frac{(1-\nu)\epsilon_{\perp} + \nu\epsilon_{\parallel}}{1+\nu} \tag{3.71}$$

where $\nu$ is the Poisson ratio which is given by

$$\nu = \frac{c_{12}}{c_{11} + c_{12}} \tag{3.72}$$

for the (001) surface and $c_{ij}$ are the elastic constants [22].

Determining $\omega_S$, $\omega_L$,$\theta_{BS}$ and $\theta_{BL}$, one can evaluate the strain straightforwardly. If the thickness of the epilayer exceeds the critical thickness, the layer relaxes giving rise to misfit dislocations; the tetragonal symmetry is cancelled and the unit cells of the layer assume a cubic symmetry. In the case of fully strained layer, $\epsilon_{\parallel}$ is zero and when the layer partially or fully relaxes, $\epsilon_{\parallel}$ is no longer zero. Thus by carrying out HRXRD, one can establish whether the sample has relaxed or not *and* also quantify the strain if the system has not relaxed.

## 3.5 Raman Spectroscopy

Raman Spectroscopy also allows one to determine this strain. Constant et al. [27] determined the internal strain in the pseudomorphic $In_xGa_{1-x}As/GaAs$structures over a wide range of

composition *x*. The quantitative measurement of strain is obtained from the phonon wave number shift between commensurate and incommensurate layers, governed by the formula

$$\epsilon_p = \frac{1}{\beta}\frac{\delta\nu}{\nu_o} \tag{3.73}$$

where *3* is a constant which depends on the material, growth direction and conditions and phonon type mode. $\nu_o$ is the wave number of the strain relaxed material for the same composition, which is evaluated from figure 3 of ref [27]. This value is compatible to the LO phonon wave number *(v)* of $In_xGa_{1x}As/GaAs$structure with InGaAs thickness 500 Å which is expected to be relaxed. $\delta\nu$ is the wave number shift.

## 3.6 Experimental

Sample of $In_{0.1}Ga_{0.9}As/GaAs$used in this work was grown by Organometallic Vapour Phase Epitaxy (OMVPE) at 100 torr pressure and 640° *C* growth temperature using alkyles trymethyle gallium, trimethyle indium and the hydride arsine. Epilayers are grown on nominal (001) GaAs substrate on a 5000 Åthick epitaxially grown GaAs buffer layer. The V/III ratio used on this growth is about 150.

On sample 9706, *RBS* and channeling have been carried out by 1.5 MeV and 3 MeV $He^{++}$ beam at Institute of Physics, Bhubaneswar, at a scattering angle of 150°. The scattering chamber is equipped with a goniometer with five[5] degrees of freedom $(x, y, z, \theta, \phi)$.On the goniometer, the *9* precision is of 0.1° and the $\phi$ rotation has a precision of 0.3°. The beam is collimated by a pair of collimators of dia 1.5mm, seperated by a distance of 0.5 meter. The details of this setup are given in [29].

On other samples, RBS and channeling have been carried out at the 2 MeV Van de Graaff accelerator at Indian Institute of Technology, Kanpur. $He^{+}$ beam of energy 1.2 MeV has been utilized at a scattering angle of 150°. The scattering chamber is equipped with a goniometer with six degrees of freedom; three translational motions $(\pm 10mm)$ along the x, y, and z directions, and three rotational motions namely the *9* rotation (180°) around the beam direction (x) with

a precision of $0.0125^{o}$, the $\phi$ rotation $(360^{o})$ around the axis perpendicular to the beam in the vertical plane with a precision of $0.018^{o}$ and the $\Psi$ rotation (±3.5") around the axis perpendicular *to* the beam in the horizontal plane with a precision of 0.007".

RBS and channeling have been carried out again on these samples duo to some ambiguity in the channeling results of IIT, Kanpur. This work is carried out at Center of Irradiation of Materials, Alabama A & M University, at 3.058 MeV $He^{++}$ beam at a scattering angle of $170^{o}$ and a solid angle of 0.2249 msr, the total FWHM is about 35-40 keV. The goniometer of this setup has four degrees of freedom; x (horizontal transversal), z (vertical transversal) with a precision of 0.0025mm each, *9* rotation (about the z-axis) of 0.(1° precision and a $\phi$ rotation (about the beam direction) of 0.001° precision. The beam is collimated by a pair of collimators of 1.5 mm and 2 mm respectively.

A brief description of the Philips XTERT Materials Research Diffractometer *{MED)* at TIFR, Mumbai, is given here.

(i)A series of Pre-aligned Fast Interchangeable X-ray *(PREFIX)* optical modules for point and line focus applications. Each PREFIX optical module is fitted to a U-shaped mounting bracket which has precisely machined, highly polished surfaces. It also has the ability to rotate ceramic insulated X-ray tube from point to line focus. Because of this feature the system can be changed from a High Resolution or Stress/Texture point focus application configuration into a normal Bragg configuration using the appropriate PREFIX optical modules for line focus applications, in a very less time without losing the alignment. (ii)A PW3040/00 Coasole comprising the X-ray generator, electronics racks with CPU and source controller. The electronics rack contains two position controls to drive the horizontal goniometer, Dual Sealer boards for the detectors and additional multiple DC Motor drive boards to drive the MRD cradle. (iii)A PW 3050/20 horizontal goniometer equipped with two optical disks for Theta and 2Theta. The goniometer is controlled by two position controls (Pos. Con. 2) which are able to drive *9* and *29* in steps of $0.0001^{o}$ with a reproducibility of $\pm 0.0001^{o}$, (iv)The MRD cradle has five following motorized movements; (a) a phi $\phi$ rotation (360°, step size $0.02^{o}$) with a reproducibility of ±0.01° and a slew speed of $70^{o}/sec$ (b) a Psi tilt $\Psi$ (180°, step size 0.01°) with a reproducibility of $\pm 0.01^{o}$ and a slew speed of $2^{o}/sec$

(c) X/Y translation for wafer mapping (±50 mm) with a step size of 0.01 mm and a precision of 10/; (d) Z translation (±5 mm) with a step size of 0.001 mm and a precision of $1\mu$ (e) Sample oscillation around any point on the X and Y table perpendicular to the diffraction plane. The cradle ran be used as a programmable automatic sample changer for multiple samples that have different heights and shapes. (v)Three PREFIX primary 4-crystal monochromators and a Ge[220] primary collimator. The Ge-crystals are factory aligned, tilted and set-up in either the Ge[440] or Ge[220] reflection to use the system in the High Resolution mode. The specifications of the assemblies are (a) 4 crystal symmetrically cut Ge[440] setting: $\Delta\theta \approx 5''$ (b) 4 crystal symmetrically cut Ge[220] setting: $AB \approx 12''$ (c) 4 crystal asymmetrically cut Ge[220] setting: $\Delta\theta \approx 18''$ (d) 2 crystal symmetrically cut Ge[220] collimator: $K\alpha 1$ and $K\alpha 2$. (vi)A PREFIX crossed slits collimators with filter slots, used for Texture or Psi-stress measurements. Opening 10 x *10mm* continuously, scale 0.02 mm. (vii)A PREFIX Fixed Divergence Slit Assembly with Masks. A programmable divergence slot assembly is optional. (viii)A PREFIX Secondary HR-Rocking Curve Assembly with rotatable slit section. (ix)A PREFIX Secondary HR-Rocking Curve/Triple Axis Optics Assembly with rotatable slit section. (x)A PREFIX Secondary parallel plate collimator (thin film attachment). (xi)A PREFIX Secondary Diffracted Beam Optics Assembly with programmable receiving slit. (xii)General Data Collector Windows Software.

Raman spectra are recorded in the backscattering geometry so as to observe the LO vibrations of the singlet type [30], which correspond to the phonons that propagate along the axis of the strained samples [31, 32]. Vertically polarized 514.5 nm argon-ion laser beam of 100 mW power was used to excite the Raman spectra. Scattered light from the samples was collected using a camera lens (Nikkon) and focussing lens. It was dispersed using a double monochromator of model Spex 14018 and detected using a cooled photomultiplier tube of model ITT-FW 130 operated in the photon counting mode. The slit width of the monochromator corresponding to 4.2 $cm^{-1}$ in terms of FWHM of the instrument resolution function was employed. The scattered light was integrated for 10 seconds and digitally recorded at 0.5 $cm^{-1}$ wavenumber interval. The optical absorption spectra are recorded using a Chemita 599 UV-VIS spectrophotometer.

## 3.7 Results and Discussion

*RBS* spectrum of 1.5 $MeV\ He^{++}$ on the sample 9706 is shown in figure 3.3. From this random spectrum and the thicknesses of the epilayer are confirmed. The atomic fraction of In is found to be 0.1. The In signal from the epilayer is easily resolvable but the Ga and As signals from epilayer could not be distinguished from those of the buffer. Picraux et al [34] have carried out RBS on $In_{0.19}\ Ga_{0.81}\ As/GaAs$ multilayered (31nm/layer) superlattice. They found that the In fraction (x=0.19) in the alternating layers gives rise to major oscillations and is resolvable upto 16 layers. These oscillations are not seen in the present studies, owing to the lesser composition of indium content [10].

In our study the Ga signal in the $In_xGa_{1-x}As$ is reduced as also the As. The amount of reduction in the yield depends on the crystalline quality of the sample material. For instance, the $\chi_{min}$ of indium for all the samples is around 10% indicating reasonably good crystallinity of the epilayer. Strain measurements by ion-channeling technique in multi-layered structures is based on the tetragonal distortions induced in the layers. These experiments for SLS have been performed in early eighties [11],[35]-[43]. Picraux et al [39] have determined strain in $GaAs_{1-x}Sb_x/GaAs$ grown by MBE. We have determined the tetragonal distortion using formula (3.14). $\Delta\theta$, the shift in the minimum yield and the corresponding tetragonal distortion, $\epsilon_t$, has been found out from figure 3.4. The results are tabulated in table 3.2. The shifting of the minimum yield towards left with respect to the substrate indicates that the distortion is compressive. This is expected since the lattice parameter of $In_xGa_{1-x}As$ is larger than that of *GaAs*. No separation in the minimum yield dip of the substrate and the buffer has been observed.

On samples 9702 and 985 series, RBS/C experiments are carried out at Alabama A & M University. 985 series samples show that the atomic fraction of indium has changed to 0.075 as against 0.1. This is later confirmed by HRXRD. The results of the available data are shown in figures 3.5 - 3.7 and are tabulated in table 3.2.

Channeling at 1.2 MeV on these samples were first carried out at Indian Institute of Technology, Kanpur. The results of this experiment shows that all the samples are relaxed. But High

Resolution XRD and Raman Spectroscopy show a finite strain in all the samples. At these low energies, the critical angle for channeling becomes larger than the angular misalignment [41] and becomes complicated and often ambiguous due to the *beam steering effects*, in that some of the channeled ions become random in one layer, although aligned in one. This steering effect can also alter the symmetry of angular scan profiles of deep layers [44, 45]. For instance, figure 3.8 shows the angular scan around <011> axis, of sample 9702. The shift in the minima of epilayer from that of substrate is less than 0.1°, giving a tetragonal distortion of $\epsilon_t$ — 0.17%. This indicates that the sample has relaxed, contradicting the experiments of HRXRD and Raman Spectroscopy. It was then decided to carry out channeling at 3 MeV and the samples (other than sample 9706) were subsequently studied at Alabama A & M University; the results of which are reported here.

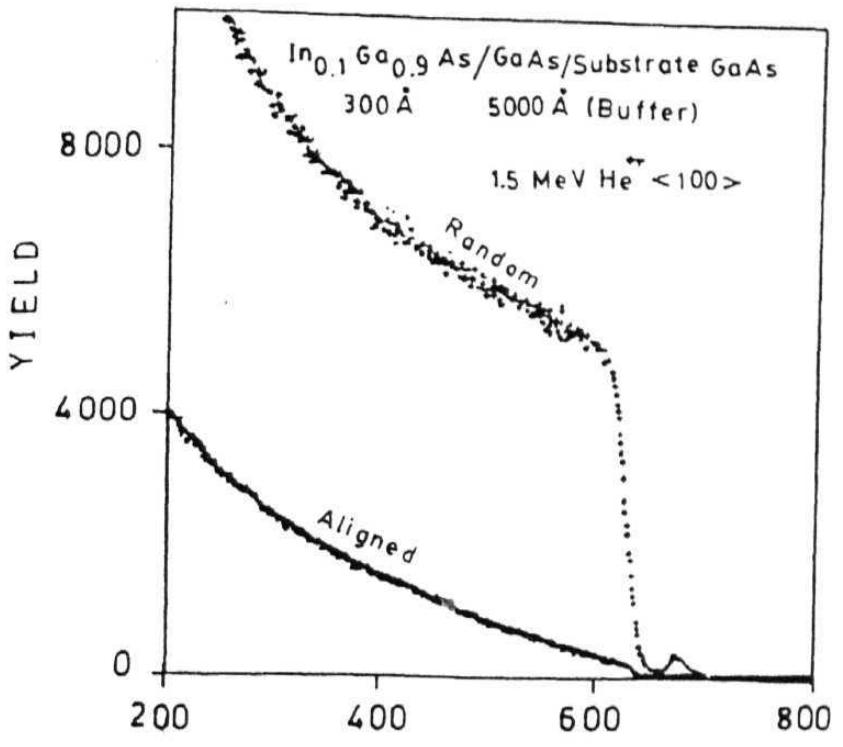


**Fig** 3.3: 1.5 MeV $He^{++}$ RBS spectrum for a scattering angle of $150^{o}$ from a single layer **of** $In_{0.1}Ga_{0.9}As$ on GaAs.

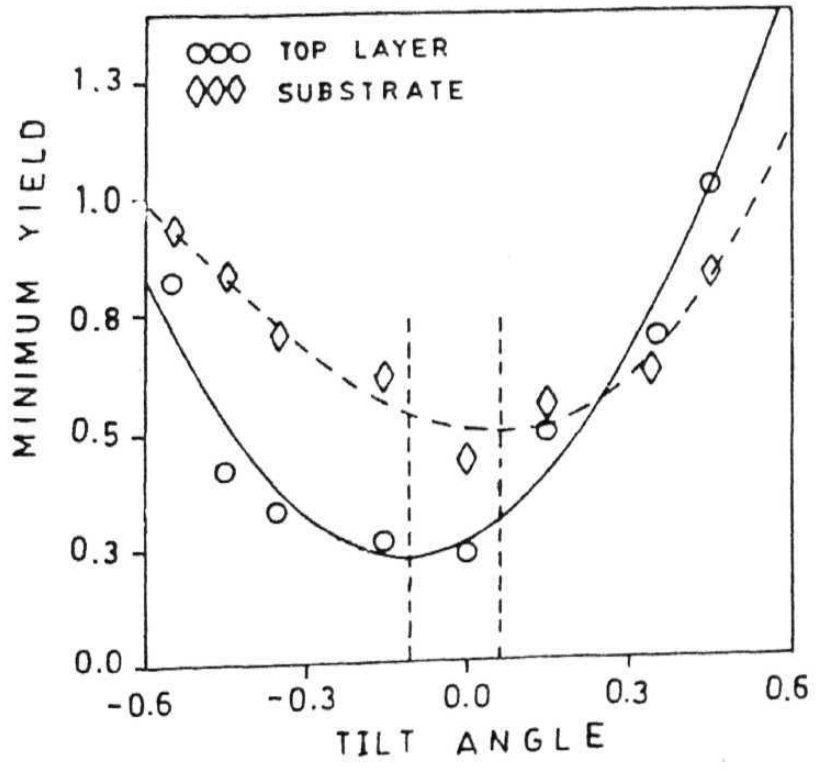


**Fig** 3.4: Channeling angular scans along the inclined <110> axes **from** a single 30-nm layer of $In_{0.1}Ga_{0.9}As$ on GaAs.

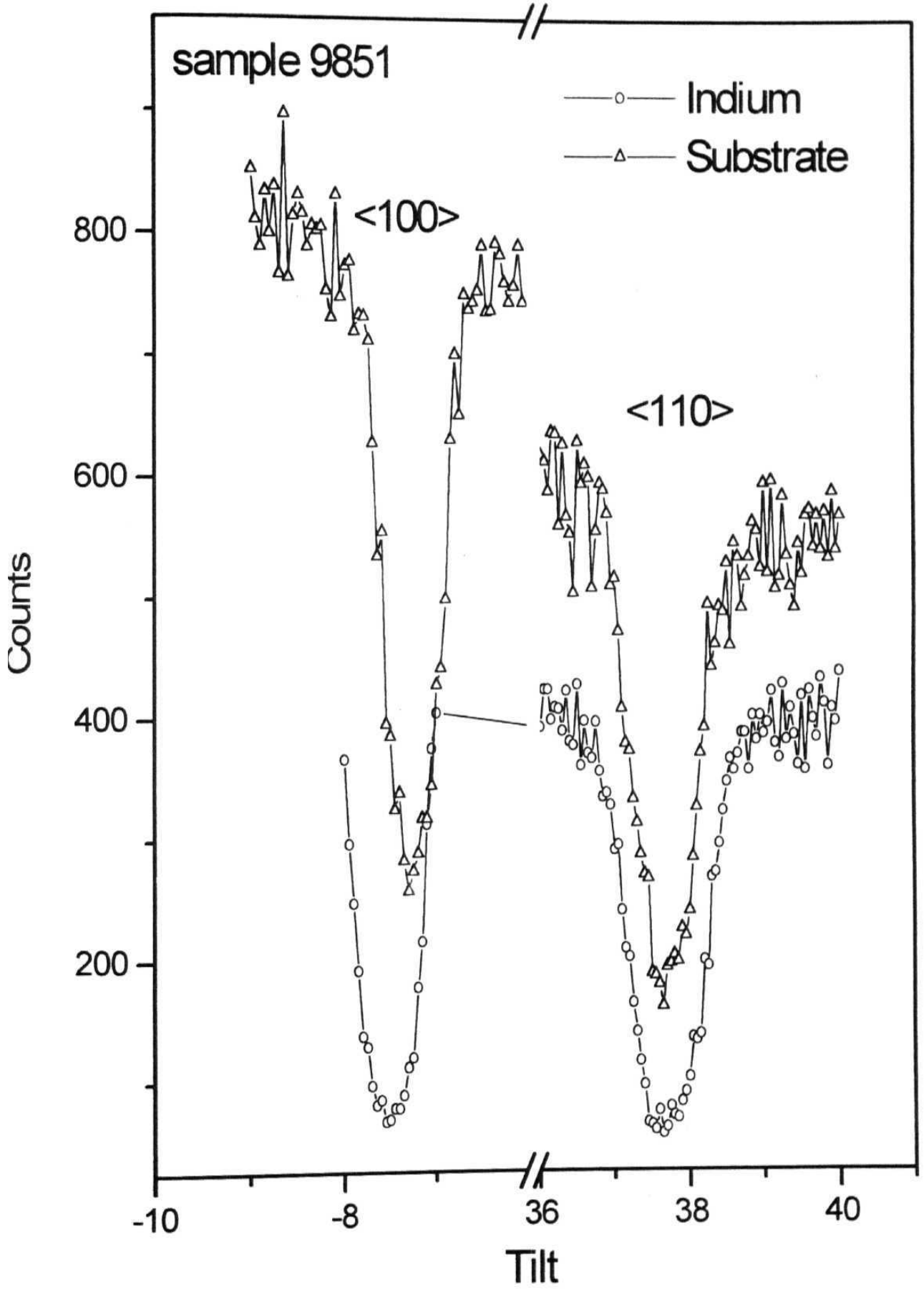


**Fig. 3.5:** Channeling angular scan around <100> and <110> axes.

$\Delta\theta = 0.2^{\circ}$ and $\theta = 45.31^{\circ}$

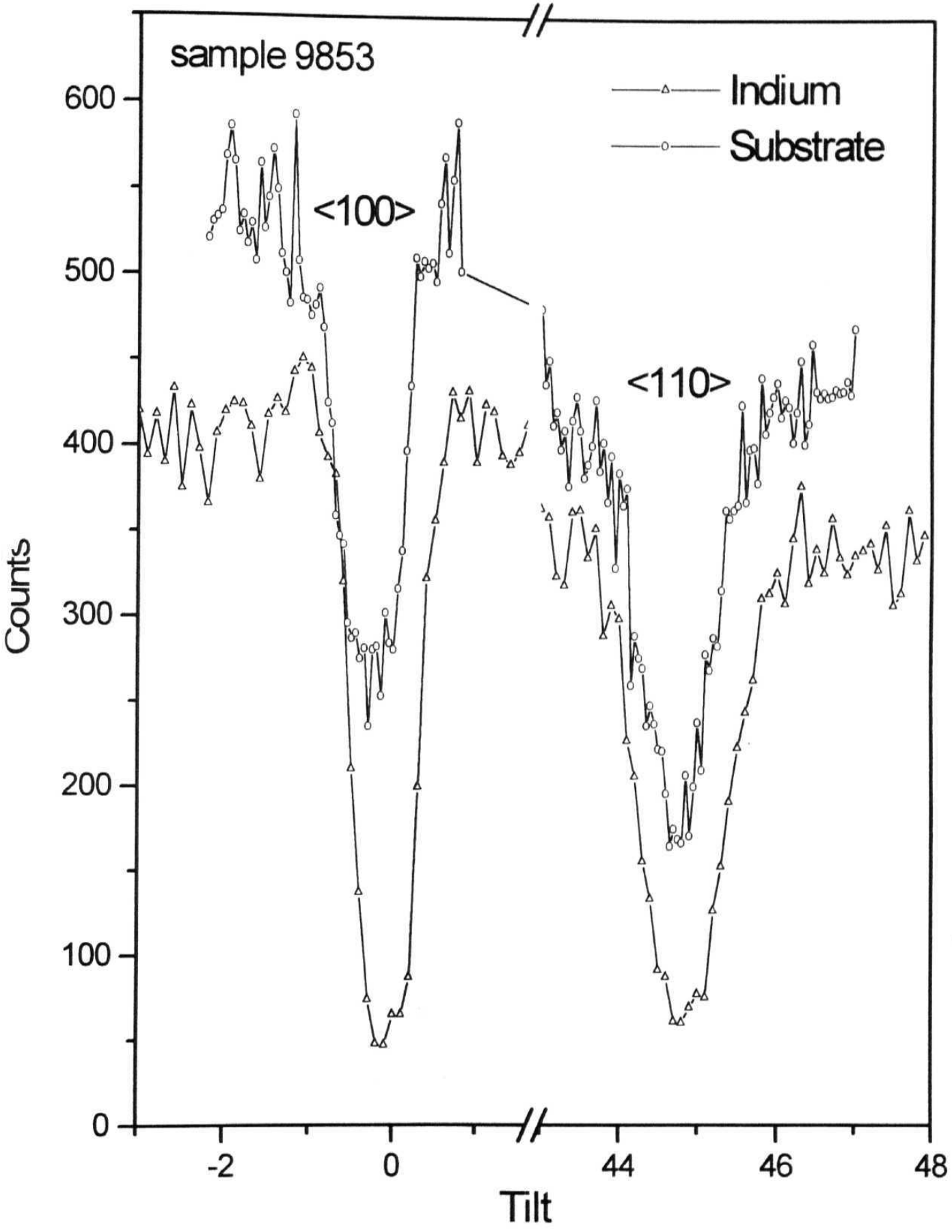


**Fig. 3.6 :** Channeling angular scan around <100> and <110> axes.

$\Delta\theta = 0.18^{\circ}$ and $\theta = 45.06^{\circ}$

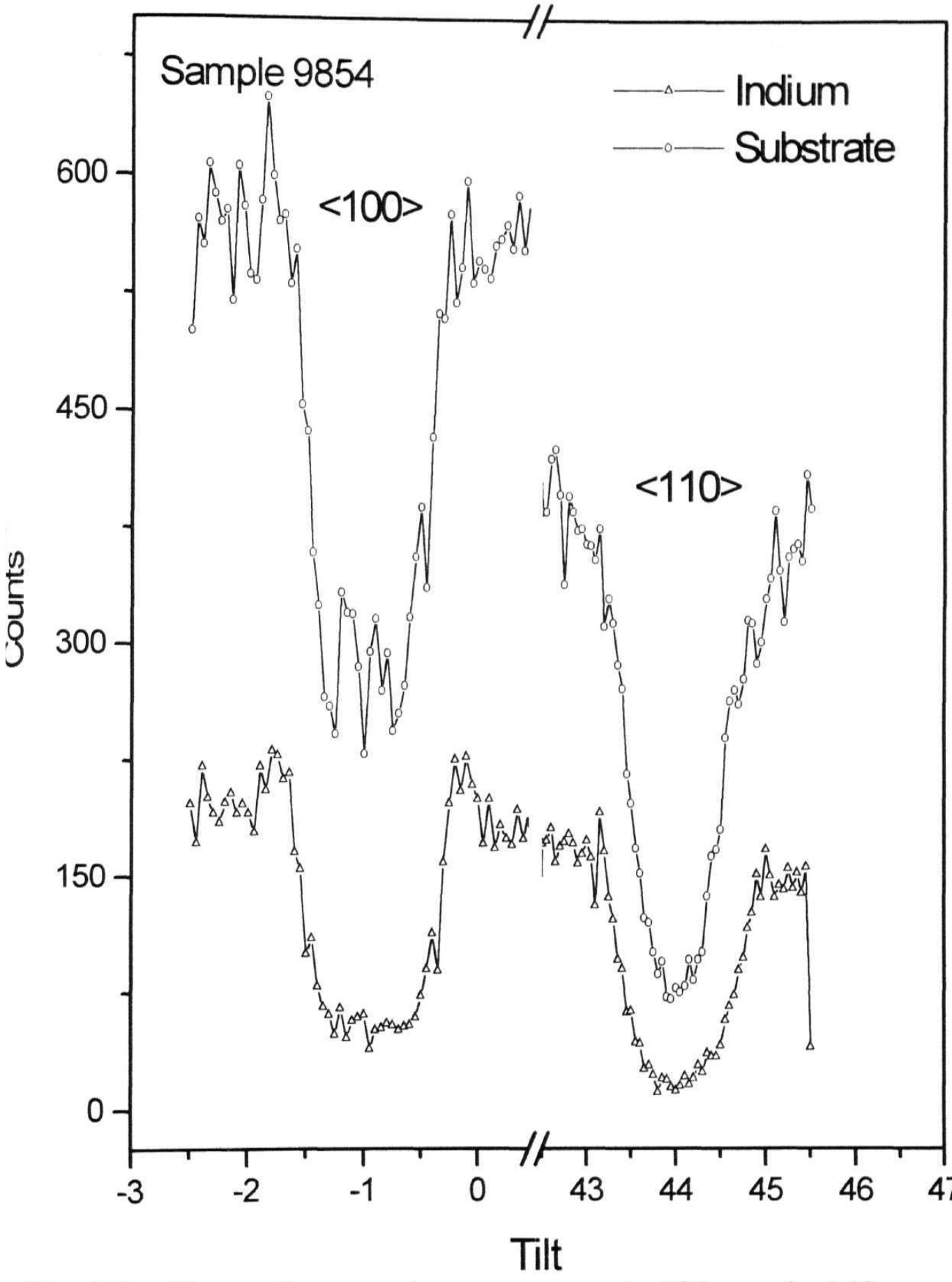


**Fig. 3.7 :** Channeling angular scan around <100> and <110> axes.

$\Delta\theta = 0.2^\circ$ and $\theta = 45.033^\circ$

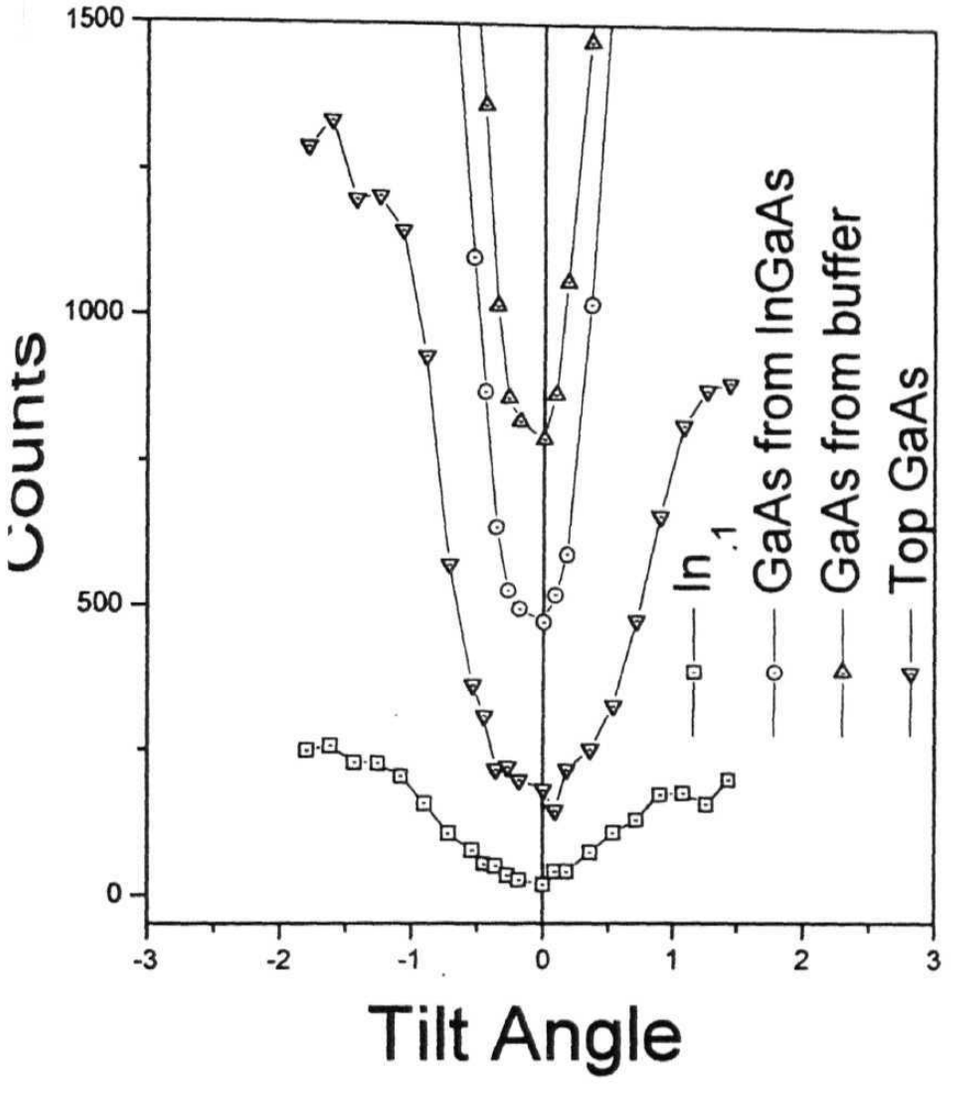


ig 3.8: Channeling angular scans along the inclined [110] axes from 25 nm GaAs and 35-nm $In_{0.1}Ga_{0.9}As$ layer on a GaAs substrate

X-ray measurements of (004) reflection along four azimuth directions give mean separation between the GaAs Bragg peak and the $In_{0.1}Ga_{0.9}As$ Bragg peak $\overline{\Delta\Omega}$ such that $\epsilon_\perp$ and $\epsilon_\parallel$ are evaluated straightforwardly. We have measured the asymmetric 224 and 224 reflections also for this sample, from which, $\epsilon_\perp$, $\epsilon_\parallel$ and hence the strain are found out and tabulated in table 3.2. Figures 3.9 - 3.13 show the X-ray spectra of all the samples.

SLS s of $In_xGa_{1-x}As/GaAs$ have been studied by Raman Spectroscopy rigorously [28] and all such studies reveal that InGaAs presents a two mode behaviour; the GaAs-like LO phonon mode and InAs-like LO phonon mode. The GaAs-like LO phonon is more dominant and the TO mode is not observed at all. The wavenumber of InGaAs is shifted from both the LO phonon modes of the bulk GaAs and the GaAs-like LO of the ternary alloy for the same composition. This feature is the superposition of the GaAs LO and the GaAs-like LO of $In_xGa_{1-x}As$ shifted by the efforts of strain in the opposite direction. $\nu_o$ is found to be 288.3 $cm^{-1}$ and $\nu$ is noted down in figures 3.14 - 3.19 for each sample. *(3* value for the indium content of 10% has been found by least square fit of the values given in table 3 of reference [27]. It comes out to be 1.6602. Strain value is then evaluated using equation (3.20). The results are tabulated in table 3.2 along with those of ion-channeling and HRXRD.

Table 3.2: The values of strain for various samples using Ion Channeling, XRD and Raman Spectroscopy.

| Sample No. | Strain ($\epsilon_t$%) By Ion Channeling | Strain ($\epsilon_\perp$%) By HRXRD | Strain ($\epsilon_p$%) By Raman Spectroscopy |
|---|---|---|---|
| 9702 | 1 | 0.96 | 1 |
| 9850 | | | 0.7565 |
| 9706 | 0.7 | 1 | 1.3 |
| 9851 | 0.7 | 0.92 | 0.945 |
| 9853 | 0.7 | 1 | 1 |
| 9854 | 0.7 | 0.85 | 0.9 |

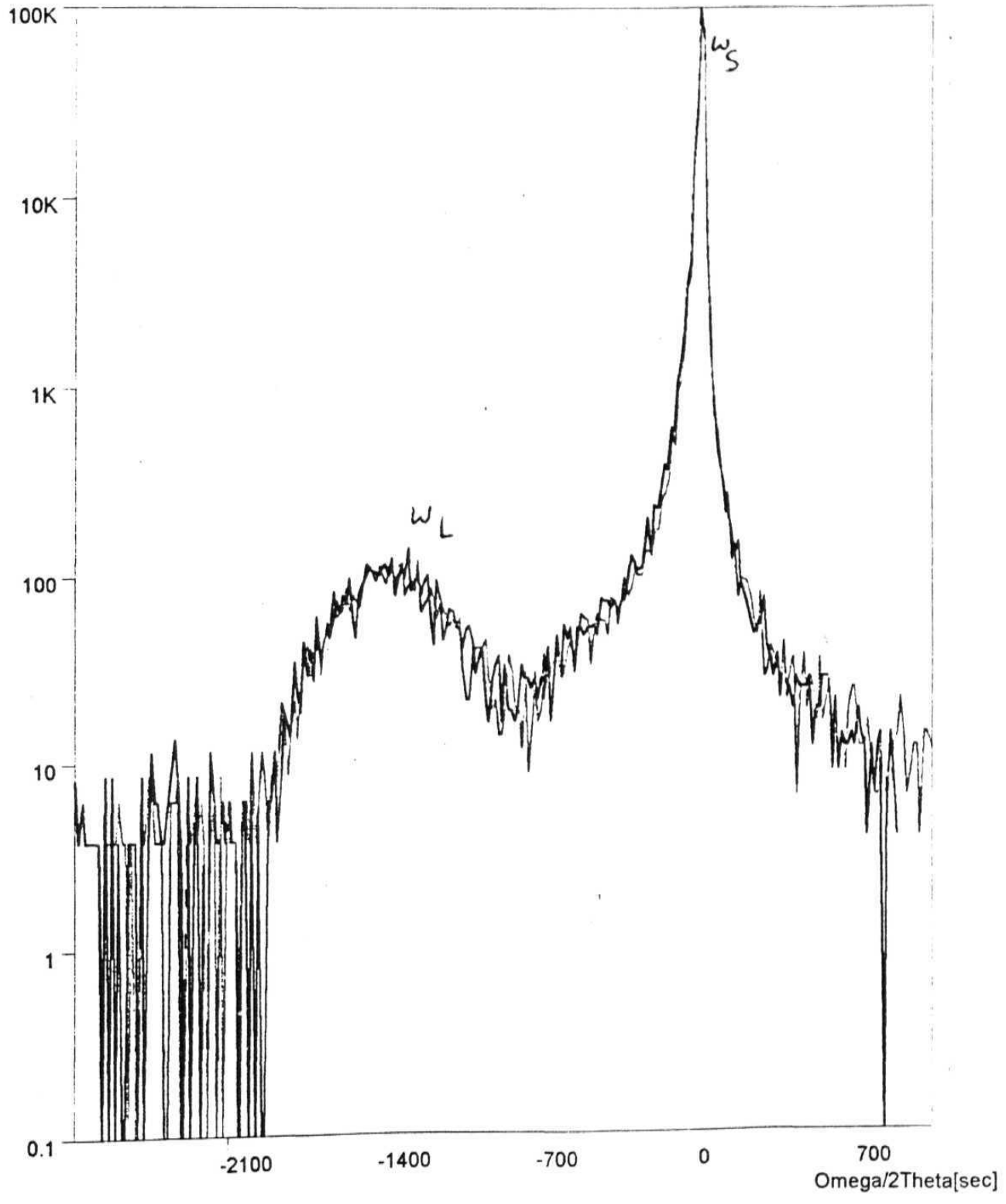


**Fig 3.9**: $\Omega/2\Theta$ scan around (004).

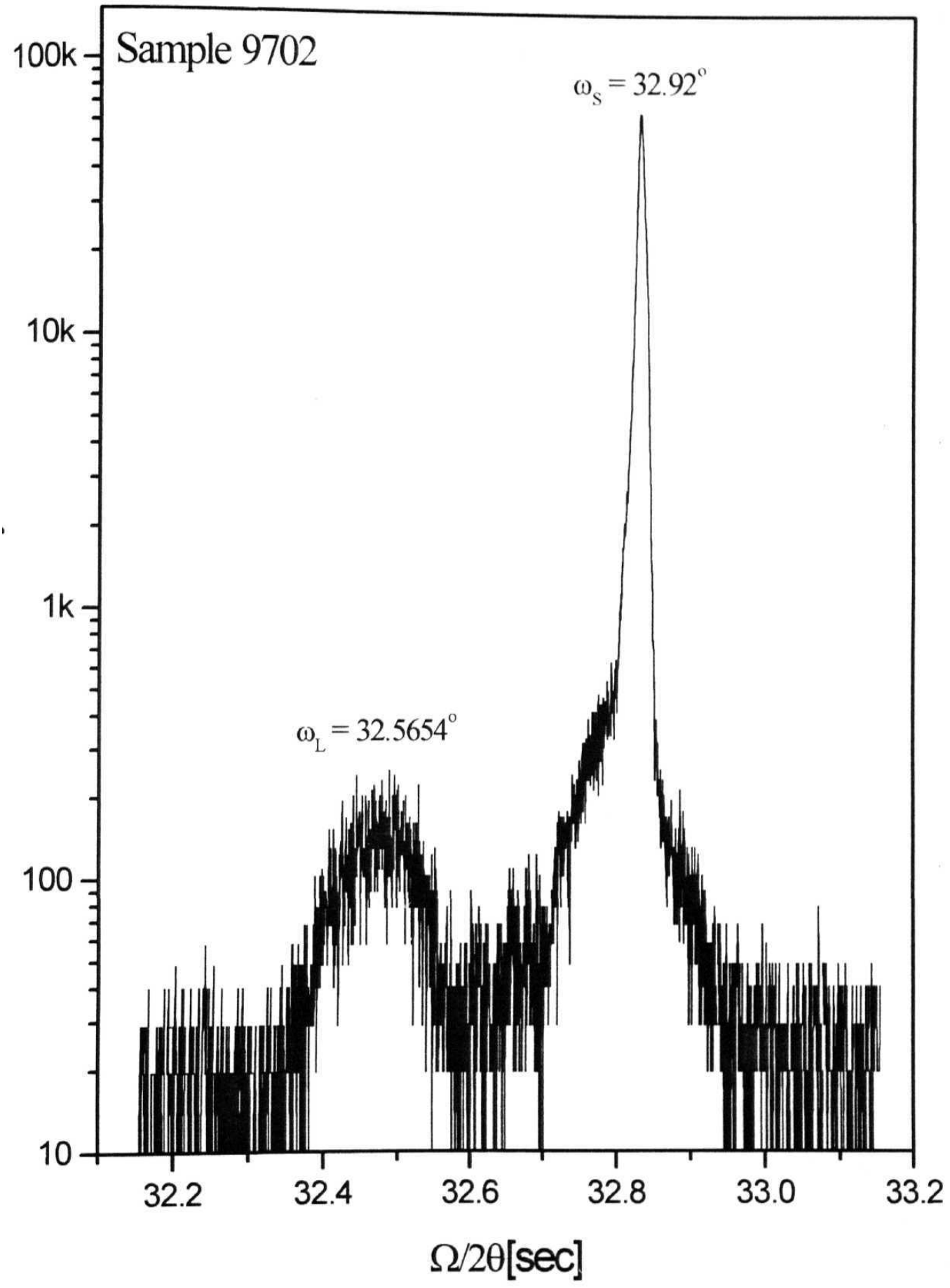


**Fig 3.10:** Ω/2θ scan around (004)

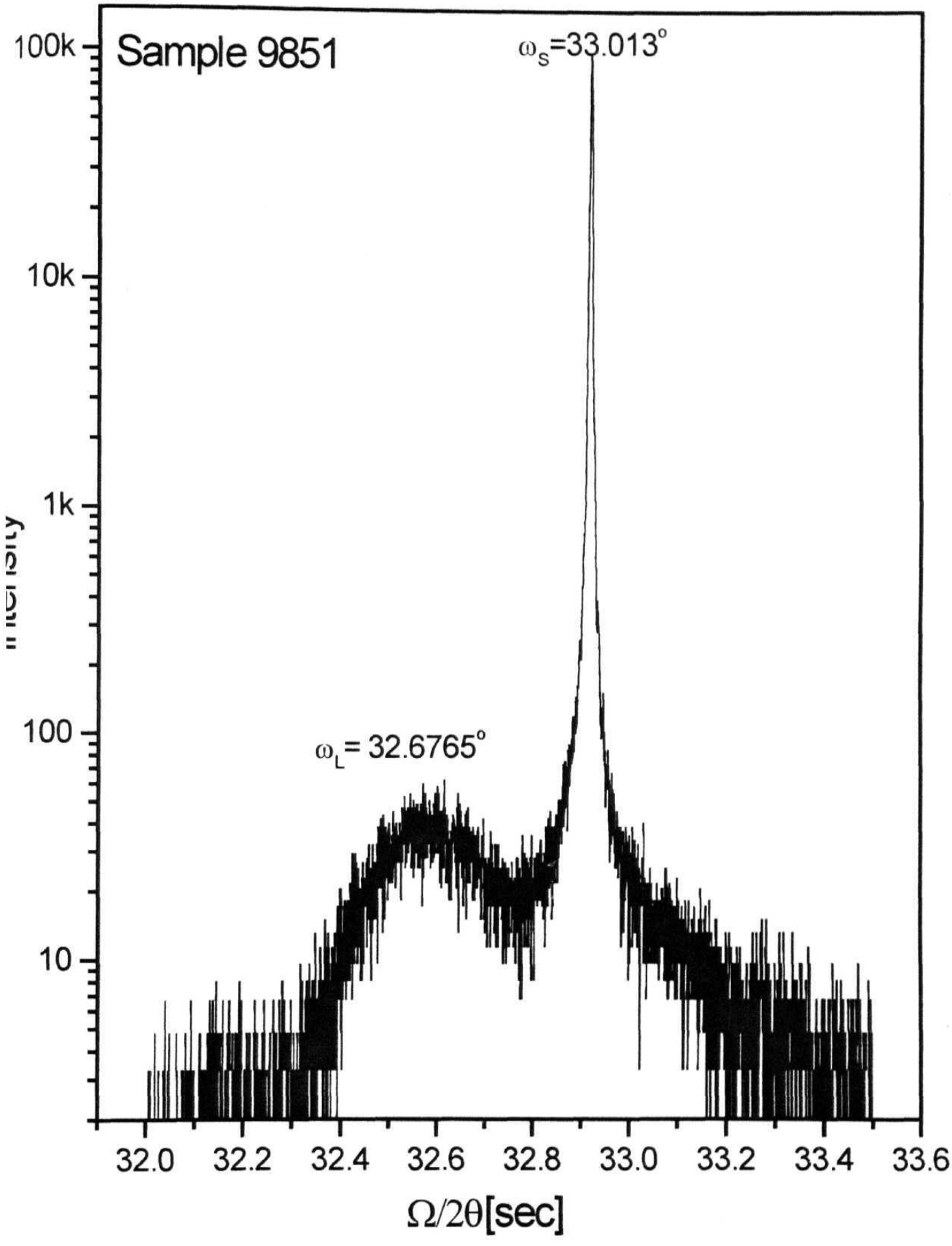


**Fig 3.11:** Ω/2θ scan around (004)

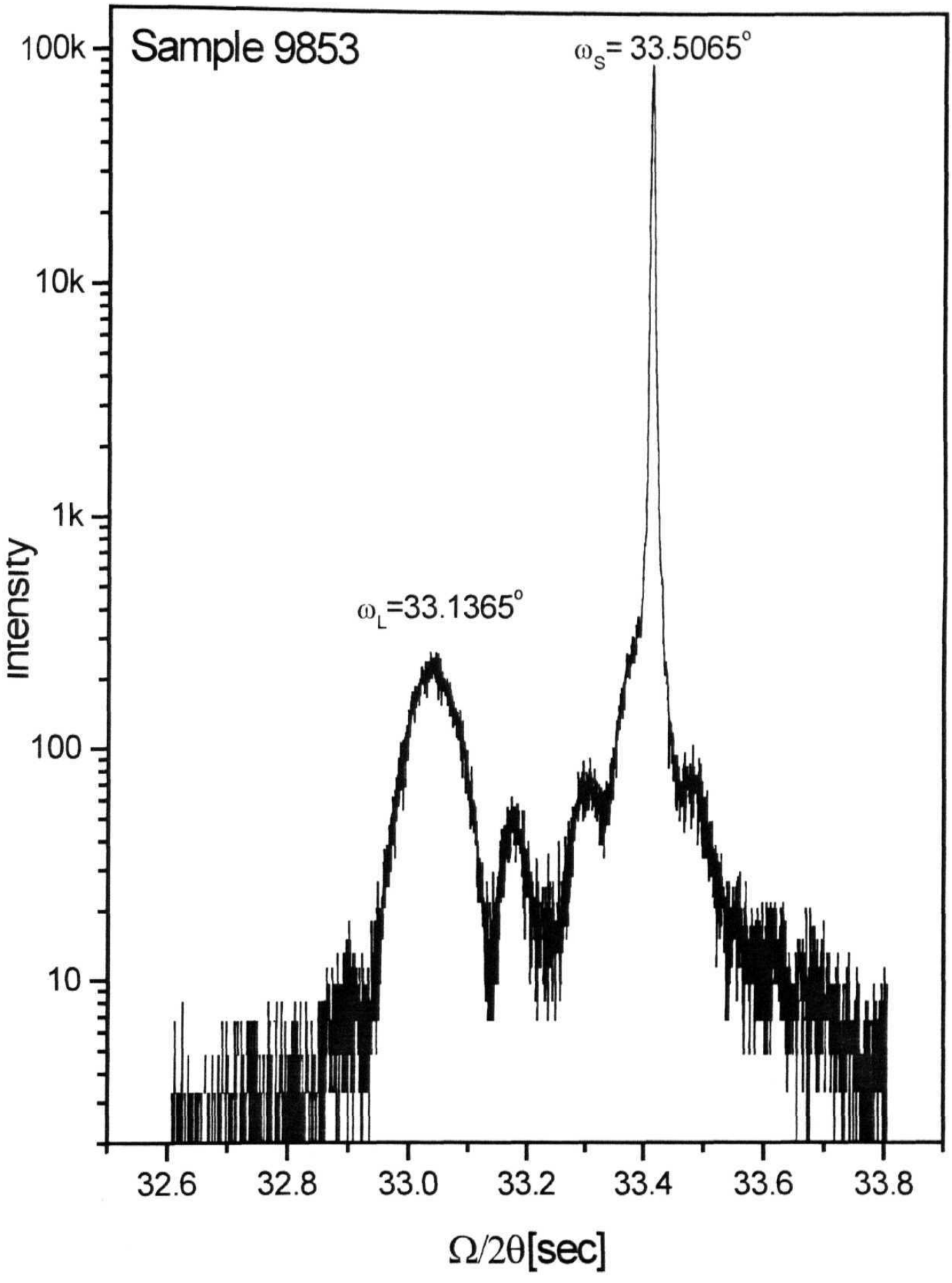


**Fig 3.12:** Ω/2θ scan around (004)

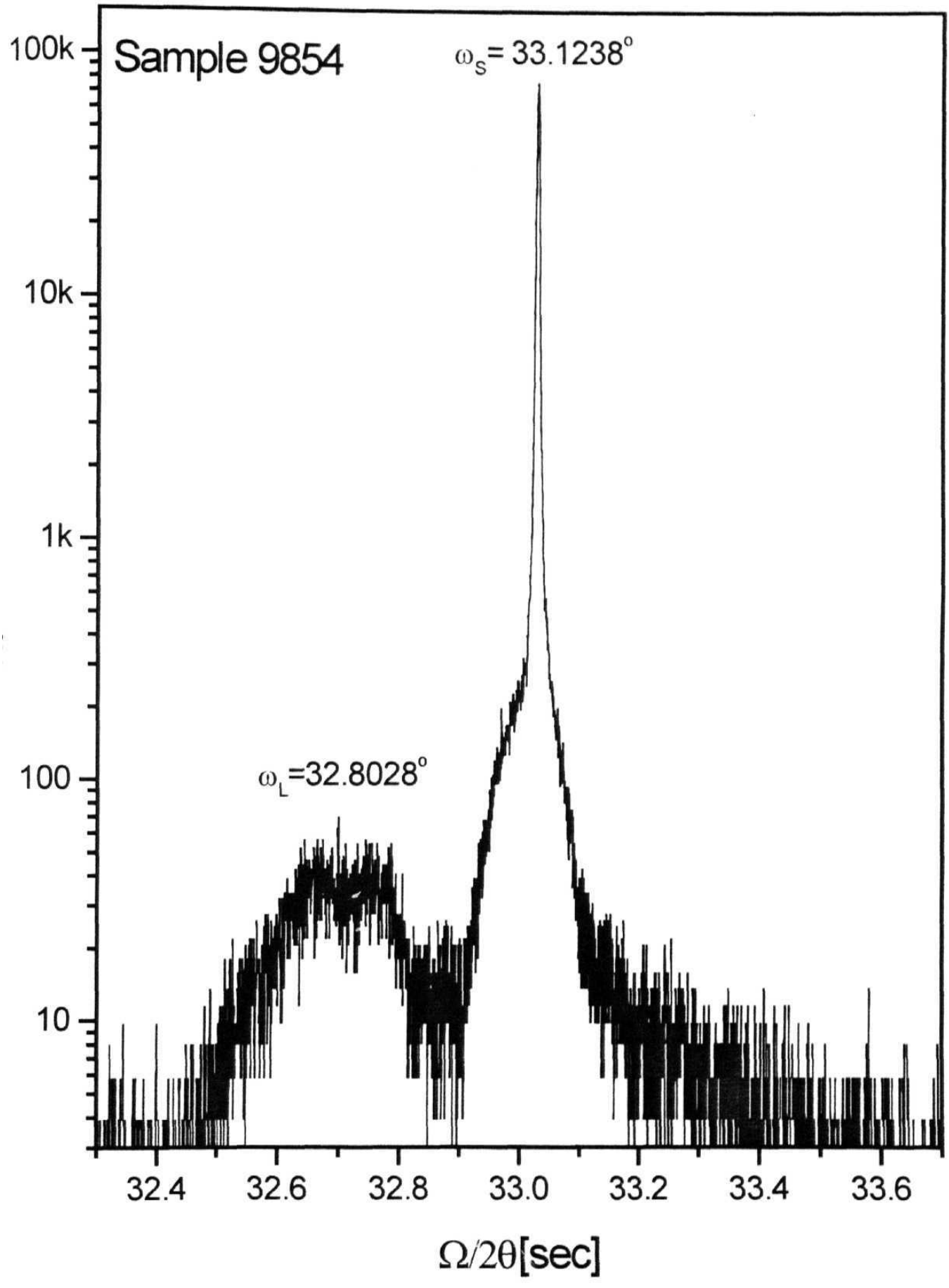


**Fig 3.13:** Ω/2θ scan around (004)

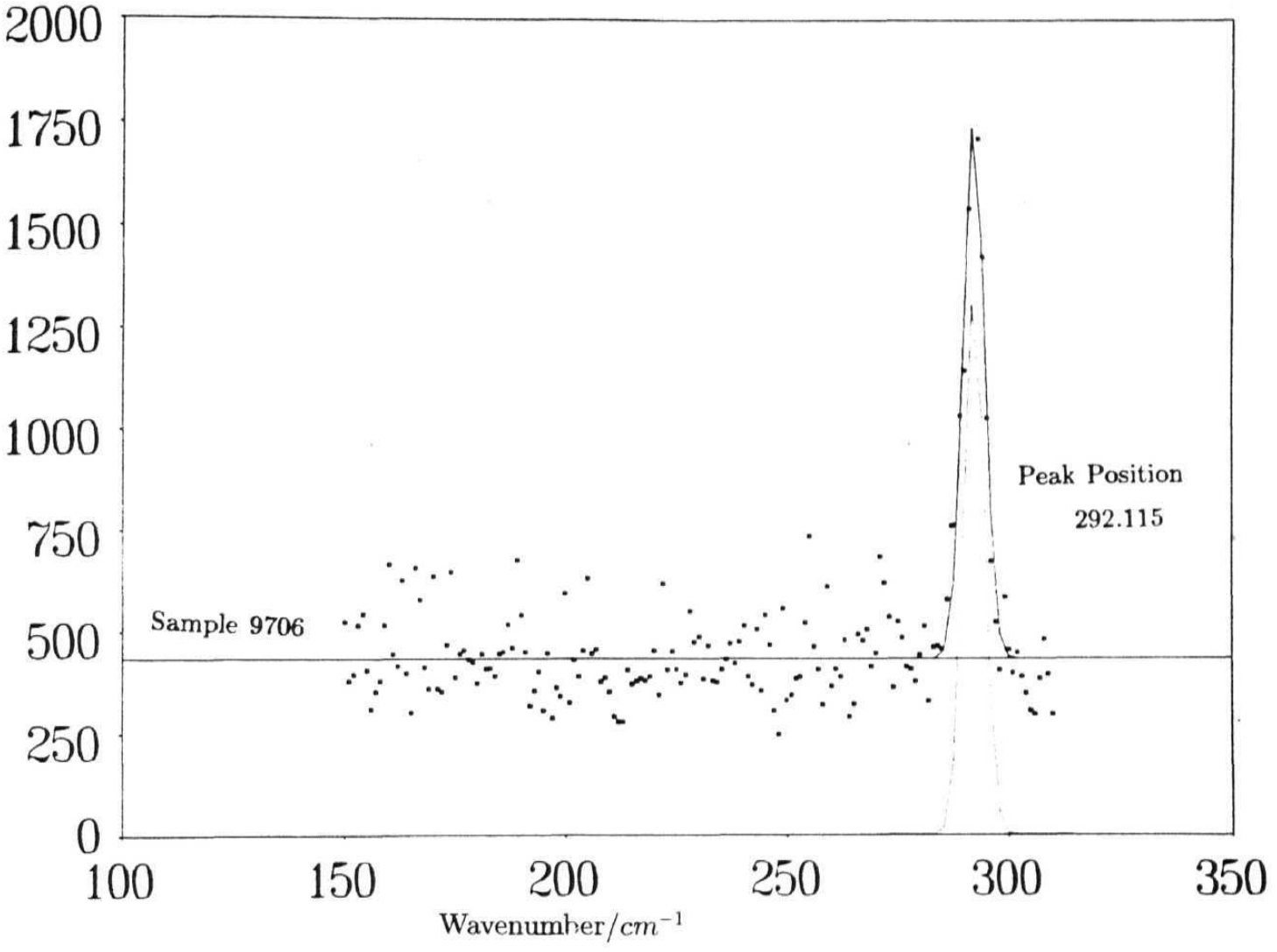


**Fig 3.14:** Raman Spectrum showing the peak, fitted using the PEAKFIT software.

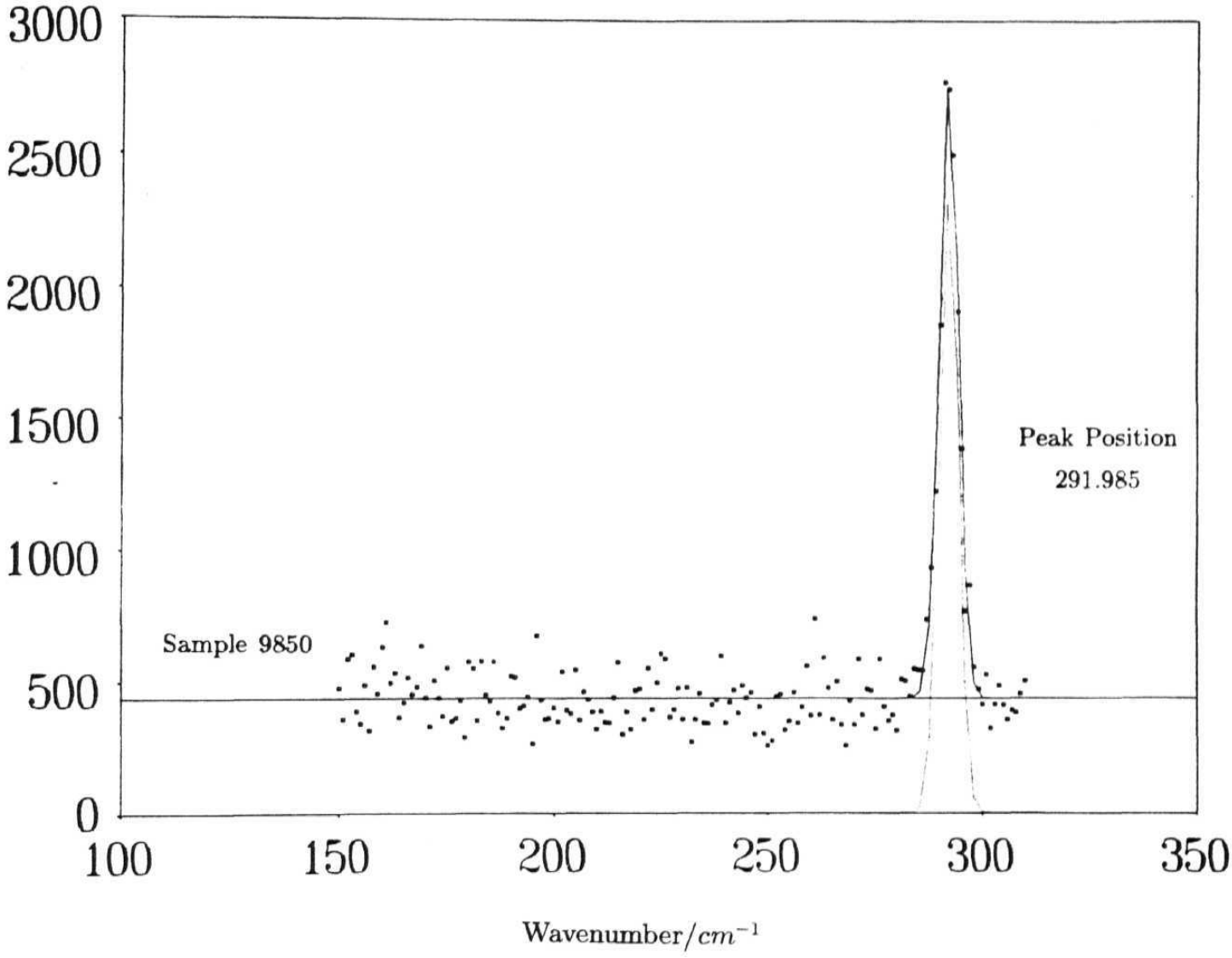


Fig 3.16: Raman Spectrum. The dashed line shows the fitted curve.

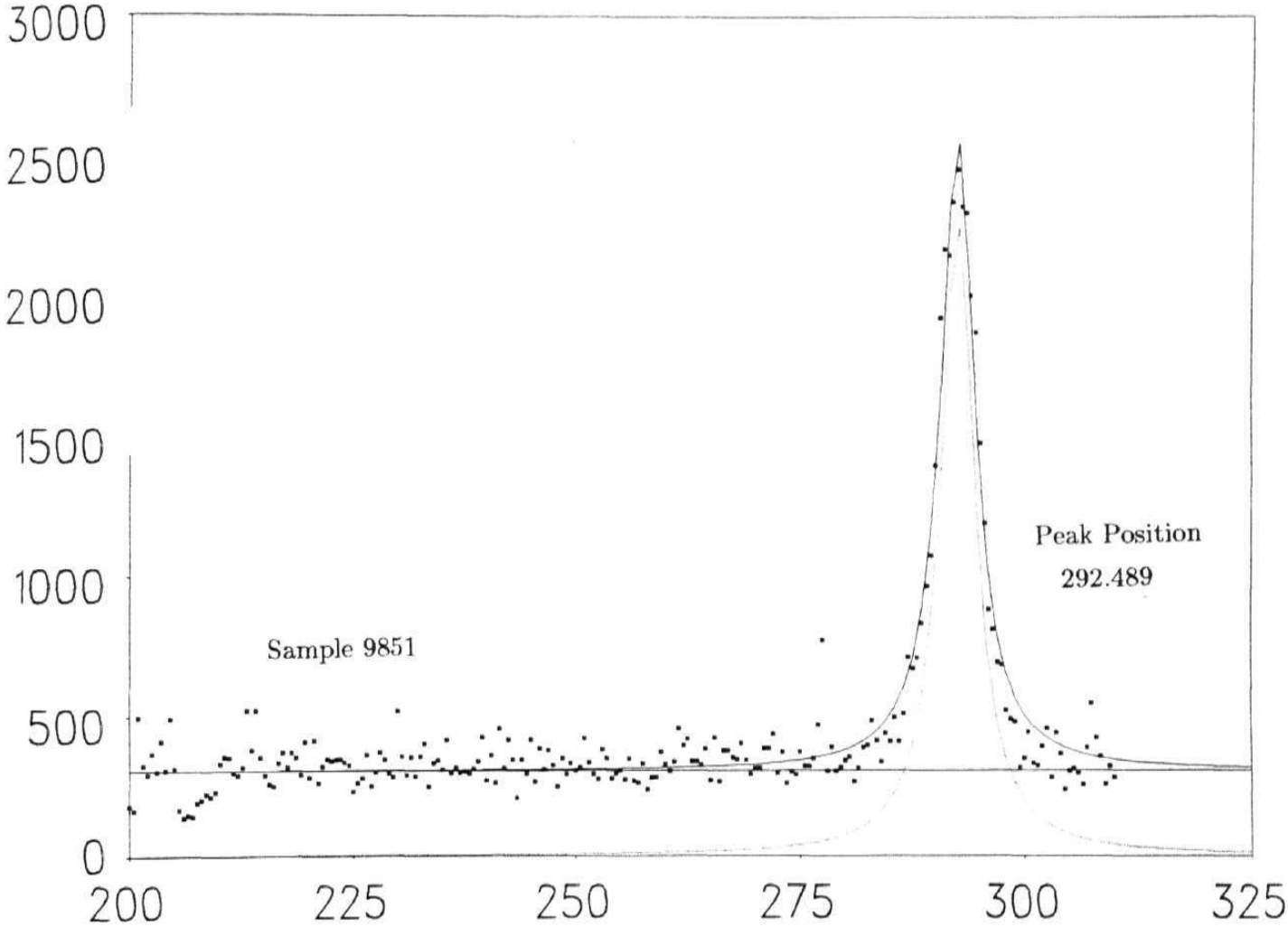


Fig 3.17: Raman Spectrum. The dashed line shows the fitted curve.

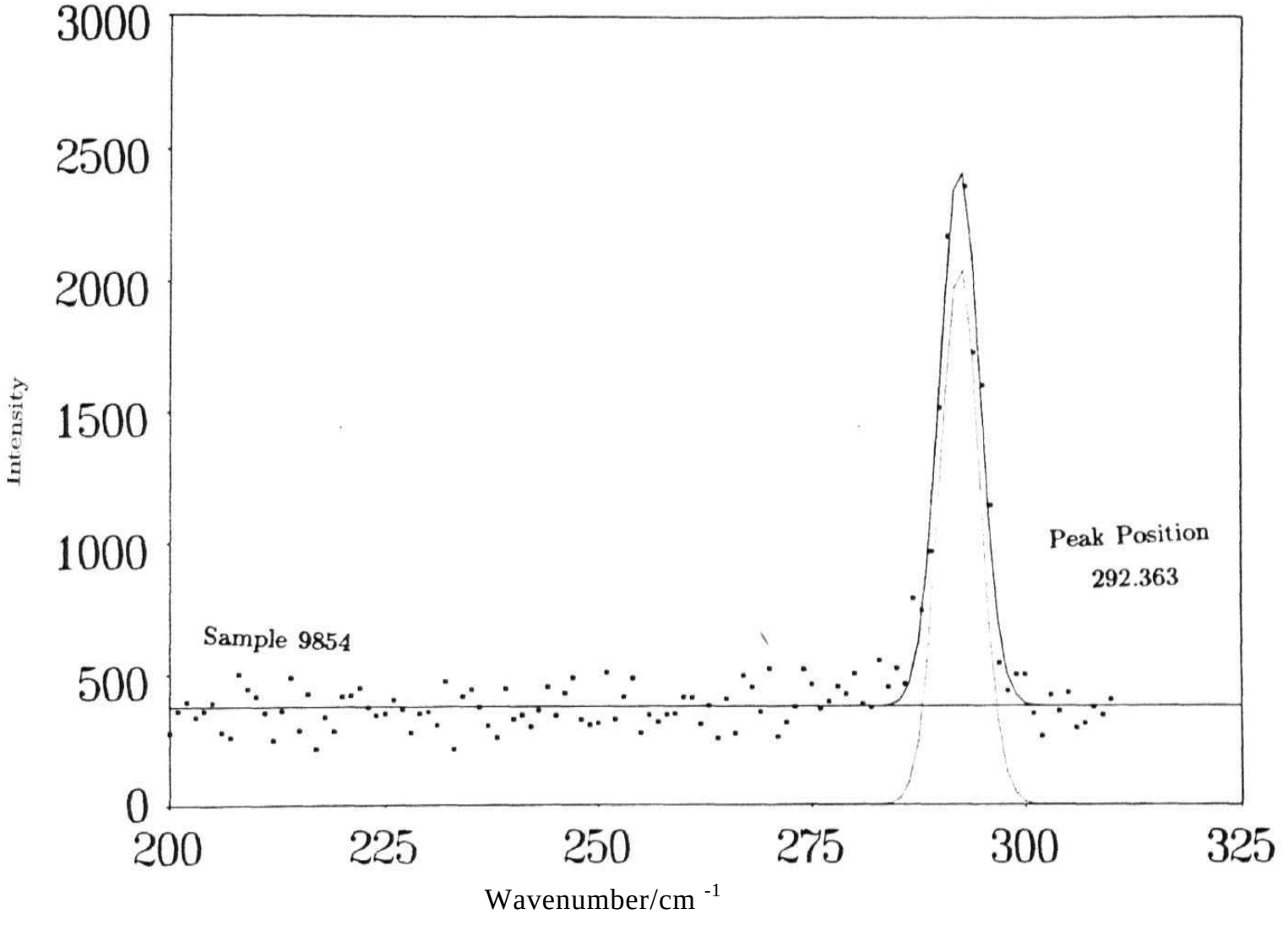


Fig 3.19: Raman Spectrum. The dashed line shows the fitted curve.

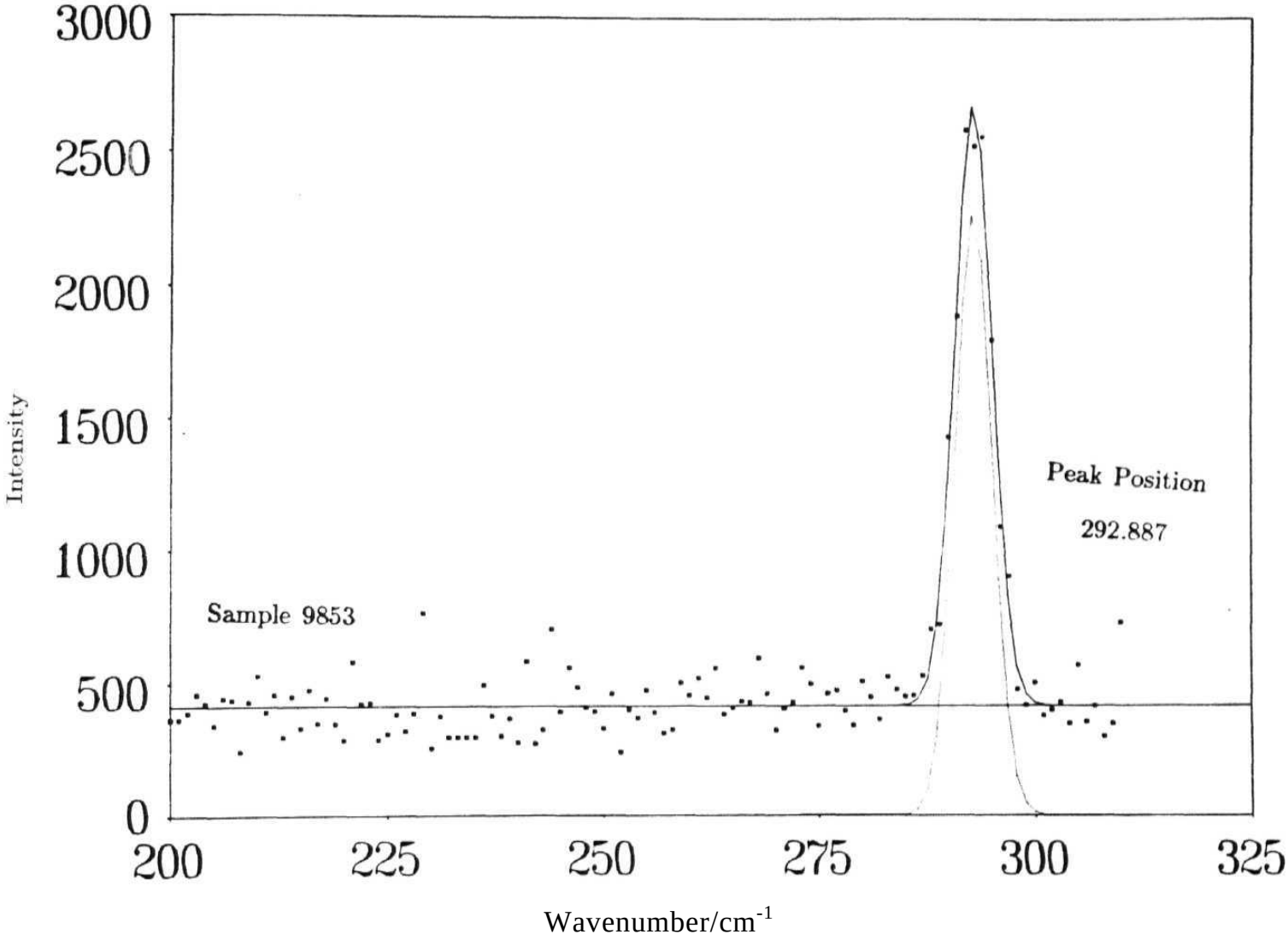


Fig 3.18: Raman Spectrum. The dashed line shows the fitted curve.

Strain values in such technologically important SLS can also be found out by empirical formula.

$$\epsilon_{\perp} = \frac{(a_L^{\perp} - a^{\perp})}{a^{\perp}} \tag{3.74}$$

and

$$\epsilon_{\parallel} = \frac{(a_L^{\parallel} - a^{\parallel})}{a^{\parallel}} \tag{3.75}$$

where $a_l^{\perp}$ and $a_l^{\parallel}$ are the lattice constants of the strained layer in the direction perpendicular and parallel to the interface respectively. $a$ and a" are the corresponding values for the free lattice of the epilayer material. The tetragonal distortion in the epilayer $\epsilon_t$ is related to $\epsilon_{\parallel}$ and $\epsilon_{\perp}$ as

$$\epsilon_t = \epsilon_{\parallel} - \epsilon_{\perp} \tag{3.76}$$

These can be calculated by finding out the lattice constants of $In_xGa_{1-x}As$ using the Vegard's law

$$a_{In_xGa_{1-x}As} = x a_{\mathrm{InAs}} + (1-x) a_{\mathrm{GaAs}} \tag{3.77}$$

and the lattice constants $a_{GaAs} = 5.6532\mathring{A}$ and $a_{InAs} = 6.0584\mathring{A}$ , we find $a_{In_{0.1}Ga_{0.9}As} = 5.6937\mathring{A}$. $\epsilon_{\parallel}$ and $\epsilon_{\perp}$ are related to each other by the elastic constants c11, c12 etc as

$$\epsilon_{\parallel} = -\frac{c_{11}}{2c_{12}}\epsilon_{\perp} \tag{3.78}$$

which again can be found by Vegard's law. Assuming fully strained epilayer, the expected value of $\epsilon_{\perp}$ is 0.014 which is higher than the $\epsilon_{\perp}$ values obtained from the two measurements described above. The lower $\epsilon_{\perp}$ value can occur if the strained layer relaxes. The critical thickness for strain of 0.01 obtained from the Matthews and Blackeslee formulation is close to 200 A. Therefore a partial relaxation of the strain in the epilayer cannot be ruled out at this stage.

The lattice constant of unstrained $In_{0.1}Ga_{0.9}$ will henceforth be named as $a_{epi}$ and that of the GaAs as $a_S$. According to the definition, the tetragonal distortion that one determines from ion channeling is the change in the lattice parameter from unstrained to strained value. X-ray scattering determines the strain from the lattice parameter the epilayer takes with respect to the substrate lattice parameter.

The two can **thus** be related as follows:

**Ion Channeling:**

$$\epsilon_t \approx \frac{\Delta\theta}{\sin\theta\cos\theta} = \epsilon_{\parallel} - \epsilon_{\perp} \tag{3.79}$$

$$\approx \frac{a_{\parallel} - a_{\perp}}{a_{\text{epi}}} \tag{3.80}$$

**XRD:**

$$\epsilon_f = \frac{a_{\parallel} - a_{\perp}}{a_S} \tag{3.81}$$

This $\epsilon_f$ is evaluated from the $\epsilon_{\perp}^{XRD}$ that is determined from X-ray measurements as follows [22]

$$\epsilon_{\perp} = \frac{a_{\perp} - a_S}{a_S} \qquad \text{and} \qquad \epsilon_{\parallel} = \frac{a_{\parallel} - a_S}{a_S} \tag{3.82}$$

When the epilayer is fully strained,

$$\begin{aligned} a_{\parallel} &= a_S \qquad \text{and so} \qquad \epsilon_{\parallel} = 0 \\ \epsilon_{xx} = \epsilon_{yy} &= \frac{a_{\parallel} - a_{epi}}{a_S} = \epsilon_{\parallel} - \epsilon_f \qquad (3.83) \\ \epsilon_z &= \frac{a_{\perp} - a_{epi}}{a_S} = \epsilon_{\perp} - \epsilon_f \\ &= -\frac{2\nu}{1-\nu}\epsilon_{xx} \qquad (3.84) \\ \therefore \quad \epsilon_f &= \frac{2\nu}{1+\nu}\epsilon_{\parallel} + \frac{1-\nu}{1+\nu}\epsilon_{\perp} \qquad (3.85) \end{aligned}$$

So, in the case of a fully strained sample, $\epsilon_{\parallel} = 0$ and hence,

$$\epsilon_f = \frac{1-\nu}{1+\nu}\epsilon_{\perp}$$

where $\nu$ is the Poisson ratio $= c_{12}/c_{11} + c_{12}$.

$$\therefore \qquad \epsilon_{\perp} = \frac{a_{\perp} - a_S}{a_S} \tag{3.86}$$

and thus,

$$\epsilon_t = -\epsilon_\perp(\frac{a_S}{a_{epi}}) \tag{3.87}$$

The strain values that are tabulated in table 3.2 can be compared straightforwardly.

# References


[1] H.C. Casey and M.B. Panish, *Hetero structure Lasers*, Academic Press, New York, 1978.

[2] L. Esaki and R. Tsu, IBM J. Res. Dev., 14, 11, 1970.

[3] G.B. Stringfellow, Rep. Prog. Phys., 45, 469, 1982.

[4] G.B. Stringfellow, P.F. Lindquist, T.F. Cast and R.A. Burmister, J. Elect. Mat,, 3, 497, 1974.

[5] M. Ettinberg, J. App. Phys., 45, 901, 1974.

[6] G.B. Stringfellow, J. Cryst, Growth, 27, 21, 1974.

[7] G.B. Stringfellow, J. Phys. Chem. Solids, 35, 775, 1974.

[8] G.C. Osbourn, J. Appl. Phys., 53, 1586, 1982.

[9] R. Hull and J.C. Bean, J. Vac. Sci. Tech A7, 2580, 1989; R. Hull and J.C. Bean App. Phys. Lett., 54, 925, 1989.

[10] J.W. Matthews, J. Vacc. Sci. Technol., 12, 126, 1975-

[11] J.W. Matthews and A.E. Blackelee, J. Cryst, Growth, 27, 118, 1974.

[12] J.W. Matthews and A.E. Blackelee, J. Cryst. Growth, 32, 265, 1974.

[13] F.C. Frank and J.H. Van der Merwe, Proc. Roy. Soc., A198, 205, 1949.

[14] F.C. Frank and J.H. Van der Merwe, Proc. Roy. Soc, A198, 216, 1949.

[15] F.C. Frank and J.H. Van der Merwe, Proc. Roy. Soc, A200, 125, 1949.

[16] J.H. Van der Merwe and C.A.B. Ball in "Epitaxial Growth" Part B, pg: 1933-528, ed: J W Matthews, Academic Press, New York, 1975.

[17] J W Mayer, J F Zeigler, L L Chang, R Tsu and L Esaki, J. Appl. Phys, 44, 2322, 1973.

[18] F.W. Saris, W.K. Chu, CA. Chang, R. Ludeke and L. Esaki, Appl. Phys. Lett, 37, 931, 1980.

[19] S.T. Picraux, L.R. Dawson, G.C. Osbourn and W.K. Chu, Nucl. Ins. and Meth, 218, 57, 1983.

[20] L.C. Feldman, J.W. Mayer and S.T. Picraux, "Materials Analysis by Ion Channeling", Academic Press, New York, 1982.

[21] W.K. Chu, J.W. Mayer and M.A. Nicolet, "Backscattering Spectrometry", Academic Press, New York, 1978.

[22] C.R. Wie, Materials Sc. and Engg., **R13**. 1, 1994.

[23] L. Vegard, Zeit. fur Physik, 5, 17-26,k (1921).

[24] E.F. Hockings, I. Kudman, T.E. Seidel, CM. Schmerz and E.F. Steigman, Journ. App. Phys., **37,** 2879-2885, (1966).

[25] J.S. Multani and J.S. Sandhu, J. Electr. Soc. Vol. 126, 1086, 1979.

[26] W.J. Bartels, J. Vac. Sc. Tech, B1, 338, 1983.

[27] M. Constant, N. Matrullo, A. Lorriaux and L. Boussekey, J. Raman Spect., 27, 225, 1996.

[28] S. Ernura, S. Gonda, Y. Matsui and H. Hayashi, Phys. Rev. B, 38, 3280, 1998.

[29] K. Sekar, P.V. Satyam, G. Kuri, D.P. Mahapatra and B.N. Dev, Nucl. Inst. Meth **B73,** 63, 1993.

[30] R. Loudon, Adv. Phys., 13, 423, 1964.

[31] E. Anastassakis, A. Pinczuk, E. Burnstein, F. H. Pollak and M. Cardona, Soild State Commun., 8, 133, 1970.

[32] F. Cerdeira, C. J. Buchenauer, F. H. Pollak and M. Cardona, Phys. Rev. B, 5, 580, 1972.

[33] Azher M. Siddiqui, Anand P. Pathak, B. Sundarvel, Amal K. Das, K. Sekar, B.N. Dev and B.M. Arora, Nucl. Inst. and Meth. (B), 142, 389, 1998.

[34] S.T. Picraux, B.L. Doyle and J.Y. Tsao in Strained-layer Superlattices: Materials Science and Technology, Vol 33 "Semiconductors and Semimetals", ed: Thomas P Pearsall, Academic Press, New York (1991).

[35] S.T. Picraux, L.R. Dawson, G.C. Osbourn and W.K. Chu, Appl. Phys. Lett, 43, 930, 1983.

[36] S.T. Picraux, L.R. Dawson, G.C. Osbourn, R.M. Biefeld and W.K. Chu, Appl. Phys. Lett, 42, 1020, 1983.

[37] S.T. Picraux, W.K. Chu, W.R. Allen and J.A. Ellison, Nucl. Ins. and Meth, **B15,** 306, 1986.

[38] S.T. Picraux, J.Y. Tsao and D.K. Brice, Nucl. Ins. and Meth, **B19/20,** 21, 1987.

[39] S.T. Picraux, L.R. Dawson, J.Y. Tsao, B.L. Doyle, S.R. Lee Nucl. Ins. and Meth, **B33,** 891, 1988.

[40] S.T. Picraux, R.M. Biefeld, W.R. Allen, W.K. Chu and J.A. Ellison, Phys. Rev. **B38,** 11086, 1988.

[41] W. K. Chu, C. K. Pan, C A Chang, Phys. Rev. **B28,** 4033, 1983.

[42] A.T. Fiory, J.C. Bean, L.C. Feldman and I.K. Robinson, J. Appl. Phys., 56, 1227, 1984.

[43] A.H. Hamdi, V.S. Speriosu, M.A. Nicolet, J.L. Tandon, Y.C.M. Yeh, J. Appl. Phys., 57, 1400, 1985.

[44] Shin Hashimoto, Y.Q. Feng and W.M. Gibson, Nucl. Inst. and Meth, B13, 45, 1986.

[45] A. Kozanecki, J. Kaczanowski, B.J. Sealy and W.P. Gillin, Nucl. Ins. and Meth, **B118,** 640, 1996.

Chapter 4

# CATASTROPHIC DECHANNELING RESONANCE STUDY OF $In_xGai_{1-x}As/GaAs$ MULTILAYERS

There are three widely used methods of ion hanneling to measure strain in SLS. First, determination of strain from the shift in the channeling dips and secondly the influence of crystal imperfections on ion channeling in SLS which results in dechanneling along the inclined directions. The third method is based on a resonance condition in which if the period of SLS structure matches with the average channeled-particle wavelength, there will be a rapid increase in dechanneling after a certain depth. This phenomenon is called *Catastrophic Dechanneling Resonance* (CDR), which is less commonly used but highly sensitive method for strain measurements in SLS. The channeled particles oscillate between the planes and have a classical trajectory wavelength which starts with all the particles in phase. Since the wavelength varies only moderately for particles of different amplitude, phase matching is retained to moderate depths. At shallow depths, the channeled yield is similar to that of a bulk crystal and after penetrating a few layers, a very strong increase in the channeled signal occurs until almost all the beam is dechanneled. This method is suitable only for thick layers since the half wavelength of channeled particles is of the order of 30nm; this must be made equal to the path length per superlattice layer along the inclined planar channeling direction- Inspite of this constraint, CDR technique is attractive for strain analysis at very low strains: it is the most sensitive of all the ion-channeling techniques for strain measurements.

The above mentioned behaviour is readily understood in a phase-plane description (fig. 4.1). The incident beam is represented by a line on a diagram of normalized transverse momentum (i.e. angle) versus normalized position in the channel.

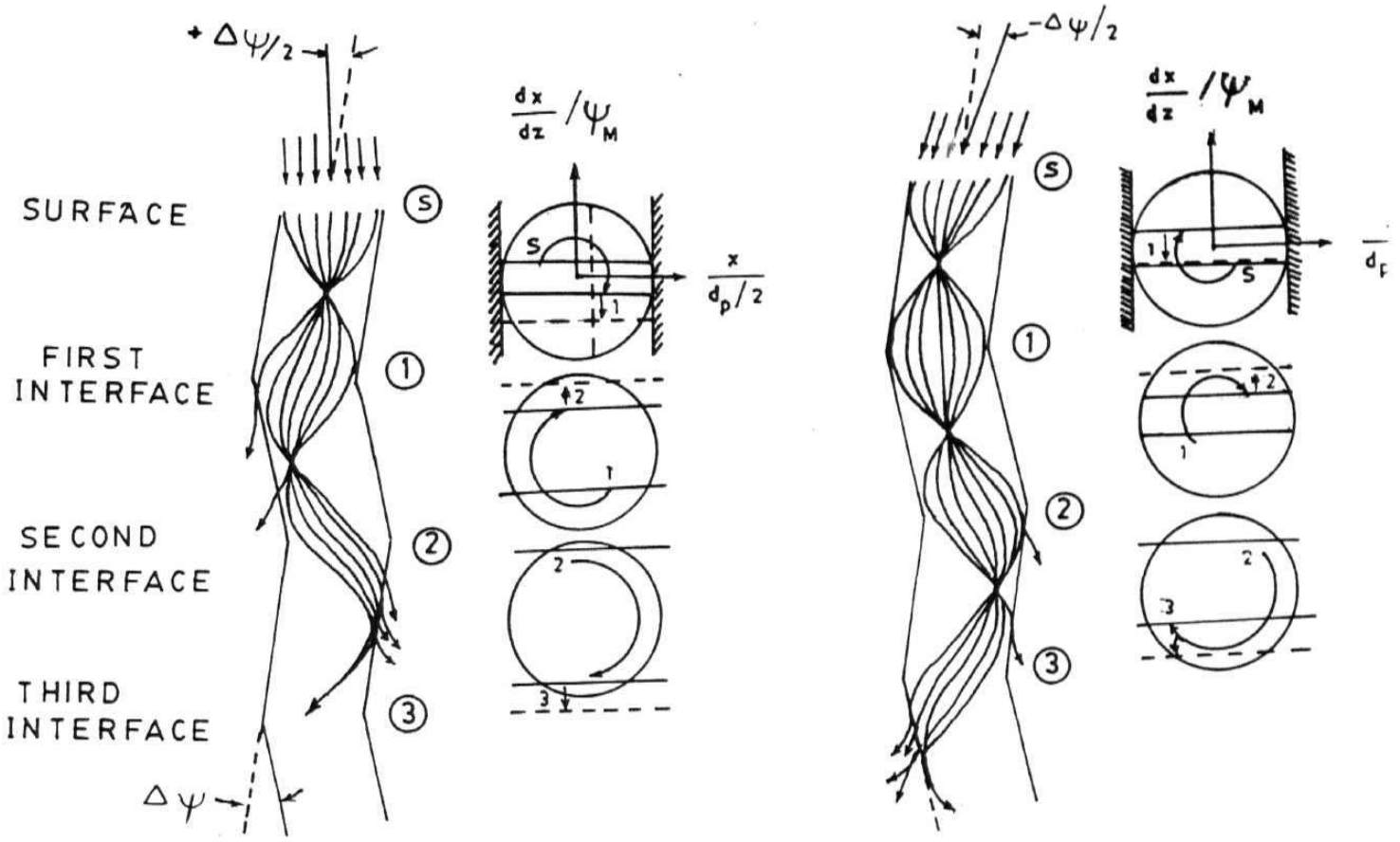


**Fig 4.1**: The calculated trajectories for 1.2 MeV $He^+$ in SLS for two different incident angles, (a) for $\psi_o = +\Delta\psi/2$ and (b) for $\psi_o = -\Delta\psi/2$.

This line rotates as the channeled beam penetrates the crystal and undergoes a vertical shift at each interface according to the sign and magnitude of the tilt angle $\Delta\psi$. As a result, in the simple modified harmonic model, the focus point of the beam moves close to the channel wall in each successive layer until the particles have sufficient transverse energy to penetrate the planes. In penetrating each layer, the beam changes direction since this corresponds to travelling a half wavelength, but the crystal planes also change their direction by $\Delta\psi$. Thus, the angle of the channeled particles relative to the crystal planes increases at each interface until they become sufficiently large so that particles can no longer be steered by the crystal planes and are *dechanneled.* The layer in which CDR occurs is directly related to the tilt angle $\Delta\psi$ at each interface and incident angle of the beam with respect to the superlattice planes.

We have undertaken systematic experimental and theoretical study [12] on strain and strain relieving mechanisms in technologically important SLS using ion channeling methods. CDR occurs when half wavelength – of oscillatory motion of a planar channeled ion beam matches the path length per layer (s) of SLS which leads to sudden increase in the dechanneling after a certain depth. Study of this resonance gives the information on the strain present in SLS. Harikumar et al [2] have theoretically studied the parameter dependence of CDR (energy, incident angle, tilt angle etc) in $GaAs_xP_{1-x}/GaP$ using Thomas Fermi type potentials and a realistic Shell model potential and their calculations [2-4] were in good agreement with experimental results [4]. Here we report, to the best of our knowledge, for the first time, the calculations of the parameter dependence of CDR for $He^4$ ion beam along (110) plane in $In_{0.1}Ga_{0.9}As/GaAs$ superlattices using Moliere potential. A similar study was earlier carried out for $In_{0.2}Ga_{0.8}As/GaAs$ using Biersack and Shell Model Potential. The Shell potential is free from the statistical nature and takes into account the detailed atomic shell structure of the target material. The shell model charge density and shell potential is earlier used successfully by Harikumar et al [5] for various other problems like stopping power, channeling radiation etc. in the related problems of ion channeling studies.

## 4.1 Dechanneling in SLS

Under CDR conditions, a large fraction of planar channeled particles is simultaneously focused onto the channel wall as a consequence of resonance. The minimum impact parameter $r_c$ defines the cut-off distance for a channeled trajectory, and if a particle approaches a plane within this distance $r_c$ of that plane, it is considered to be dechanneled. The equation of motion for the planar channeled particle in an SLS is given by [1-5]

$$\frac{d^2X}{dz^2} + \frac{1}{2E_z}\frac{d}{dX}Y_2(X) = \sum_{j=1}^{n}(-1)^j \Delta\psi\delta(z - js) \tag{4.88}$$

where x and z are the transverse and longitudinal displacements of the channeled particle respectively and x is measured from the midpoint between the planes. $E_z$ is the longitudinal energy and almost equals the incident energy E, n is the number of layers and tilt $\Delta\psi$ is a result of the elastic accommodation of the strain and is a direct measure of strain in SLS. $Y_2(x)$ is the averaged continuum model planar potential due to two planes surrounding the particle trajectory. The well known Moliere potential for planar channeling situation can be written as ([2] and further references therein)

$$Y(y) = 2\pi N d_p Z_1 Z_2 e^2 \sum_{j=1}^{3} a_i \frac{e^{-b_i y}}{b_i} \tag{4.89}$$

Here $Z_1$ and $Z_2$ are the atomic numbers of the projectile and the target atoms (SLS) respectively, e is the electronic charge, N is the bulk density of atoms in the crystal, $d_p$ is the interplanar distance, y is the distance measured from the plane and $a_i$ and $b_i$ are fitting constants. The total transverse energy $E_\perp$ is conserved and is given by [6]

$$E_\perp = E(\frac{dx}{dz})^2 + Y_2(x) \tag{4.90}$$

where dx/dz= $\psi$ is the incident angle. From this we get

$$dz = \sqrt{E}\frac{dx}{\sqrt{E_\perp - Y_2(x)}} \tag{4.91}$$

which yields after integration, the wave length of particle trajectory as a function of transverse energy as

$$\lambda = 4\sqrt{E}\int_0^a \frac{dx}{\sqrt{E_\perp - Y_2(x)}} \tag{4.92}$$

Here $a$ is the amplitude of motion defined by $Y_2(a) = E_\perp$.

Corresponding planar Shell potential is given by [2, 3]

$$Y_S(y) = 2\pi N dp Z_1 e^2 \sum_j \frac{\omega_j}{2n_j} \sum_{k=1}^{2n_j} k(2\xi_j)^{2n_j-k} \sum_{m=o}^{2n_j-k} e^{-2\xi_j y} \frac{y^m}{m!\ (2\xi_j)^{2n_j-k-m+1}} \tag{4.93}$$

where $n_j$ is the principal quantum number, $\omega_j$ is the occupation number of the j-t'ı shell, $\xi_j$ is the optimized orbital exponent.

For each incident angle $\psi_o$, the trajectory calculations are carried out for 200 incident particles spaced uniformly between the planes(i.e varying the initial transverse displacement $x_o$ from $\frac{+d_p}{2}$ and $\frac{-d_p}{2}$. The trajectory is traced by numerically integrating (equation 4.1)for a given initial $\psi$ ($\psi = \psi_o$), $x(= x_o)$ *and* $z(= z_o)$. A particle is said to be dechanneled if it penetrates within a minimum impact parameter $r_c = 1.25a_T$ of that atomic plane. When a particle crosses the first interface ($z = s, j = 1$) there should be a change in $\psi$ by an amount equal to $-\Delta\psi$. At second interface ($z = 2s, j = 2$), this amount should be $+\Delta\psi$ because of opposite tilt. We have used this criterion for checking the program for various values of $\Delta\psi$ and $\psi$. Distribution of $x_o$ and $\psi_o$ are tabulated and sorted to give the depth profile of dechanneling. Total distribution of incident particle is normalized to unity which implies that total dechanneling corresponds to a situation where yield $\chi$ becomes unity. All the numerical calculations were carried out at MicroVax II system with the help of IMSL Math/Lib$^{TM}$.

## 4.2 Modified Harmonic Model

Let $\psi_c$ be the *critical angle* for channeling, and $x_c$ be the *critical distance* defined such that $r_{min} = d_p/2 - x_c$. Since the *transverse energy* is conserved, *critical transverse energy* $E_{\perp,c}$ can be written as

$$E\,\psi_c^2 \;=\; Y_2(x_c) \tag{4.94}$$

Equation (4.90) can be simplified if the potential is approximated by a simple harmonic potential, $Y_2(x) \propto x^2$, giving

$$\frac{(dx/dz)^2}{\psi_c^2} + \frac{x^2}{x_c^2} = r_p^2 \tag{4.95}$$

In the modified-harmonic model all particles have the same wavelength (equation 4.92) because of the harmonic nature of the potential and motion of a particle in the phase plane is on a circle of radius $r_p$ with co-ordinates $(2x/x_c,(dx/dz)/\psi_c)$ as shown in figure 4.1 [8, 9]. (For simplicity the *critical distance* $x_c$ on the phase circle was shown as *dp/2* ). Unit circle (Fig. 4.1) corresponds to *critical transverse energy* for particles to remain channeled [10]. A uniform incident beam of particles is represented by a horizontal line *S* on a diagram of normalized transverse momentum (angle) versus normalized lateral position in the channel. This assumption is possible because in *harmonic approximation* the wavelength is independent of transverse energy [8]. For larger incident angles $(+\psi_o)$, the line will be placed higher above the *x - axis* and for negative incident angles the line will be placed below the *x - axis.* This line rotates as the channeled beam penetrates the crystal, and undergoes a vertical shift at each interface according to sign and magnitude of the tilt $\Delta\psi$ [4]. Since the *path length per layer* s is half the wavelength (A) of the beam (See Fig. 4.2), while penetrating each layer the beam changes its direction. At the interface the crystal plane also changes its direction by $\pm\Delta\psi$ with respect to the sign of the incident angle. Thus, the angle of the channeled particles relative to the crystal planes increases at each interface until they become sufficiently large so that continuum potential can no longer restrict the motion of the particles with in the plane and consequently dechanneling of the particles occur. Since the outer circle corresponds to the maximum transverse energy for which particles remain channeled, the complete dechanneling situation corresponds to the shifting of line *S* completely outside the circle (shown in Fig. 4.1.)

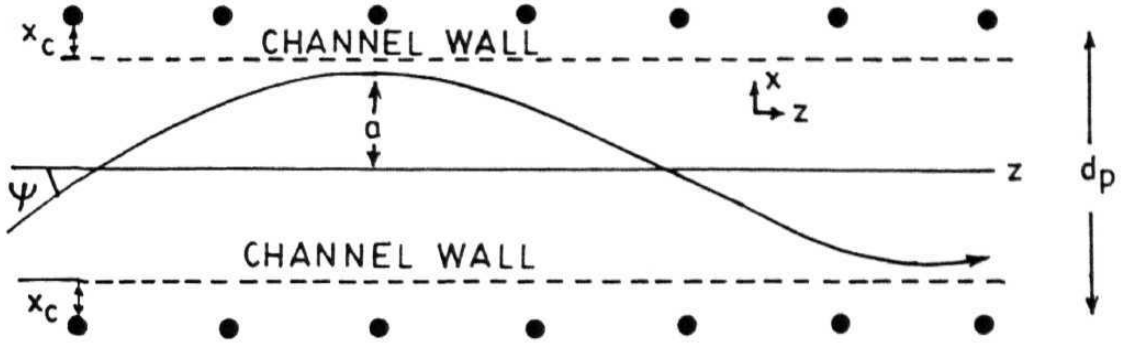


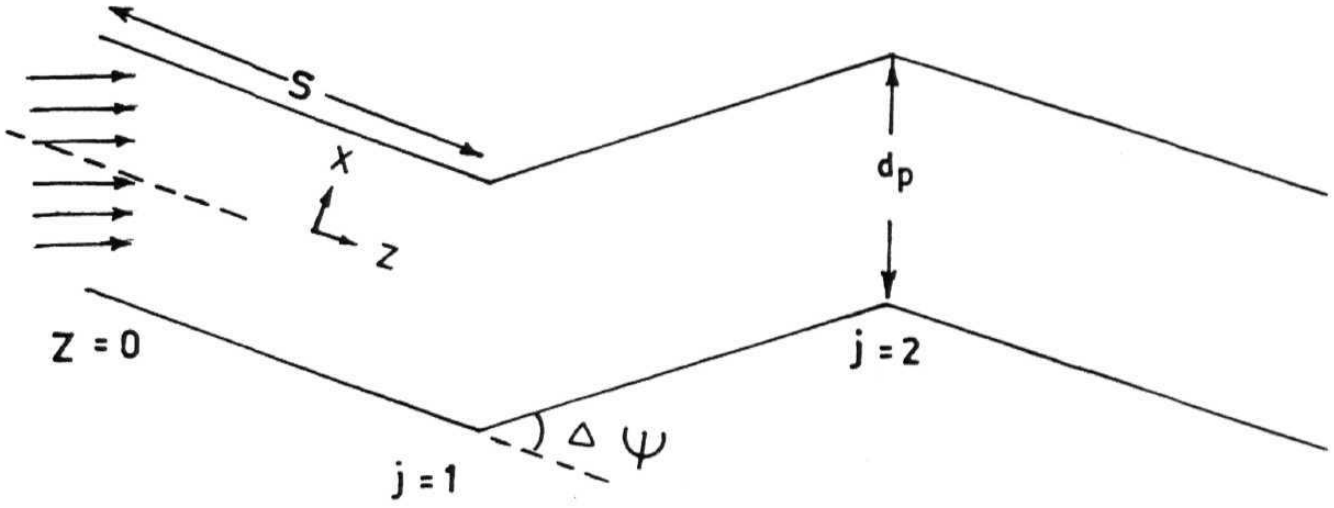


Fig 4.2: (a) The trajectory of a planar channeled particle. $d_p$ is the inter-planar spacing, $r_c$ is the minimum impact paramter for channeling, $\psi$ is the incident angle and a is the amplitude of motion of a charged particle. (b) Schematic diagram of <110> planar channel of an SLS. $\Delta\psi$ is the tilt angle and *s* is the path length per layer of the SLS.

## 4.3 Results and Discussions

The calculated trajectories for 1.2 MeV $^4He$ channeled in a **SLS** for incident angles $\psi_o = -\Delta\psi/2$ and $\psi_o = +\Delta\psi/2$ respectively are also shown in figure 4.1 from where it is evident that there is a delay in depth for catastrophic dechanneling of one layer for $\psi_o = -\Delta\psi/2$ case. Since the starting line in the *phase plane* is below the origin for particles incident at an angle $\psi_o = -\Delta\psi/2$, its evolution out of the circle at each interface trails that of particles incident at an angle $\psi_o = +\Delta\psi/2$ by exactly one layer.

Moving the incident angle to increasingly larger negative values shifts the line *S* lower on the unit circle and thereby delays the focusing of the channeled particle into the planar wall [10]. It can be inferred from above mentioned *phase-plane analysis,* that if one reduces the incident direction $\psi_o$ by $\Delta\psi$ it delays the depth of the *CDR* by one layer. Let $D_c(\psi_o)$ denote the depth of the *CDR*, then

$$D_c(\psi_o) - D_c(\psi_o - \Delta\psi) = -1 \tag{4.96}$$

and hence

$$\frac{\Delta D_c(\psi_o)}{\Delta\psi} = \frac{-1}{\Delta\psi} \tag{4.97}$$

Thus the *CDR* depth versus incident angle should have an average slope $-1/\Delta\psi$ and thus be a measure of strain in the *Strained Layer superlattices.* Using the phase plane analysis we can calculate the CDR depth as a function of incident angle $\psi_o$. It can be shown that the jumps in the *CDR* depth at interface *j* occur at the corresponding incident angle $\psi_o$ such that [9]

$$j - 1 = \psi_c/\Delta\psi(A - \psi_o/\psi_m) \tag{4.98}$$

Where $A = [1 - ((1 - \chi_c)d_p/2x_c)^2]^{1/2}$ and $\chi_c$ is the dechanneling level. The *Catastrophic Dechanneling depth* increases when the angle of incidence is varied from $-\psi_o$ to $+\psi_o$ and is shown explicitly in figure 4.3. The calculations were done for the dechanneling depth corresponding to a dechanneling level $\chi_c = 0.85$ (i.e. 85 % of the particles were dechanneled at this depth).

Thus slope of the lino in figure 4.4 which is calculated using *modified harmonicapproximation* (equation 4.98) is equal to the reciprocal of tilt angle Al". This model allows rapid evaluation of results without the extensive numerical calculations. The staircased structure shown for *CDR* depth calculations using *Moliere potential* contains both strain and potential information and to a first approximation, the slope of the straight line passing through these staircased structure is equal to the reciprocal of the strain tilt angle $\Delta\psi$.

This CDR study has been made in the energy range of 0.5 to 2.0 MeV to follow up the experiments at the low energy accelerators available in India. We can still go further down in the energy range but then one has to consider the electronic energy loss of the probe beam in SLS. As mentioned earlier, CDR technique can be effectively used to determine the strains in SLS; its sensitivity is due to the fact that the tilt angle $\Delta\psi$ is of the order of critical angle for channeling $\psi_c$ [4]. This calculation is done for $In_{0.2}Ga_{0.8}A/;GaAs$, 200 A, six layered each (s=282.2 A ) and $In_{0.1}Ga_{0.9}As/GaAs$,300 A , six layered each (s=424.26 A) assuming that this thickness is within the critical layer thickness of the sample such that misfit dislocations are not generated. The probe is $He^4$. The average dechanneling fraction $\chi$in the second layer is taken as the criterion for fixing the CDR energy. For $In_{0.2}Ga_{0.8}As/GaAs$case, $\Delta\psi$ = 0.782° and since the critical angle for channeling is less than the tilt angle, ($\psi_c$ = 0.39° for 0.7 MeV $He^4$ ions) the complete dechanneling of the probe beam occurs at the second layer itself (Fig 4.5) indicating thereby that this sample is not suitable for CDR studies. The critical angle and the tilt angle are in competition with each other and this calculation is done assuming two tilt angles. For $In_{01}Ga_{0.9}As/GaAs$we find the CDR energy to be 1.2 MeV by varying the energy over a considerable range. This is shown in figure 4.3 which shows the depth Vs dechanneling fraction for (i) +0.15° (ii) *0*° and (iii) $-0.15^{o}$ incident angles. We have assumed here a tilt of 0.2° at each interface which we had experimentally determined in an earlier study [7], on these samples. Incident Angle Asymmetry (1AA) is observed wherein the particles that are incident at an angle in positive direction are dechanneled between the 2nd and 3rd layer whereas those with 0° incidence and negative angle incidence go quite deep inside. This asymmetry in the incident angle can be understood qualitatively from the phase plane analysis based on *modified harmonic model* discussed above [8, 9].

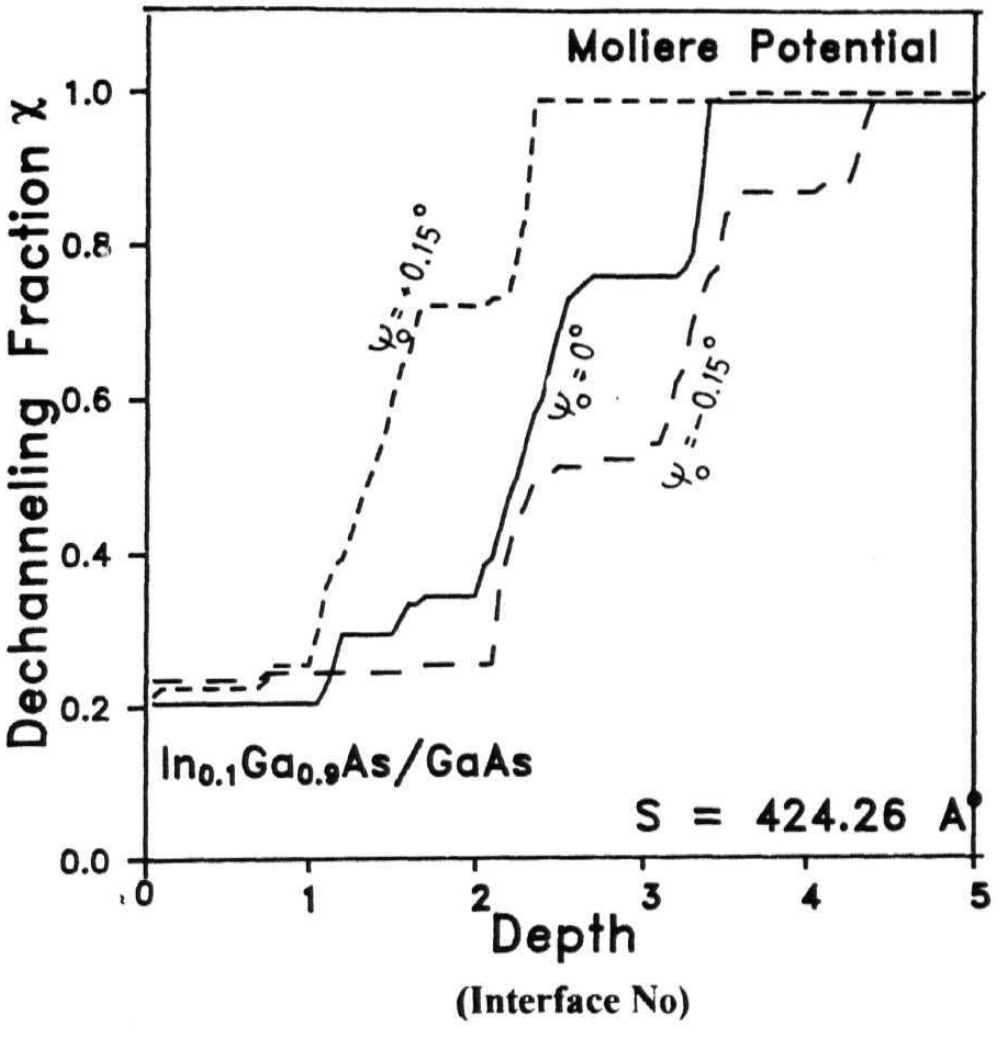


**Fig 4.3: Dechanneling Fraction χ Vs CDR depth calculated using Moliere planar potential for $In_xGa_{(1-x)}As/GaAs$ structure with x = 0.2, $\Delta\Psi$ = 0.782° (dashed line) and x = 0.1, $\Delta\Psi$ = 0.391° (solid line)**

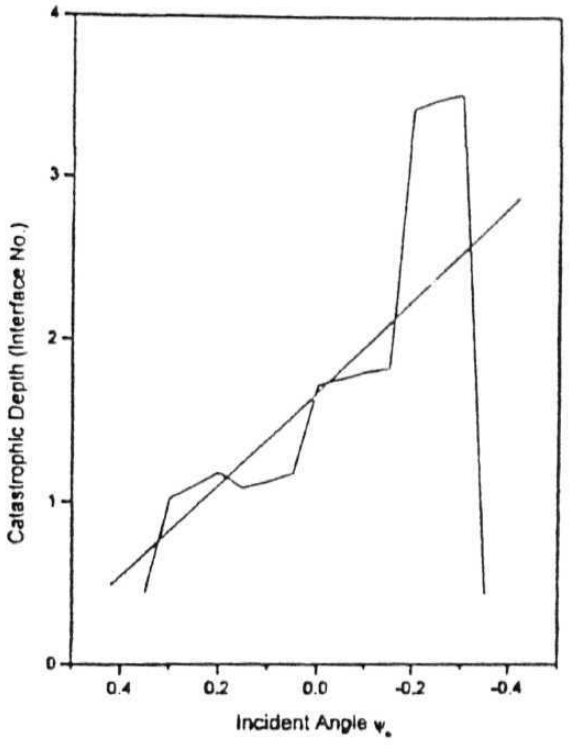


Fig 4.4: Catastrophic depth as a function of incident angle for a static Moliere potential.

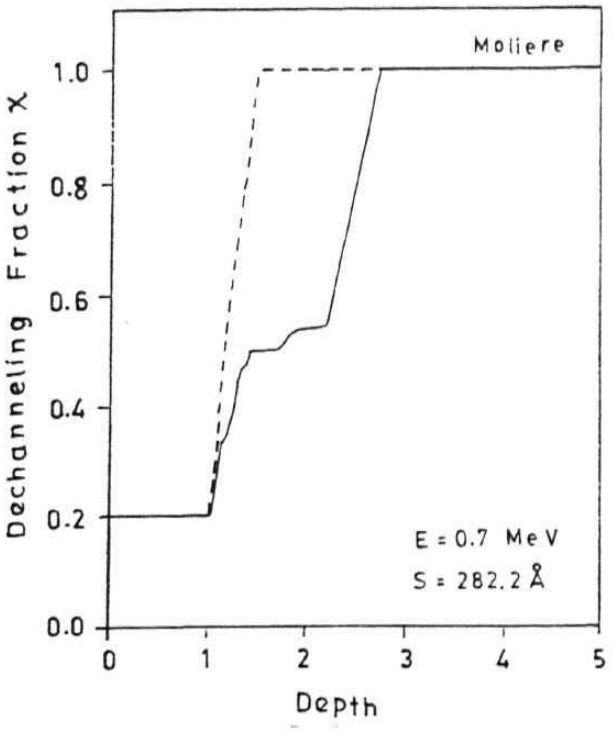


**Fig 4.5: χ Vs CDR depth calculated using** Moliere pianar potential for InxGa(1-x)As/GaAs structure with x = 0.2. Av = 0.782° (dashed line) and x = 0.1. Δψ = 0.391" (solid line).

# References


[1] V. Harikumar and A. P. Pathak, Journ. Phys. Cond. Matt., 7, 7805, 1995.

[2] V. Harikumar and A. P. Pathak, Phys. Stat. Sol.(b), **177,** 269, 1993.

[3] A. P. Pathak and Harikumar V., Nucl. Inst, Meth. **B99,** 499, 1995.

[4] S. T. Picraux, B. L. Doyle and J. Y. Tsao, ed: Pearsall P. Thomas Semiconductors and Semimetals, 33, New York, Academic Press, 1991, Strained-layer Superlattices: Materials Science and Technology.

[5] V. Harikumar and A. P. Pathak, Phys. Stat. Sol.(b), **182,** 51, 1994.

[6] J. A. Ellison, S. T. Picraux, W. R. Allen and W. K. Chu Phys. Rev. B, 37, 7290, (1988).

[7] Azher M. Siddiqui, Anand P. Pathak , B. Sundaravel, Amal K. Das, K. Sekar, B. N. Dev and B. M. Arora, Nucl. Inst, Meth. B 142, 389, 1998.

[8] W. K. Chu, J. A. Ellison, S. T. Picraux, R. M. Biefeld and G. C. Osbourn, Phys. Rev. Lett., 52, 125, (1984).

[9] S. T. Picraux, W. K. Chu, W. R. Allen and J. A. Ellison Nucl. Inst. Meth., B 15, 306, (1986).

[10] S. T. Picraux, W. R. Allen, R. M. Biefeld, J. A. Ellison and W. K. Chu, Phys. Rev. Lett,, 54, 2355, (1985).

Chapter 5

# CONCLUSIONS

With a preview to ion channeling, the dechanneling due to defects in solids and the utilization of ion channeling for defects and/or strain in synthetically modulated structures like semiconductor superlattices have been addressed to, in this thesis. The first extensive and comprehensive treatment of channeling is that due to Lindhard [1] with the following assumptions that (i) angles of scattering for a particle are small, and (ii) collisions occur with one string or plane of atoms at a time. This continuum approximation due to Lindhard describes completely the channeling phenomena, and provides analytically handy expressions. The case of a particle in a channeled in a crystal with point defects and/or with extended defects (like stacking faults or dislocations) need to be addressed to, in detail. A detailed knowledge of interatomic potentials for such channeled particles is needed for proper understanding and interpretation of various observations. Utilization of ion channeling for defects studies and characterization is another area of special interest. This thesis is an effort to address these two problems and hence is divided into two parts viz. (i) theoretical work on the interatomic potential for a positively charged particle, channeled in a crystal with point defects and (ii) characterization of Strained-Layer Superlattices (SLS) by channeling and compare it with other characterization techniques like XRD and Raman Spectroscopy.

The interaction potential between a positively charged probe particle and impurities in a lattice (target) has been discussed in detail. Extensive research has been done regarding the interatomic potentials which were derived by various methods; each of them applicable to a certain regime. Out of these, Lindhard's potential [1], statistical potential, power law potential proposed by *Pathak*[2], exponential forms like Moliere potential [3] and the Biersack's Universal potential [4] are most frequently used potentials [5]. At small nuclear seperations, the most appropriately used

is the screened Coulomb potential with a screening function given by the Thomas-Fermi model [6]. This model possesses the distinct advantage of simplicity combined with increasing validity for heavier atoms, apart from providing an initial hypothesis for some of the reliable theoretical potentials at close separations.

The interaction between an external probe particle and a host lattice *with impurities* is described by a *modified screened* Coulomb potential which is based on the static screening concept connected to a dielectric function $\epsilon(q)$. The formulation is then extended to include higher order terms in the dielectric function which defines the screening parameters of this potential. This is covered in chapter 2 along with a discussion on the pions and muons in materials research. The weakly decaying nature of the potential thus derived manifests itself in dechanneling process and scattering cross-section. The formulation also highlights the role played by the atomic electrons of the impurity and conduction electrons of the host lattice. The dechanneling cross-section, which is then derived for this modified double screened potential for $\alpha$-particles dechanneling by hydrogen or carbon impurities in palladium crystal and muon dechanneling by oxygen impurity in tantalum, is modified for various charge states of impurity in different planar directions, when the effect of both the atomic electrons of the impurity and conduction electrons of the host lattice are considered. These are compared with earlier calculations and available experimental results and are tabulated [7].

Rutherford Backscattering Spectroscopy /Channeling is a very powerful technique using which one can determine the thickness, composition, uniformity defect densities and. can be readily applied to superlattices [8, 9, 11]. Ion channeling is a special case of RBS and is one of the sensitive characterization techniques which provides a measure of crystalline quality. It also allows one to determine the strain in epitaxial layered structures. This is accomplished by carrying out angular scans along the off-normal axis using which, the strain in the epilayers is evaluated [10]. The difference between the dips on angular axis of these angular scans between epitaxial layers is a direct measure of the strain between the layers. We have grown some samples of SLS at the OMVPE facility of TIFR, Mumbai. Chapter 3 of the thesis covers the growth and characterization of SLS by Ion Channeling, which is compared with XRD and Raman Spectroscopy.

Strain values in such technologically important SLS can also be found out by empirical formula based on Vegard's law.

$$a_{In_xGa_{1-x}As} = xa_{InAs} + (1-x)a_{GaAs} \tag{5.99}$$

and the lattice constants $a_{GaA_s} = 5.6532$ Åand $a_{InAs} = 6.0584$ Å, we find $a_{In_{0.1}Ga_{0.9}As} = 5.6937$ Å. In table 3.2, we have tabulated the results of strain analysis by ion channeling, HRXRD and Raman Spectroscopy.

Another method of determination of strain in SLS by ion channeling is based on a resonance condition in which if the period of SLS structure matches with the average channeled-particle wavelength, there will be a rapid increase in dechanneling aft r a certain depth. This phenomenon is called Catastrophic Dechanneling Resonance $CDR$ and occurs when the half wavelength $(\frac{\lambda}{2})$ of the oscillatory motion of the channeled ion matches with the path length per layer *(s)* of the *SLS* [12]. This technique is attractive for strain analysis and at very low strains: it is the most sensitive of all the ion-channeling techniques for strain measurements. In contrast, axial channeling angular scan is the most versatile; each layer strain can be determined over a wide range of strain magnitudes and layer thickness for both single-strained layers and superlattices. $CDR$dependence on various parameters like energy of the incident ion, incident angle, tilt angle etc. have been studied using Moliere potential have been carried out on $In_{0.2}Ga_{0.8}As/\ GaAs$ and $In_{0.1}Ga_{0.9}As/GaAs$superlattices with $He^4$ as the probe along the (110) direction [13]. CDR studies are described in detail in chapter 4 of the thesis.

## 5.1 Future Plan of Work

We have developed a theoretical formulation for dechanneling by point defects. The dechanneling cross-section of $\alpha$-particles in palladium with carbon and hydrogen impurities and muons in tantalum crystals with oxygen impurities are calculated along various planar directions. The interaction potential used here is a modified double screened potential; the screening effects have been incorporated using dielectric mechanism including the higher order terms in the Fourier component of the screening potential. This gives fluctuations in the local charge density (Friedal

oscillations). To get a better perspective of this interaction, the obvious choice is to generalize the screening effects to incorporate the electron-electron interaction and work in this direction is in progress.

$In_{0.1}Ga_{0.9}As/GaAs$ samples were grown, systematically varying the thickness of the samples from 100 A to 500 A keeping the indium constant. Ion channeling has been carried out at Institute of Physics, Bhubaneswar; High Resolution XRD has been carried out at Tata Institute of Fundamental Research, Mumbai and Raman Scattering work has been done at Indira Gandhi Centre for Atomic Research, Kalpakkam. The analysis is carried out from the point of view of theory of Matthews and Blackeslee on the onset of misfit dislocation upon strain relaxation.

All along, the samples were grown keeping the composition of indium constant and varying the thickness systematically. We plan to grow some samples keeping the thickness constant and vary the composition of indium systematically and then characterize them by ion channeling, in order to complete the study of the onset of misfit dislocations at a given thickness and composition.

# References


[1] J. Lindhard, Kgl. Danske, Vindenskab, Selskab, Mat. Fys. Medd., 34, No. 14 (1965).

[2] A. P. Pathak, Rad. Eff., **61,** 1, (1982).

[3] G. Moliere, Z. Naturforschung, A2, 133 (1974).

[4] D.J. O'Connor and J.P. Biersack, Nucl. Inst. Meth, **B15,** 14 (1986).

[5] V. Harikumar and A.P. Pathak, Phys. Stat. Sol. (h), **177,** 269 (1993).

[6] D. S. Gemmel, Rev. Mod. Phys. 46, 129 (1974).

[7] Azher M. Siddiqui, A. Kiran and Anand P. Pathak, Modern Physics Letters (B), 11, 1231, 1996.

[8] J W Mayer, J F Zeigler, L L Chang, R Tsu and L Esaki, J. Appl. Phys., 44, 2322, 1973.

[9] F W Saris, W K Chu, C A Chang, R Ludeke and L Esaki, Appl. Phys. Lett., **37,** 931, 1980.

[10] Azher M. Siddiqui, Anand P. Pathak, B. Sundarvel, Amal K. Das, K. Sekar, B.N. Dev and B.M. Arora, Nucl. Inst, and Meth. (B), 142, 389, 1998.

[11] S T Picraux, L R Dawson, G C Osbourn and W K Chu, Nucl. Ins. and Meth, **218,** 57, 1983.

[12] V. Harikumar and A. P. Pathak, Journ. Phys. Cond. Matt., 7, 7805, 1995.

[13] Anand P. Pathak, S.V.S. Nageswara Rao and Azher M. Siddiqui, Nucl. Instr. and Meth. **(B), 161-163,** 488, 2000.